X-ray Binaries

History

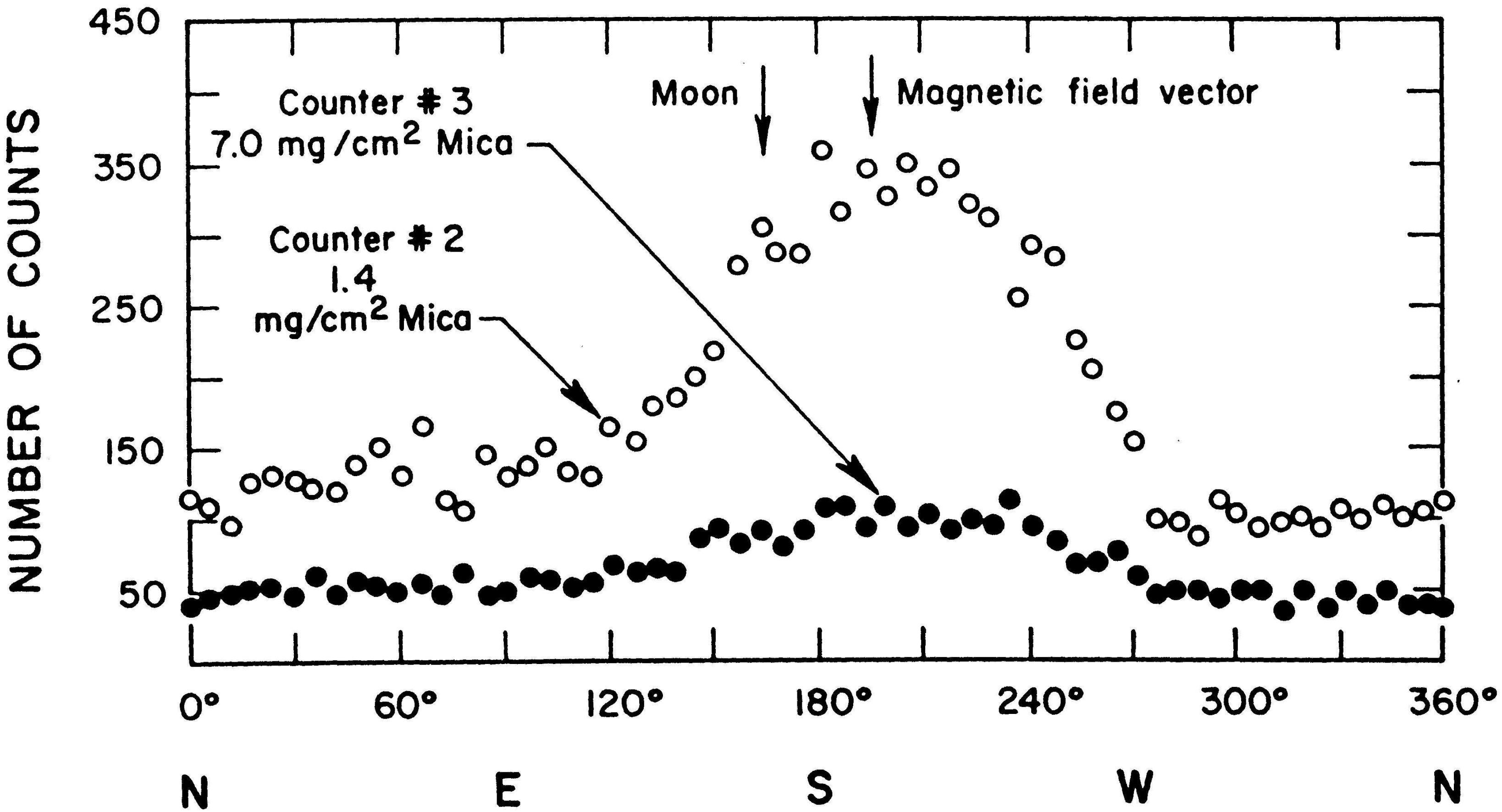

X-ray scan of the galactic plane during an Aerobee flight in June 1962 (Giacconi et al.): First discovery of an extrasolar X-ray source.

The moon was not detected in the X-rays (first detection by ROSAT in the 1990s).

Intermezzo: The name of the game

X-ray binaries are named in arcane ways. Typical nomenclatures:

- Constellation + X + number, earliest discoveries, e.g., Her X-1, Cyg X-3, but also LMC X-3.
- Name in the Ariel catalogue, e.g., A 0535+26
- Name in 4th Uhuru catalogue, e.g., 4U 1957+115
- ROSAT all sky survey, e.g., RX J1940.1-1025 (and analogously for Beppo-SAX [SAX xxx], EXOSAT [EXO xxx], Ginga [GS xxx], Granat [GRS xxx], GRO [GRO xxx])

See SIMBAD for explanations (`http://cdsweb.u-strasbg.fr/`).

History

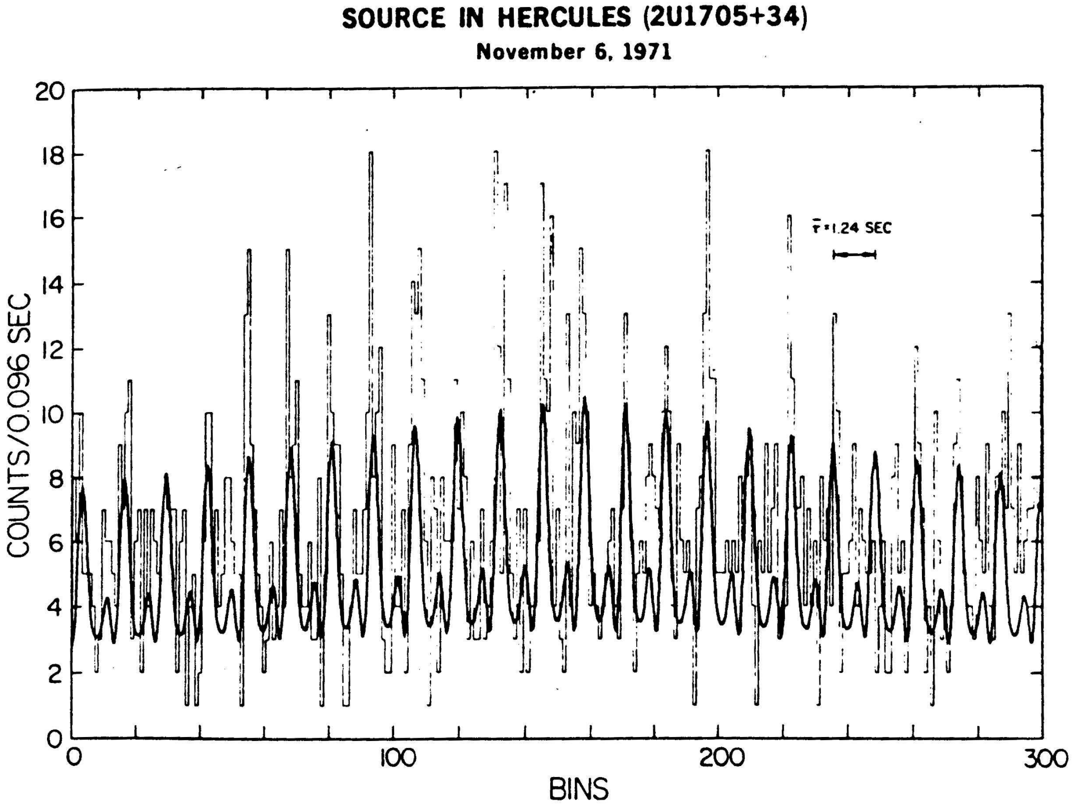

Tananbaum, 1973

First clue regarding the nature of the X-ray sources: detection of 1.24 s pulsations from Her X-1 $\Longrightarrow$ Pulsating X-ray binaries as accreting, rotating neutron stars.

Optical Appearance

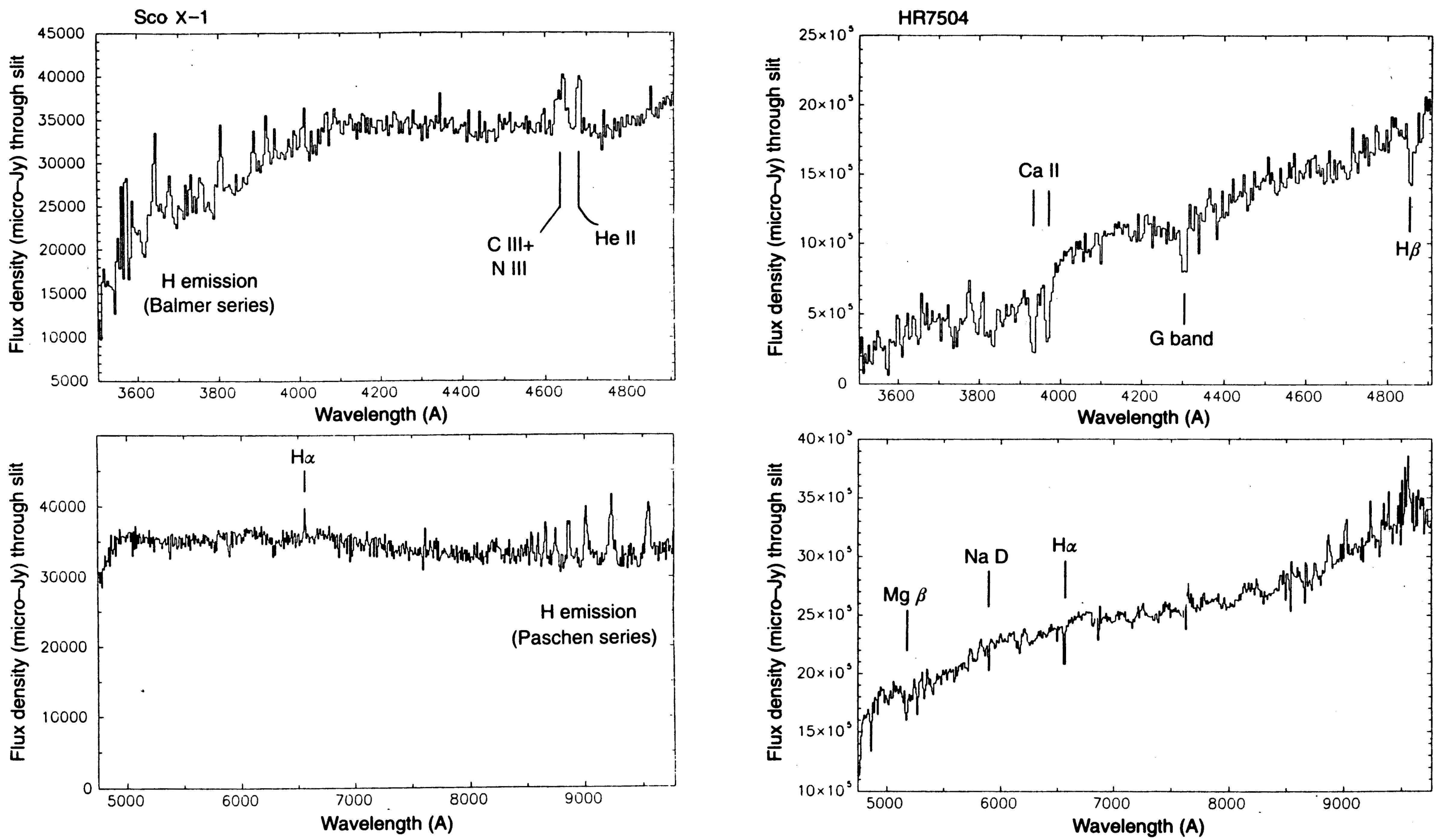

Charles & Seward, 1995, p. 156

Optical appearance of XRB unspectacular (Sco X-1 has $m_V \approx 17$), but very blue optical spectrum, prominent emission lines (e.g., HII 4686 Å) $\Longrightarrow$ evidence for an accretion disk.

Mass Determination, I

Mass determination from velocity curve.
Kepler's 3rd law:

$$\frac{(a_\mathrm{X}+a_\mathrm{S})^3}{P_\mathrm{orb}^2} = \frac{G(M_\mathrm{X}+M_\mathrm{S})}{4\pi^2} \tag{3.1}$$

where X: X-ray object, S: normal star, and a_i: distance from center of mass ($M_\mathrm{X}a_\mathrm{X} = M_\mathrm{S}a_\mathrm{S}$).
Observed velocity (projected onto sky) gives a_j:

$$K_j = \frac{2\pi a_\mathrm{j}\sin i}{P} \quad \text{since} \quad \mathrm{v} = 2\pi r/P \tag{3.2}$$

(for $j = \mathrm{X, s}$), where i is the inclination. Since

$$(a_\mathrm{X}+a_\mathrm{S})^3 = \left(a_\mathrm{X} + a_\mathrm{X}\frac{M_\mathrm{X}}{M_\mathrm{S}}\right)^3 = \frac{a_\mathrm{X}^3(M_\mathrm{X}+M_\mathrm{S})^3}{M_\mathrm{S}^3} \tag{3.3}$$

Kepler's law gives after some algebra

$$f_\mathrm{X}(M_\mathrm{X}, M_\mathrm{S}) = \frac{M_\mathrm{X}^3\sin^3 i}{(M_\mathrm{S}+M_\mathrm{X})^2} = \frac{PK_\mathrm{S}^3}{2\pi G} \tag{3.5}$$

the mass function (minimum mass of compact object). More precise mass only possible when determination of i possible (e.g., eclipses).

Mass Determination, II

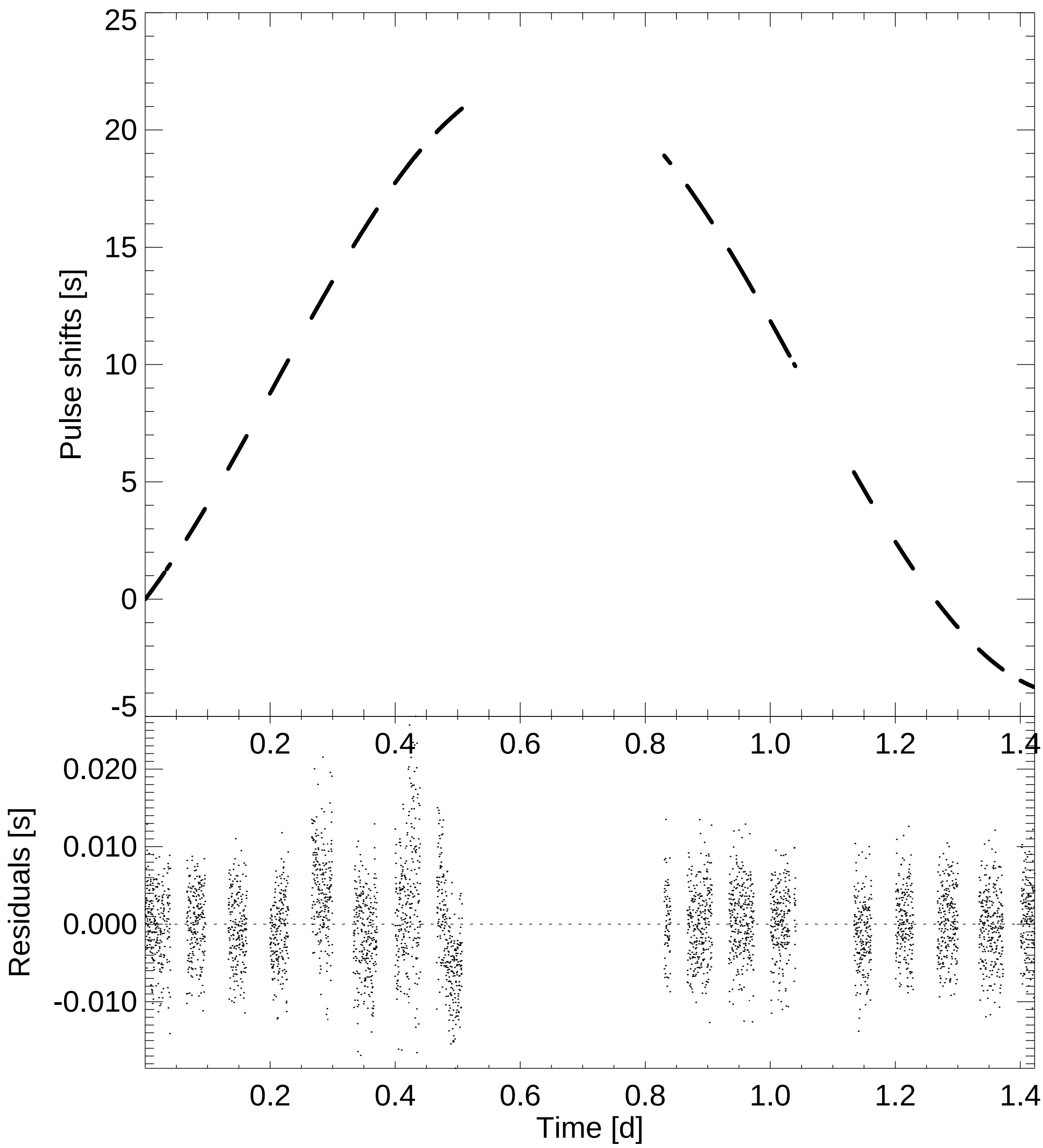

(Stelzer, 1997, Diplomarbeit AIT, Abb. 6.14)

Pulse arrival times for Her X-1 change sinusoidally as a result of the orbital motion $\Longrightarrow$ Determination of K and $a \sin i$.

Mass Determination, III

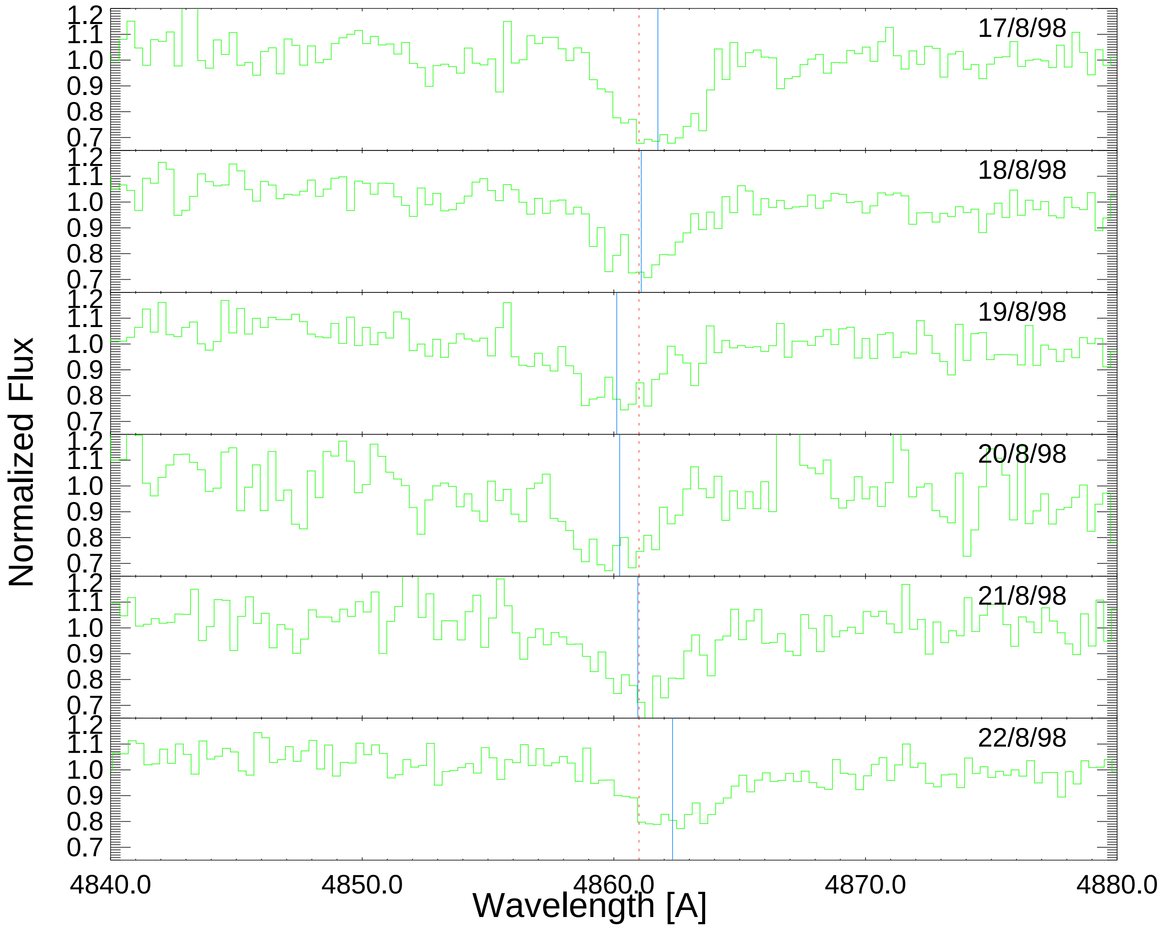

(Pottschmidt et al., 2001)

Determination of the RV of the black hole in Cyg X-1 (Observatoire de Haute Provence, 1998 August [1.52m, Aurelie]) using the Hβ line (4861Å).

Masses of XRBs

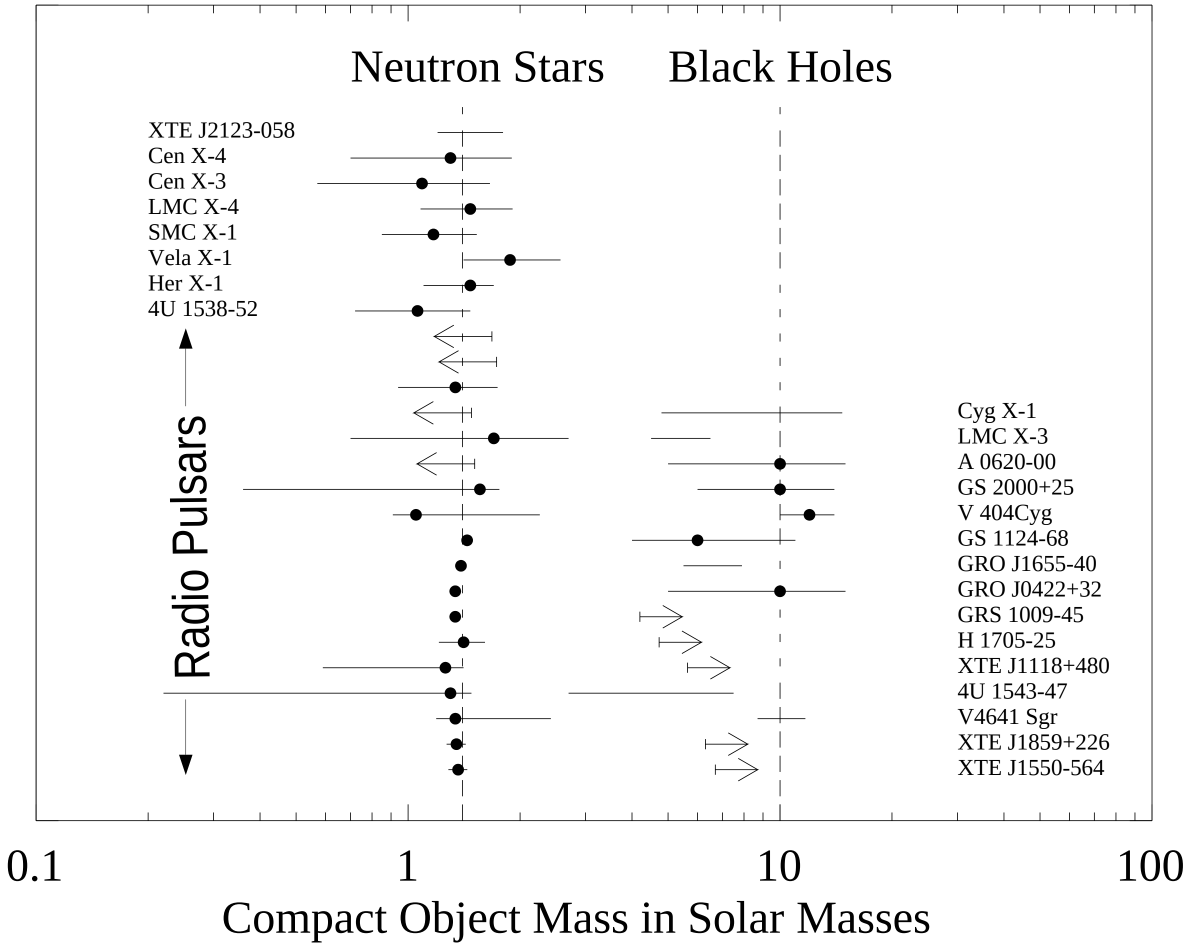

Kalemci, priv. comm.)

Almost all measured neutron star masses are consistent with the canonical value of 1.4 $M_\odot$!

Mass/Orbits

Table 2.6 X-ray/Optical Orbital Parameters of X-ray Binaries

	Source	Type[a]	P_{orb}(d)	$a_x \sin i$(lt-s)	$f_x(M/M_\odot)$	K_c(km s^{-1})	$f_c(M/M_\odot)$[b]	$M_X(M_\odot)$	References
	A. Neutron Star Primaries[c]								
1	LMC X-4	H	1.41	26.31±0.03[d]	9.86±0.04	37.9±2.4	0.008	1.38±0.25	[246,272]
2	Cen X-3	H	2.09	39.664±0.007	15.386±0.001	24±6	0.003	1.06(+0.56, -0.53)	
3	4U1538-52	H	3.73	52.8±1.8	11.4±1.2	19.8±1.1	0.003	1.3±0.2	[284,394]
4	SMC X-1	H	3.89	53.46±0.05	10.84±0.03			1.6±0.1	[387,395]
5	Vela X-1	H	8.96	113.0±0.4	19.29±0.21	21.8±1.2	0.010	1.77±0.21	
6	Her X-1	L	1.70	13.1831±0.0003	0.8513±0.0001	83±3	0.10	0.98±0.12	[116]
7	4U1907+09	H	8.38	83±3	8.8±1.0				[84]
8	4U0115+63	H	24.3	140.13±0.16	5.007±0.019				
9	2S1553-54	H	30.6	164±22	5.0±2.1				
10	V0332+53	H	34.3	48±4	0.101±0.025				
11	GX301-2	H	41.5	371.2±3.3	31.9±0.8				[404]
12	EXO2030+375	H	46[e]	240±15[e]	7.1±1.3[e]				[364]
13	4U1626-67	L	0.029	<0.010	$<1.3\times10^{-6}$				[273]
14	4U1700-37	H	3.41			18±3	0.002	1.8±0.4	[199]
15	Cen X-4	L	0.63			146±12	0.20		[95,308]
	B. Black Hole Candidates								
16	LMC X-3	H	1.70			235±11	2.3±0.3	>7[f]	[91]
17	LMC X-1	H	4.23			68±8	0.14±0.05		[224]
18	Cyg X-1	H	5.60			74.6±0.13	0.241±0.013	>7[f]	[156]
19	A0620-00	L	0.32			442±4	2.90±0.08	>3.4[g]	[306,307]
20	Nova Mus '91	L	0.43			409±18	3.07±0.40	>2.9[g]	[393]
21	GS2023+338	L	6.47			210.6±4	6.26±0.31	>5.6[g]	[54]

Footnotes:
[a] H = HMXB and L = LMXB.
[b] For entries 1-15 the errors are large and asymmetric, and are not given. They can be computed easily using the expression for $f_c(M)$ given in the text and the values tabulated here for P_{orb}, K_c, and ΔK_c.
[c] Data in Part A are adopted from Tables 3 and 4 in [342], and from the supplementary references cited above.
[d] August 1989 Ginga observations; see [272] for a summary of the results of two other recent X-ray timing observations of LMC X-4.
[e] Parameters for Model III [364].
[f] Model dependent (see text).
[g] Firm 2σ limits set by the value of the mass function (see text).

(van Paradijs & McClintock, 1995, Tab. 2.6)

Reminder: Accretion

Spherically symmetric accretion: maximum luminosity is Eddington luminosity,

$$L_{\text{Edd}} = \frac{4\pi G M_{\text{X}}(m_{\text{p}} + m_{\text{e}})c}{\sigma_{\text{T}}}$$

$$= 3.23 \times 10^4 \left(\frac{M_{\text{X}}}{M_\odot}\right) L_\odot \quad (3.6)$$

($L_\odot = 3.9 \times 10^{33}\,\text{erg}\,\text{s}^{-1}$).

Efficiency η of accretion process is defined by

$$L = \eta \dot{M} c^2 \quad (3.7)$$

where $\dot{M}$ mass accretion rate. For accretion onto a neutron star,

$$\eta = \frac{GM}{Rc^2} \quad (3.8)$$

For typical X-ray luminosities of $\sim 10^{39}\,\text{erg}\,\text{s}^{-1}$ and $\eta \sim 0.1$, one finds typical mass transfer rates of

$$\dot{M} = 10^{-9} \dots 10^{-7}\,M_\odot\,\text{a}^{-1} \quad (3.10)$$

Roche Lobe Overflow, I

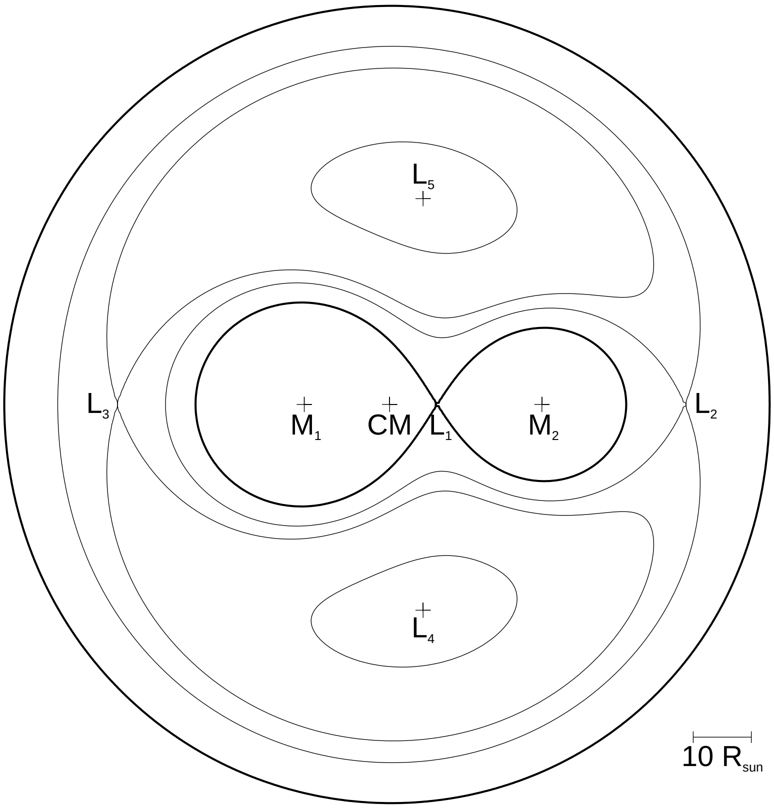

Wilms 1998

Assume both stars are point masses on circular orbits $\Longrightarrow$ Effective potential in *co-rotating coordinate system*: sum of the gravitational potentials and centrifugal potential:

$$\phi(\mathbf{r}) = -\frac{GM_1}{|\mathbf{r}-\mathbf{r}_1|} - \frac{GM_2}{|\mathbf{r}-\mathbf{r}_2|} - \frac{1}{2}(\omega \times \mathbf{r})^2 \qquad (3.12)$$

the Roche potential.

Stellar evolution: donor state eventually fills Roche lobe $\Longrightarrow$ Roche Lobe Overflow.

Roche Lobe Overflow, II

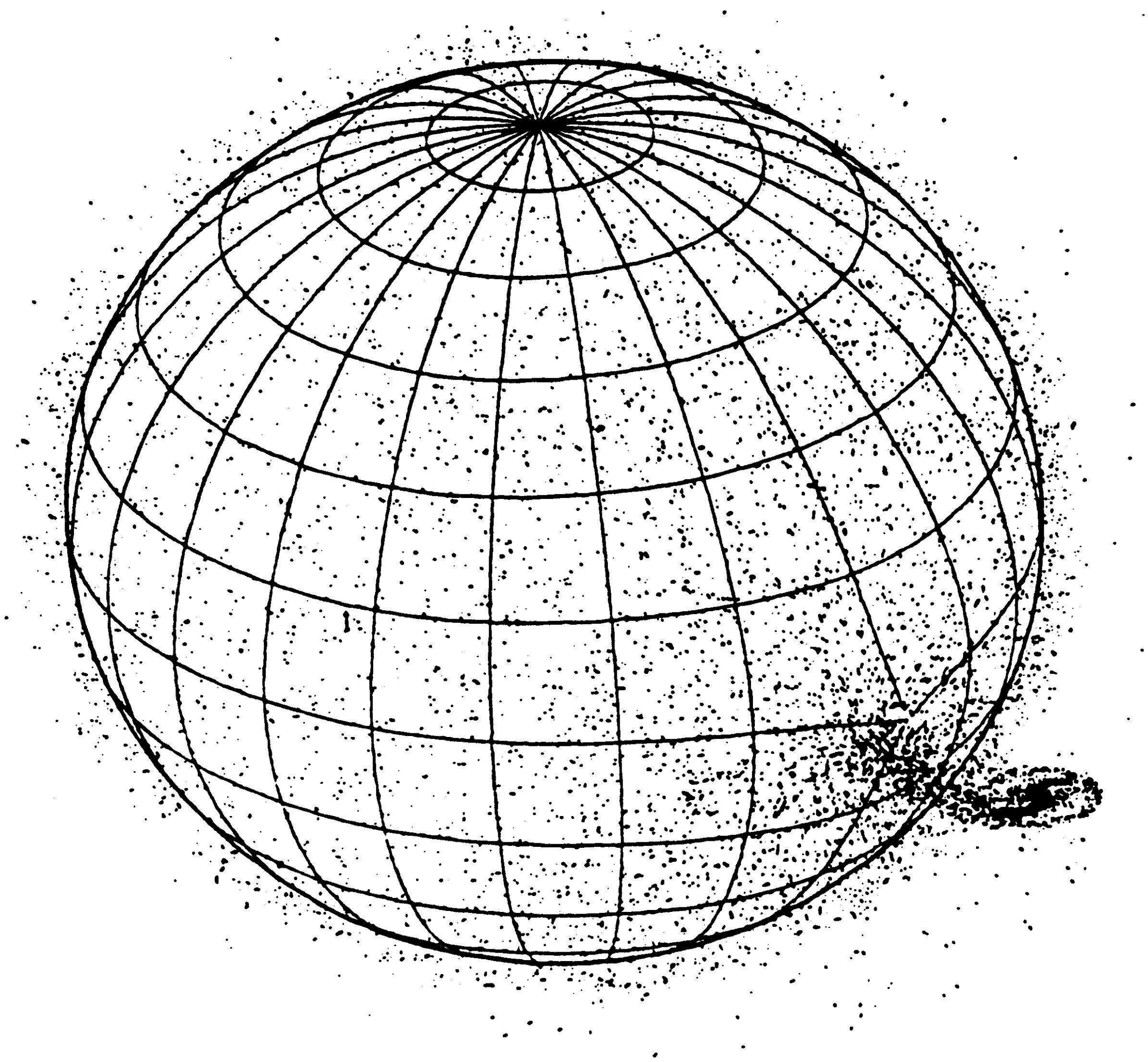

(Dennerl, Dissertation MPE)

Roche Lobe Overflow: Matter streams over Lagrange point L_1 from donor onto compact object. Preservation of angular momentum: Formation of accretion disk.

Typical objects: Her X-1.

Roche Lobe Overflow, III

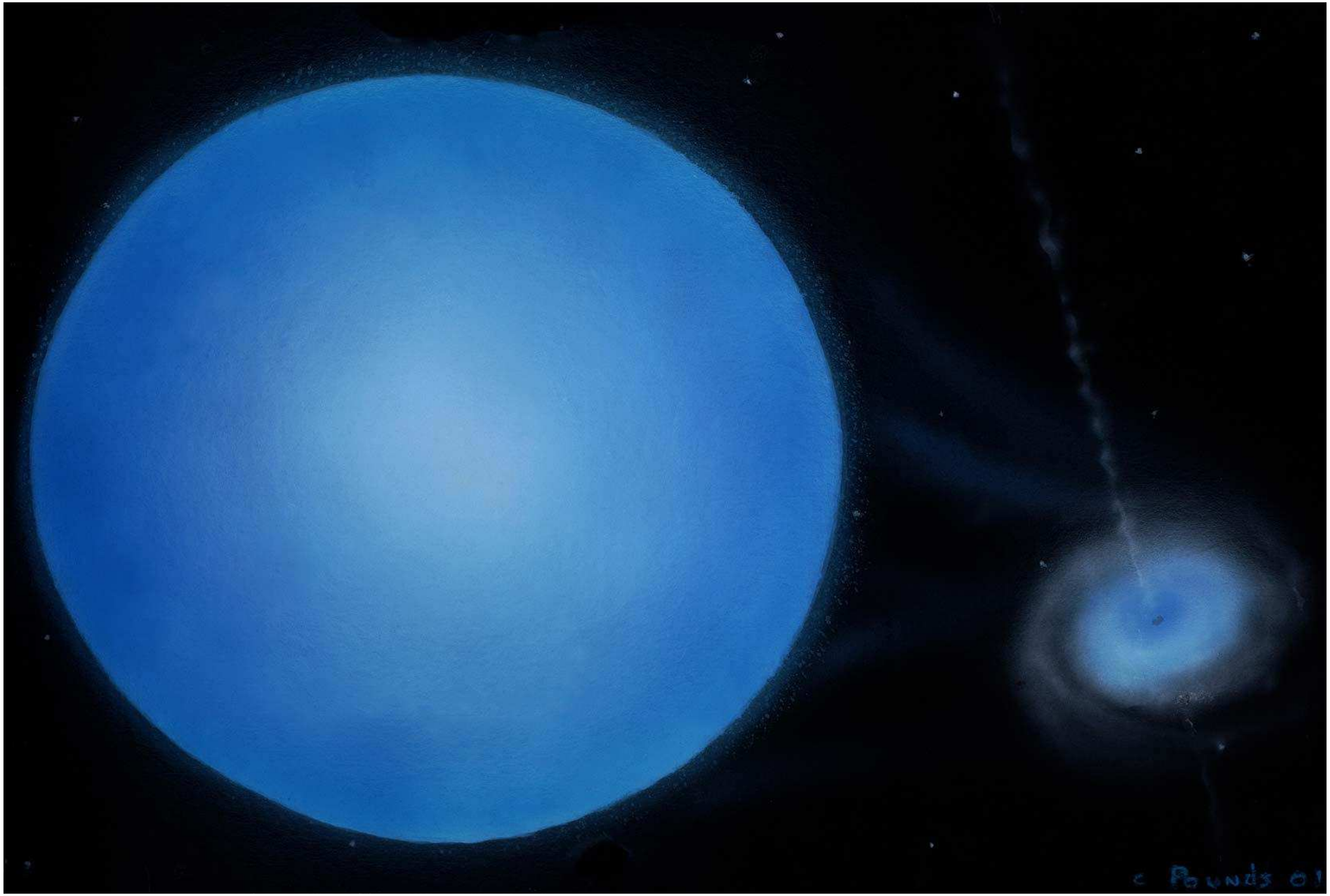

(NOAO Press Release 01/12)

Stellar Wind Accretion, I

Early type stars (spectral type O, B, mass $M \gtrsim 10\,M_\odot$) have strong winds, driven by radiation pressure in absorption lines. Typical Mass loss rates $\dot{M} = 10^{-7\ldots-5}$. Velocity profile parameterizable as

$$\mathrm{v}(r) \approx \mathrm{v}_\infty(1 - R_\star/r)^\beta \quad \text{with} \quad \beta \sim 0.5\ldots1.0 \tag{3.13}$$

and end-velocity $\mathrm{v}_\infty \approx 1000\,\mathrm{km\,s^{-1}}$.
A fraction of the wind ($10^{-4}\ldots10^{-3}$) can accrete onto compact object: Bondi-Hoyle accretion.

Stellar Wind Accretion, II

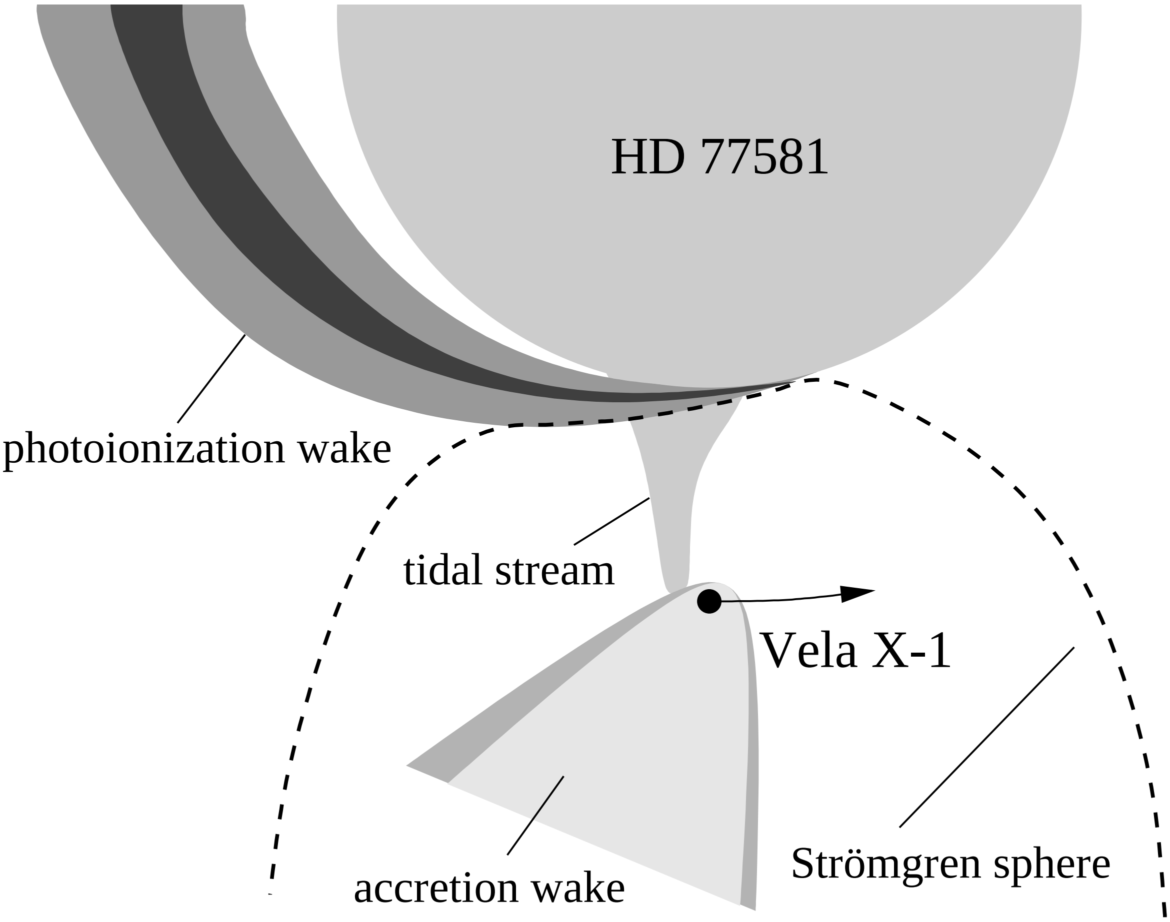

Principal components for wind-accretion:

- Ionized Strömgren region (wind ionized by X-rays from compact object).
- Accretion shock around compact object (orbital velocity typically $>$ velocity of sound!).
- Ionization wake where material is overdense.

Possibly formation of small disk around NS.

Typical Objects: Vela X-1

Stellar Wind Accretion, III

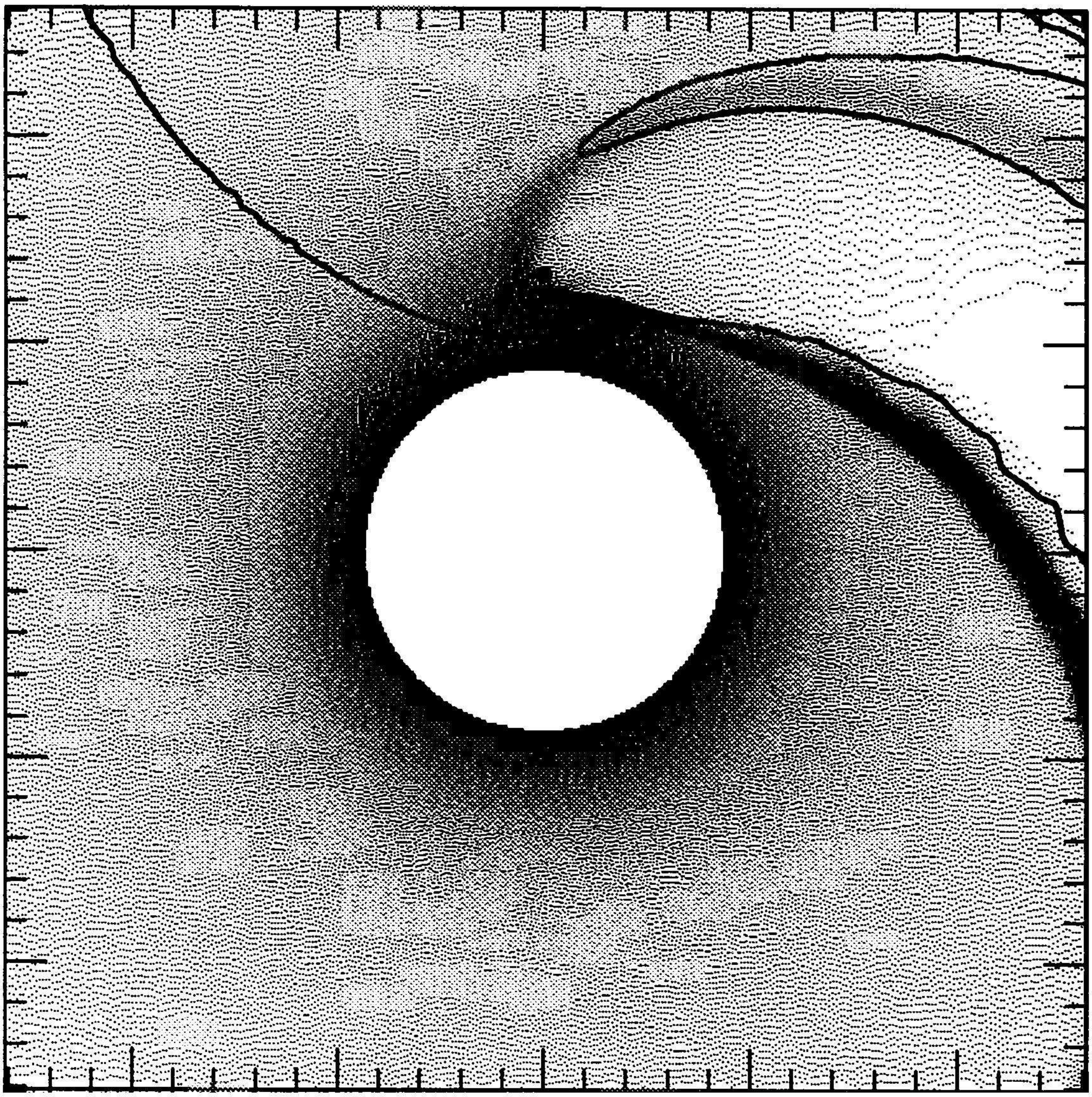

(Blondin (1994), Fig. 4)

Realistic hydrodynamical computations are difficult (asymmetry of accretion process, ionization of wind, large range of length-scales involved,. . .).

Stellar Wind Accretion, IV

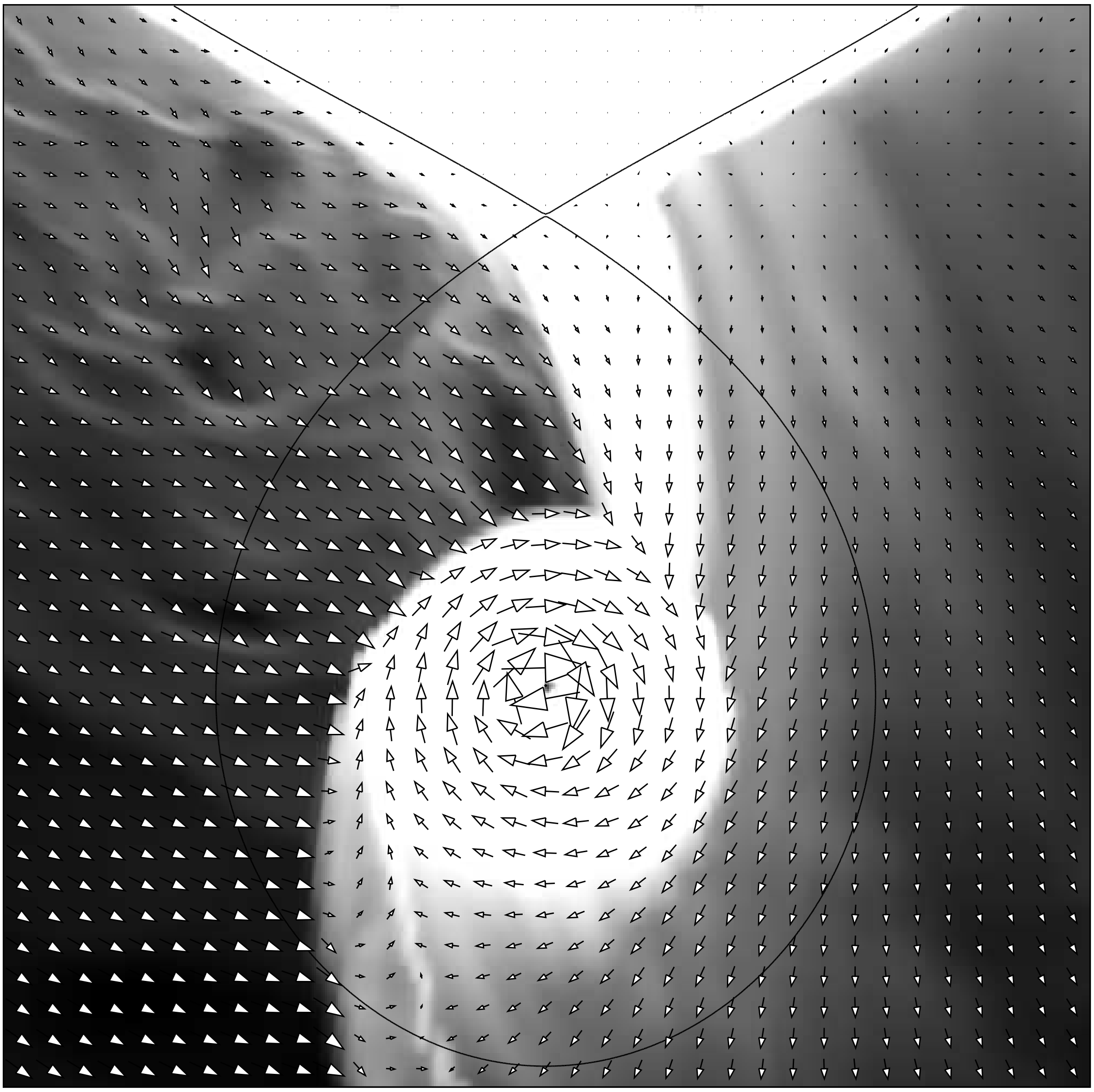

(Blondin, priv. comm.)

Velocity field from HMXB accretion (simulation for LMC X-4).

Be Accretion

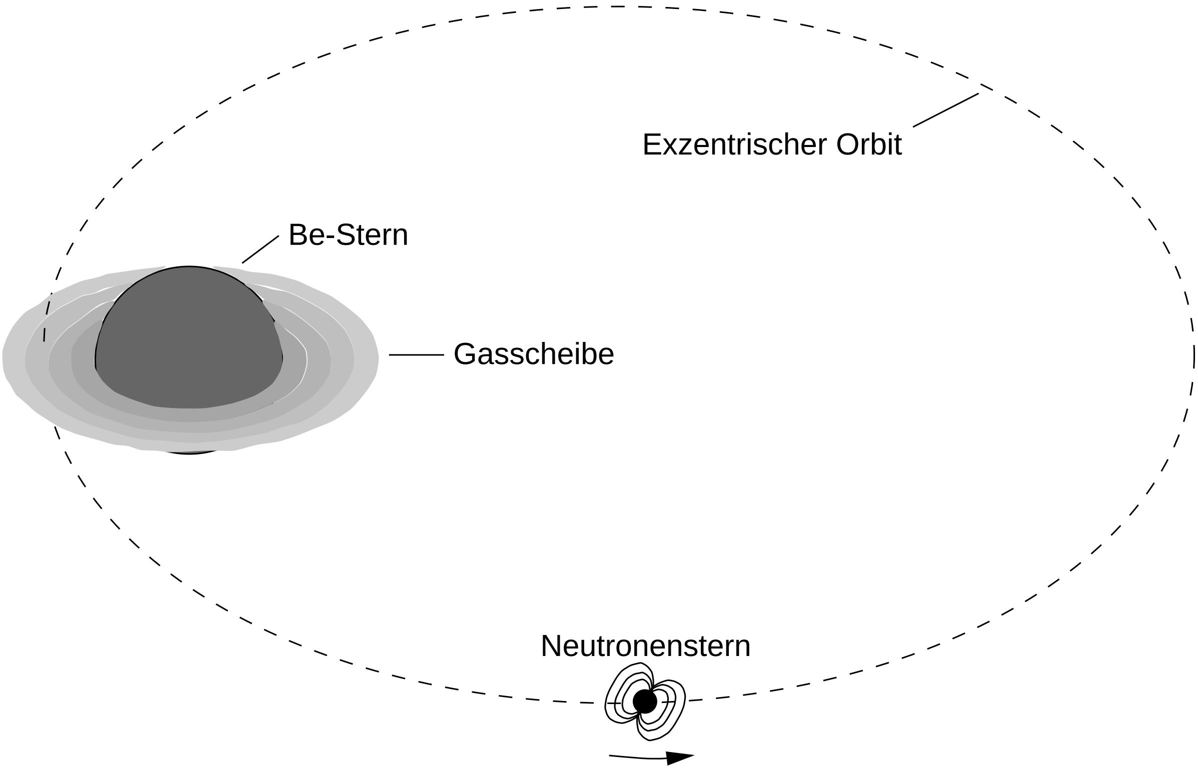

(Kretschmar 1996, Dissertation AIT, Abb. 2.6)

Some early type stars (O9–B2) have very high rotation rates $\Longrightarrow$ Formation of disk-like stellar wind around equator region. Line emission from disk: Be phenomenon.

Collision of compact object with disk results in irregular X-ray outbursts.

Exact physics not understood at all.

Typical Objects: A0535+26.

Low-Mass XRB

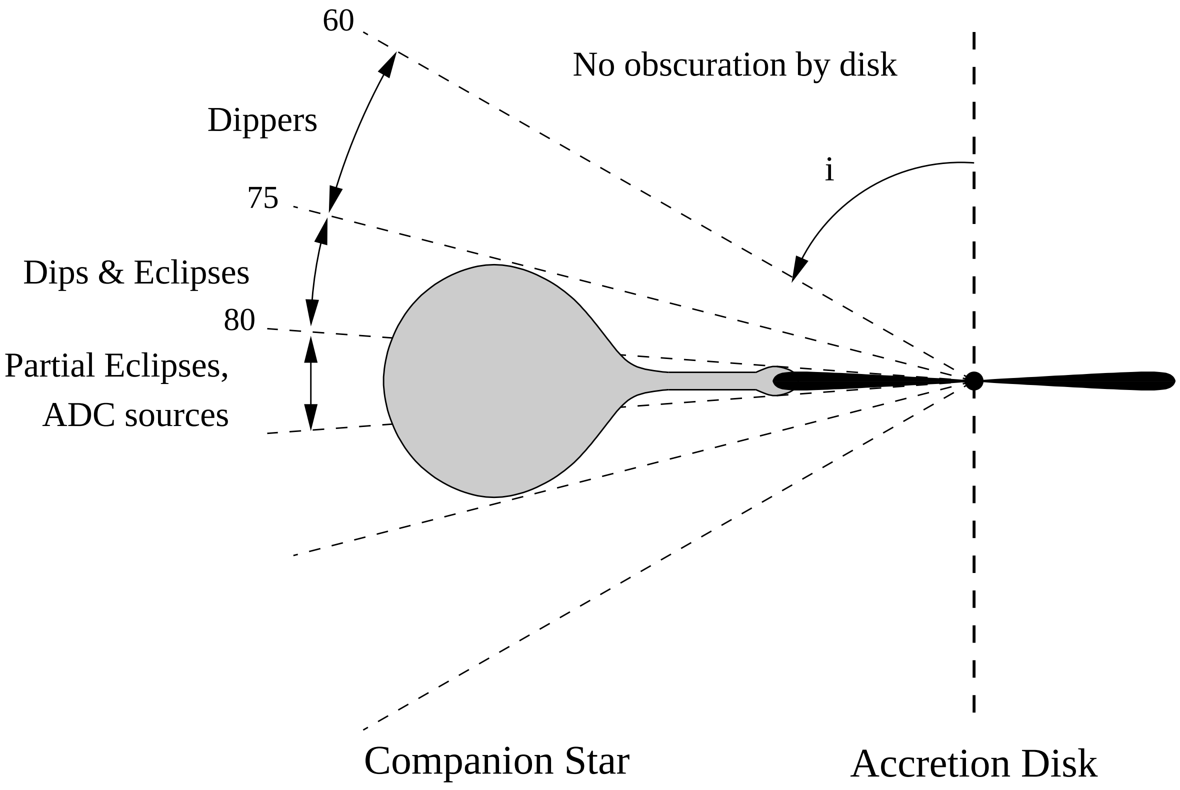

(after Charles & Seward, 1995, Fig. 8.3)

Low-Mass X-ray Binaries: Donor star has late spectral type (A and later), i.e. $M \lesssim 1.2\,M_{\odot}$.

$\Longrightarrow$ No stellar wind, systems are dominated by Roche Lobe overflow. Observed phenomenology mainly due to neutron star and the accretion disk, depending on viewing angle.

$\Longrightarrow$ Optical appearance: accretion disk and X-ray heated surface of donor star.

LMXB: Properties

Table 8.1. Properties of low-mass X-ray binaries

Source	Period (hrs)	X-ray type	Visual magnitude	Optical modulation	Companion star
4U1820–30	0.19	Burster	–	–	White dwarf
4U1626–67	0.7	Burster	19	Yes	Degenerate
A1916–05	0.83	Burster	21	Yes	Degenerate
X1323–619	2.9	Burster, dipper	–	–	
MXB1636–536	3.8	Burster	17	Yes	
EXO0748–676	3.8	Burster, dipper, transient	17		
4U1254–69	3.9	Burster, dipper	19	Yes	
4U1728–16	4.2	ADC[a] ?	17	Yes	
X1755–338	4.4	Dipper	18.5	Yes	
MXB1735–444	4.6	Burster	17	Yes	
Cyg X-3	4.8		(IR)	Yes(IR)	
4U2129+47	5.2	ADC	16	Yes	
2A1822–371	5.6	ADC	16	Yes	
MXB1659–29	7.2	Burster, dipper	19		
A0620–00	7.3	Transient	12–19	Yes	K
LMC X-2	8.2?		19	Yes	
4U2127+11	8.5	ADC	16	Yes	
4U1956+11	9.3		18	Yes	
CAL 87	10.2	ADC	19	Yes	
GX339–4	14.8	Multi-state	15–21	Yes	
Sco X-1	19.2	Prototype LMXB	12–14	Yes	
4U1624–49	21	Dipper	–	–	
CAL 83	25	ADC	17	Yes	
Her X-1	40.8	Dipper	15	Yes	F
GS2023+338	155	Transient	12–19	Yes	K0
2S0921–630	216	ADC	16	Yes	
Cyg X-2	235	Dipper	15	Yes	F giant

[a] ADC = accretion disc corona

Charles & Seward, 1995, Tab. 8.1

Accretion Disk Coronae

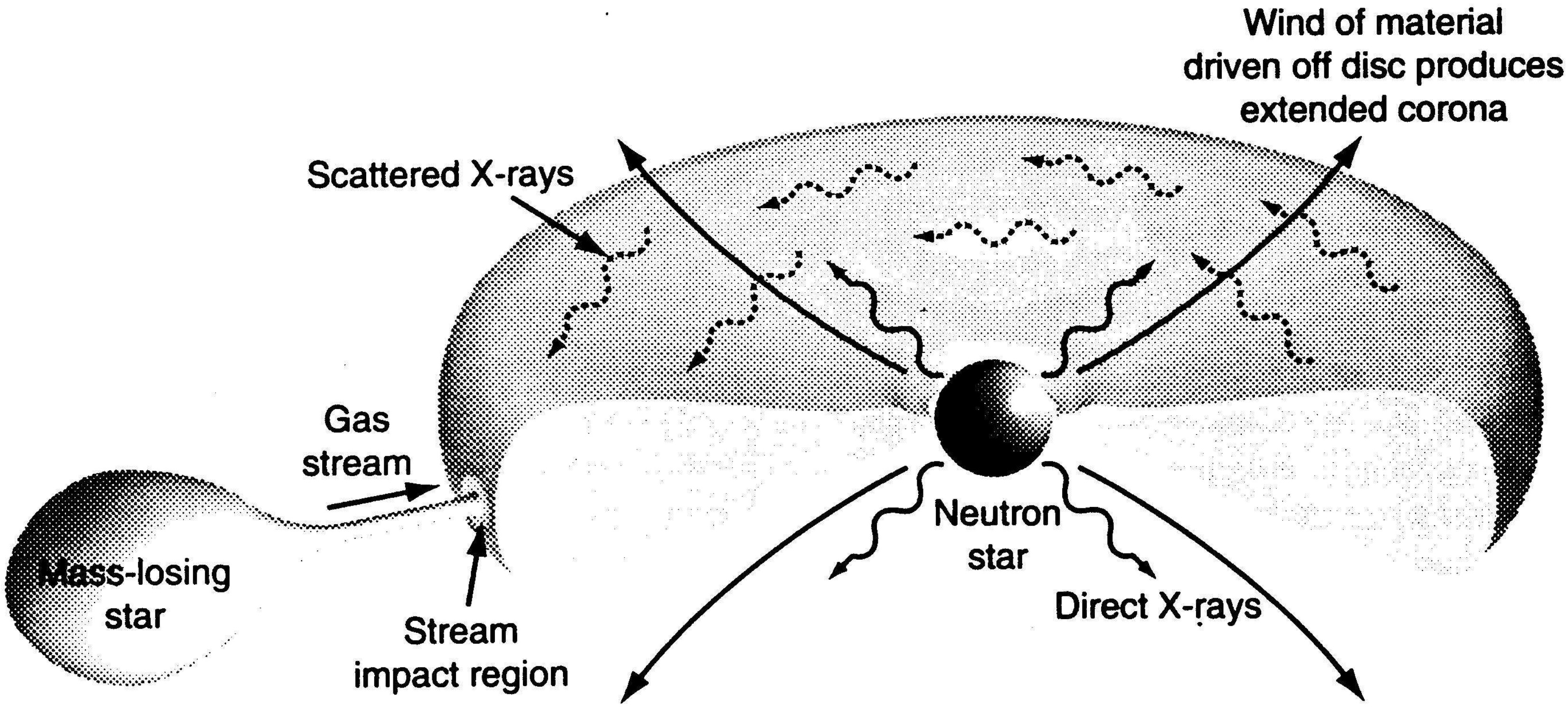

Charles & Seward, Fig. 8.8

Eclipses

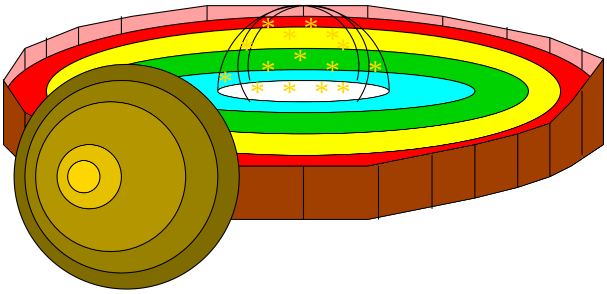

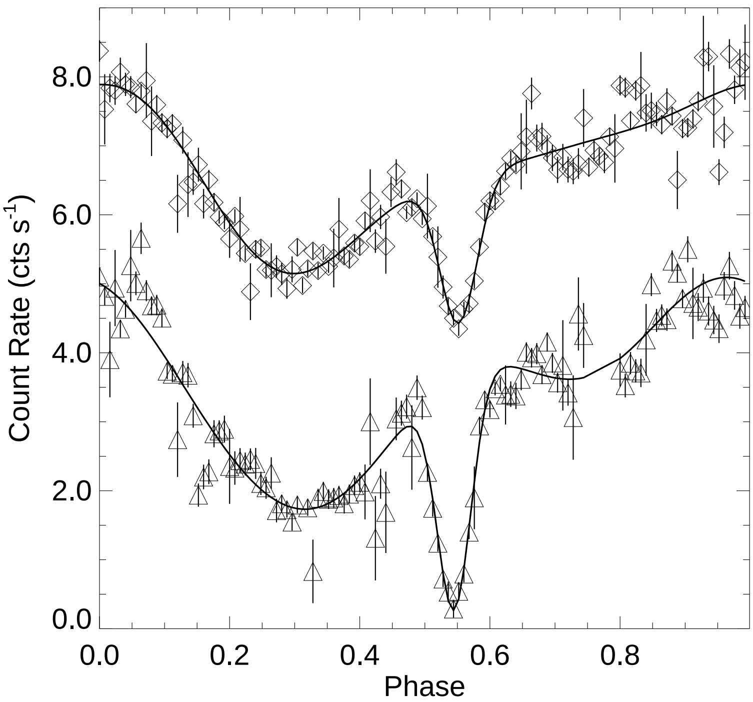

(Nowak et al., 1999)

Partial and broad eclipse from the LMXB 2A1822−371 as seen with ASCA.

Dips

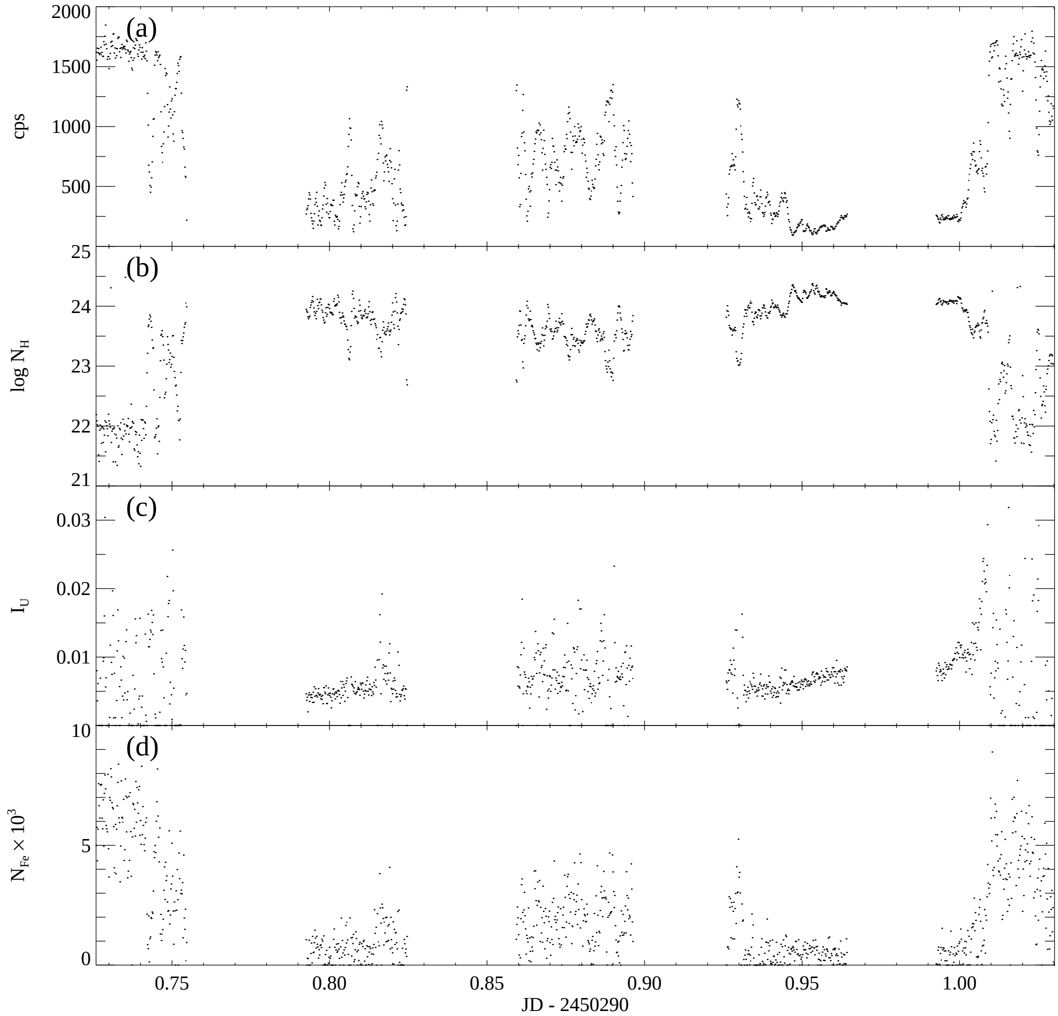

(Stelzer et al. (1999))

Temporal evolution of the absorbing column N_{H} with time over a pre-eclipse dip of Her X-1: Substructures as spray from impact of accretion stream onto disk.

Her X-1: 35 d cycle, I

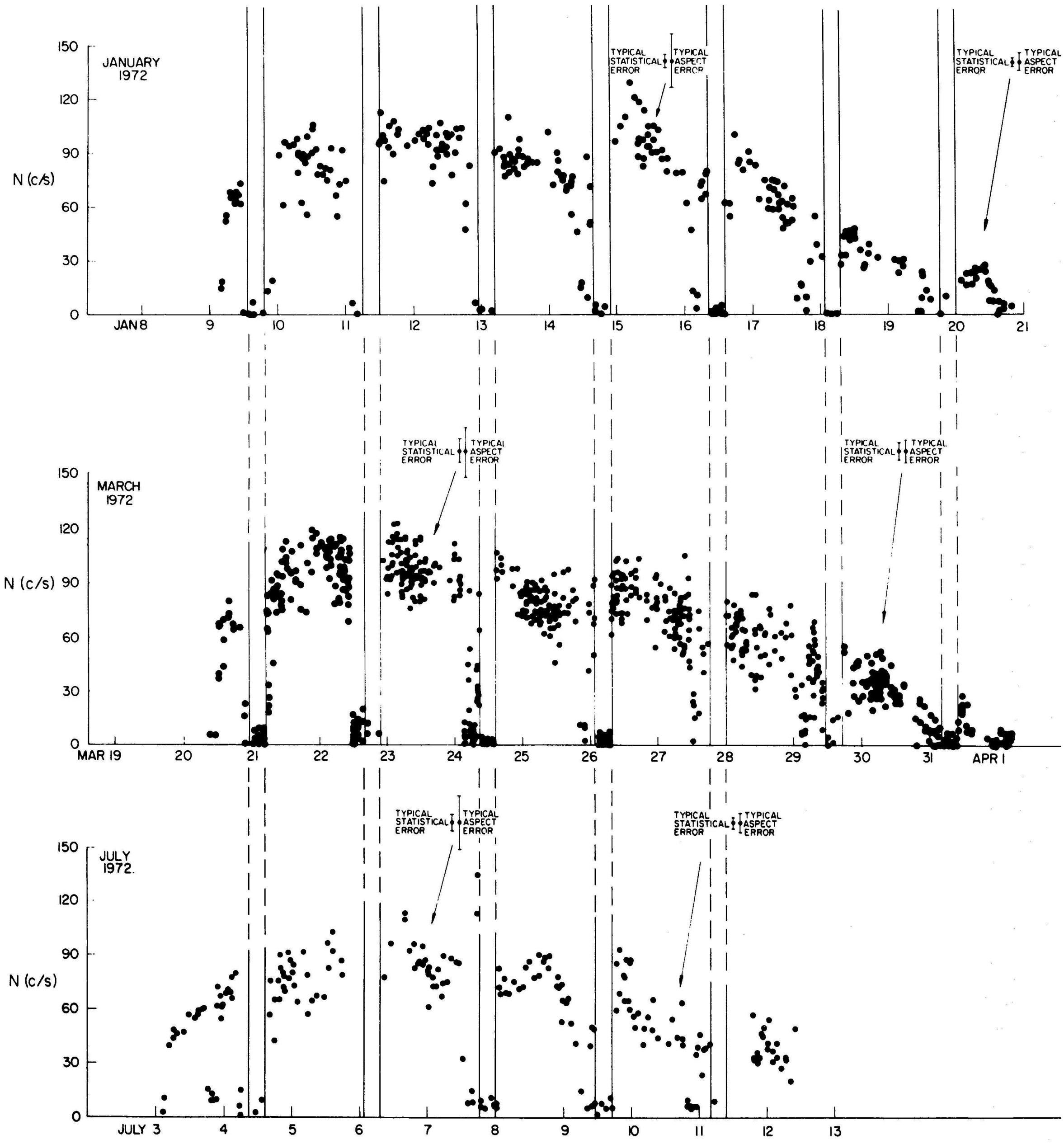

Giacconi et al. (1973)

Her X-1 shows “on” and “off” states with a periodicity of ∼35 d.

Her X-1: 35 d cycle, II

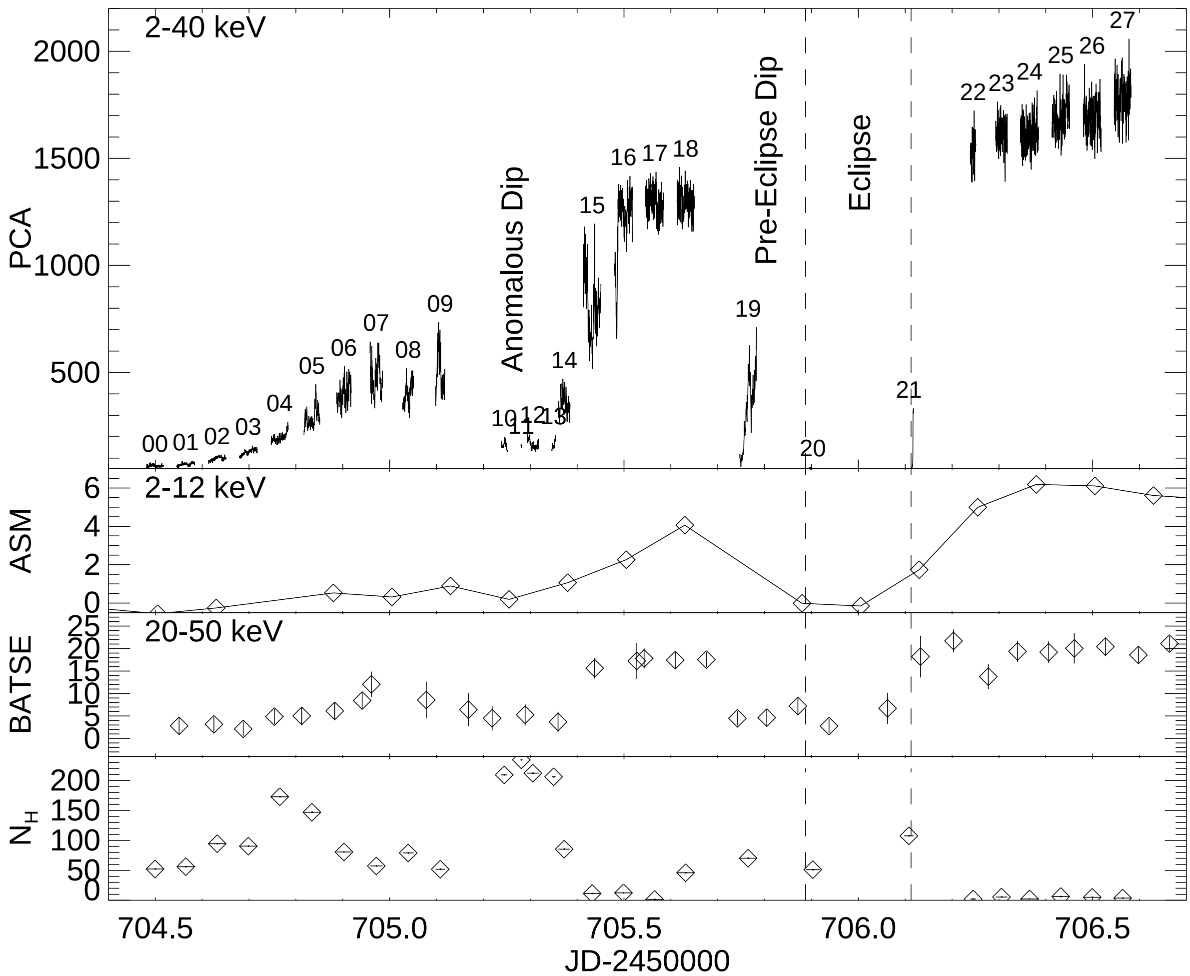

(Kuster et al., 1999)

Turn on of Her X-1 as observed with RXTE.

Absorbing column N_{H} decreases with time $\Longrightarrow$ Turn on caused by motion of covering accretion disk out of line of sight $\Longrightarrow$ Precessing warped disk.

Warped Disks

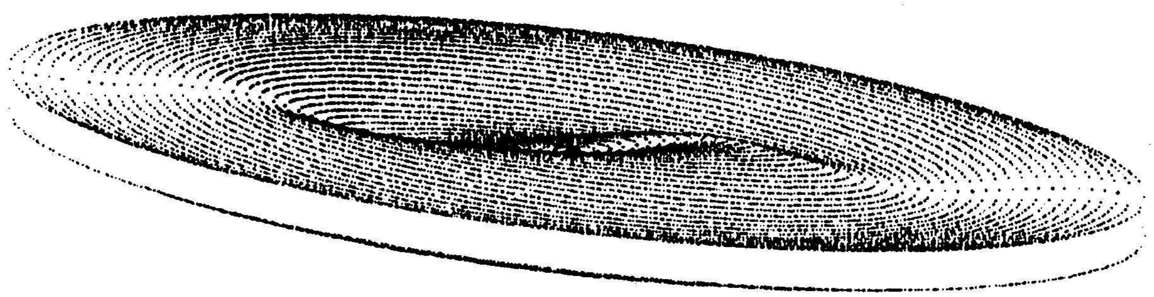

Schandl (1996)

What is the physical cause for the warping?

Torque perpendicular to plane of symmetry of disk.

Possible causes:

- Tidal torques (ruled out by precession frequency of disk).
- Wind due to X-ray heating of disk (Schandl, 1996),
- Radiation pressure (Maloney, Begelman & Pringle, 1996)

Evolution of pulse profi les, I

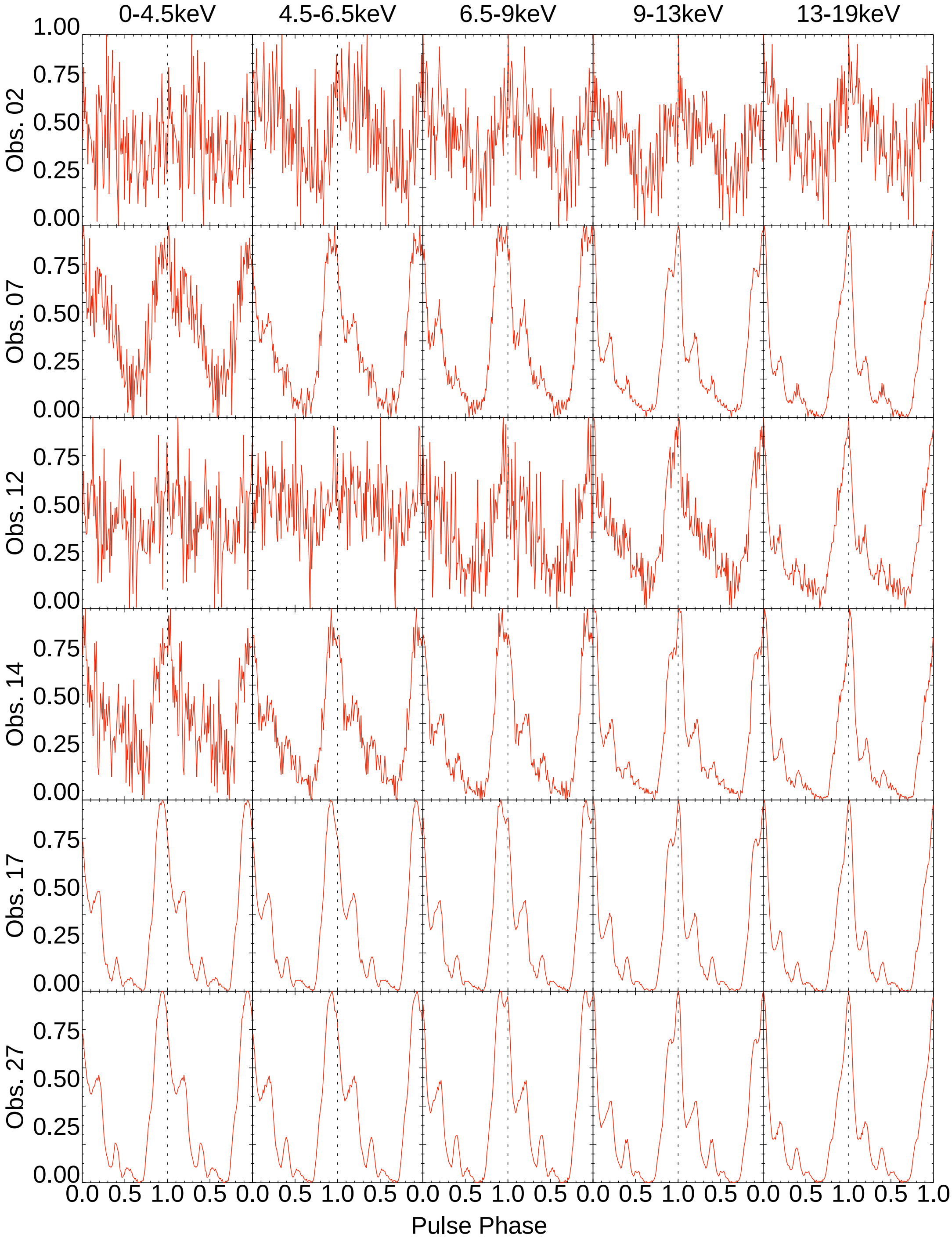

(Kuster et al., 1999)

Pulse profile does not change during start of main on.

Evolution of pulse profi les, II

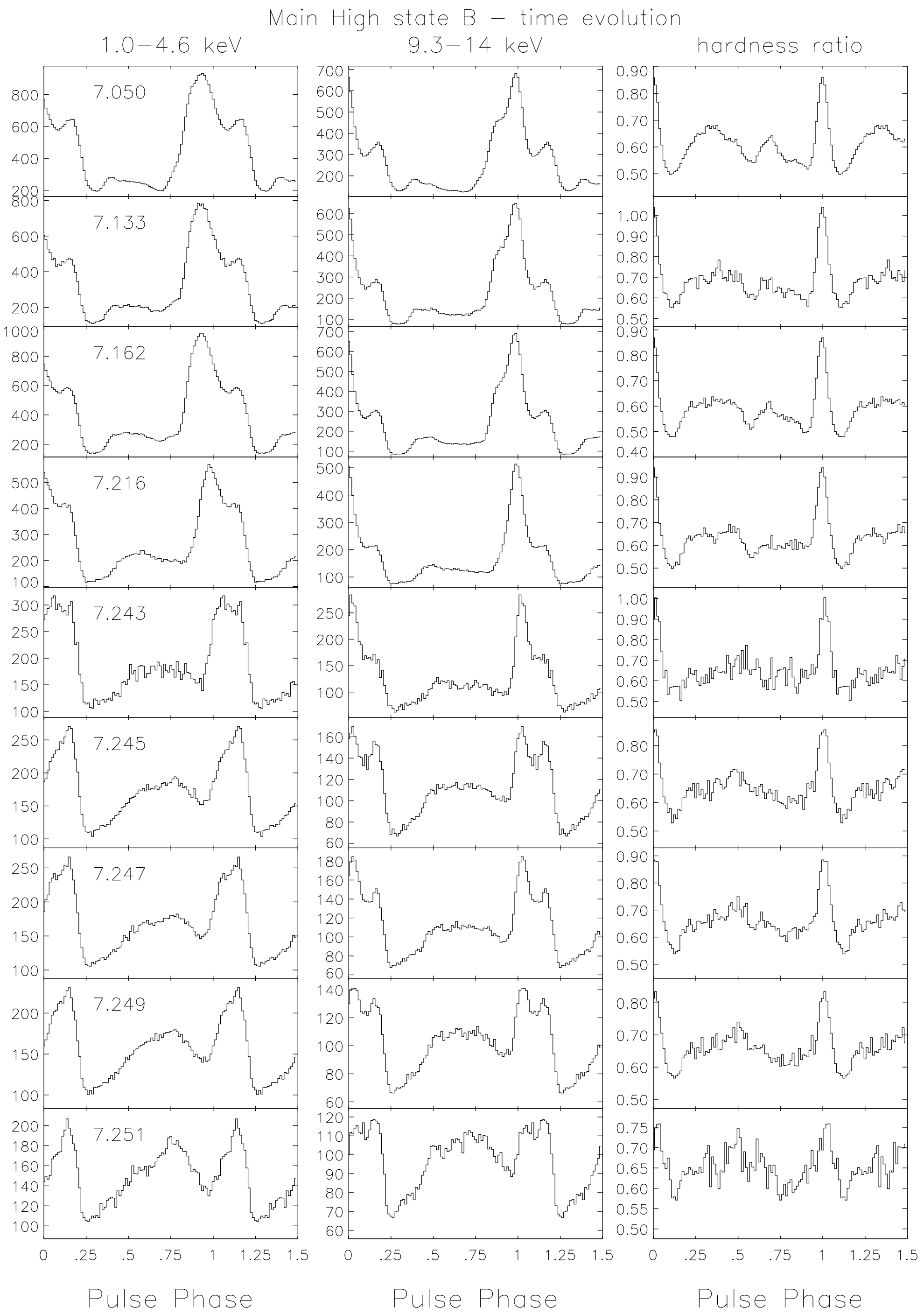

(Scott, priv. comm.)

Evolution of profile during main on.

Pulse profile does change

Explanation

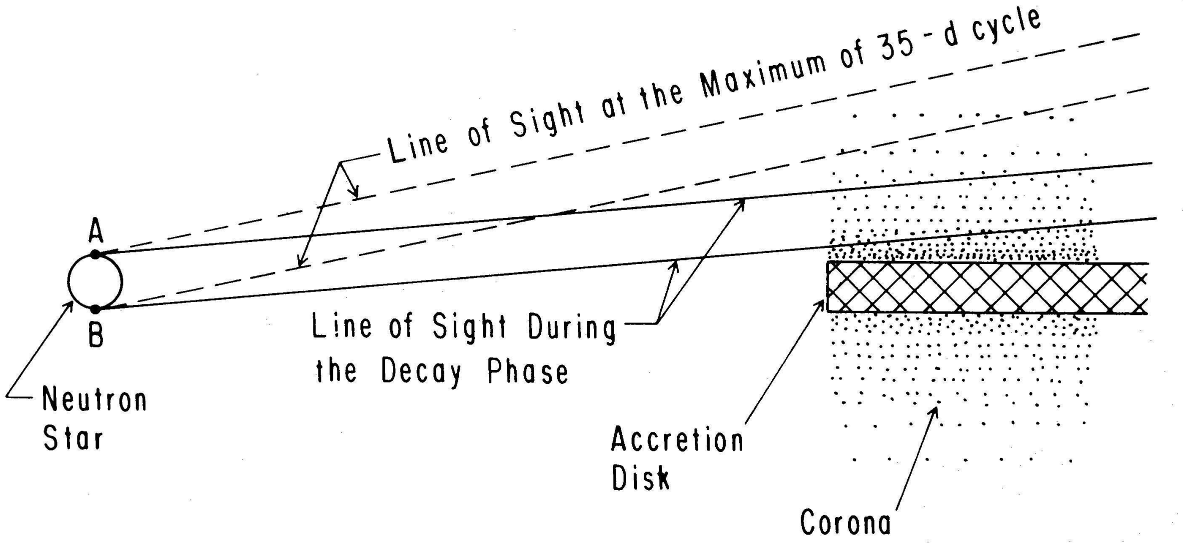

(Bai, 1981)

Evolution of pulse profile as evidence for covering: Begin of turn on: covering at outer radii, end of turn on: covering at inner radii (Note different scale heights!).

X-Ray Bursts, I

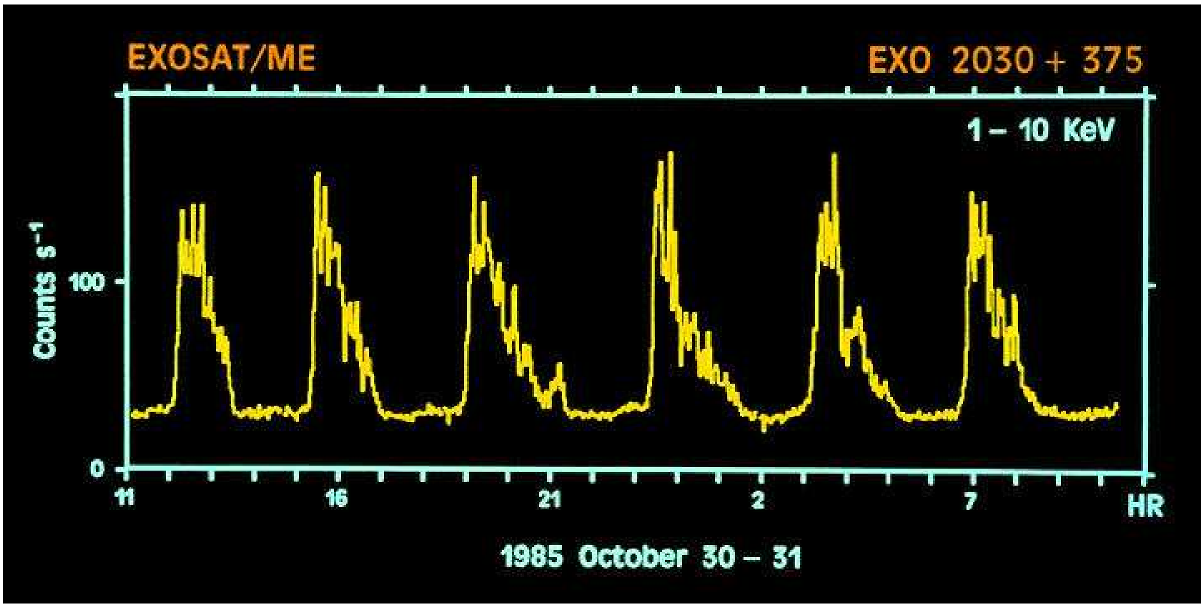

NASA GSFC

X-ray bursts from EXO 2030+375 as seen with EXOSAT.

Interpretation: Thermonuclear explosions on NS surface.

X-Ray Bursts, II

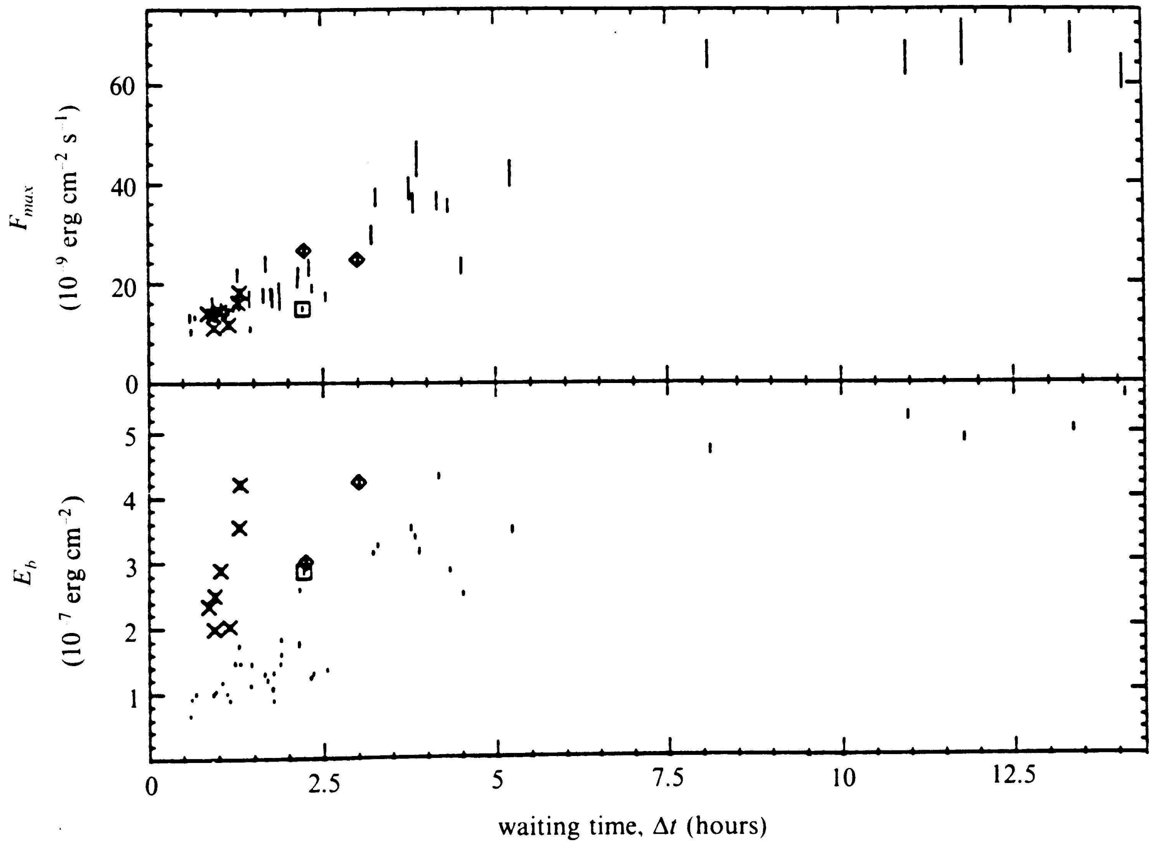

(Lewin et al., 1995, Fig. 4.10)

Peak flux and total fluence of bursts are correlated with distance to the next burst.

Explanation: Accretion of hydrogen onto surface $\Longrightarrow$ hydrogen burns quietly into helium (thickness of layer $\sim 1\,\mathrm{m}$) $\Longrightarrow$ thermonuclear flash when critical mass reached

Rapid Burster

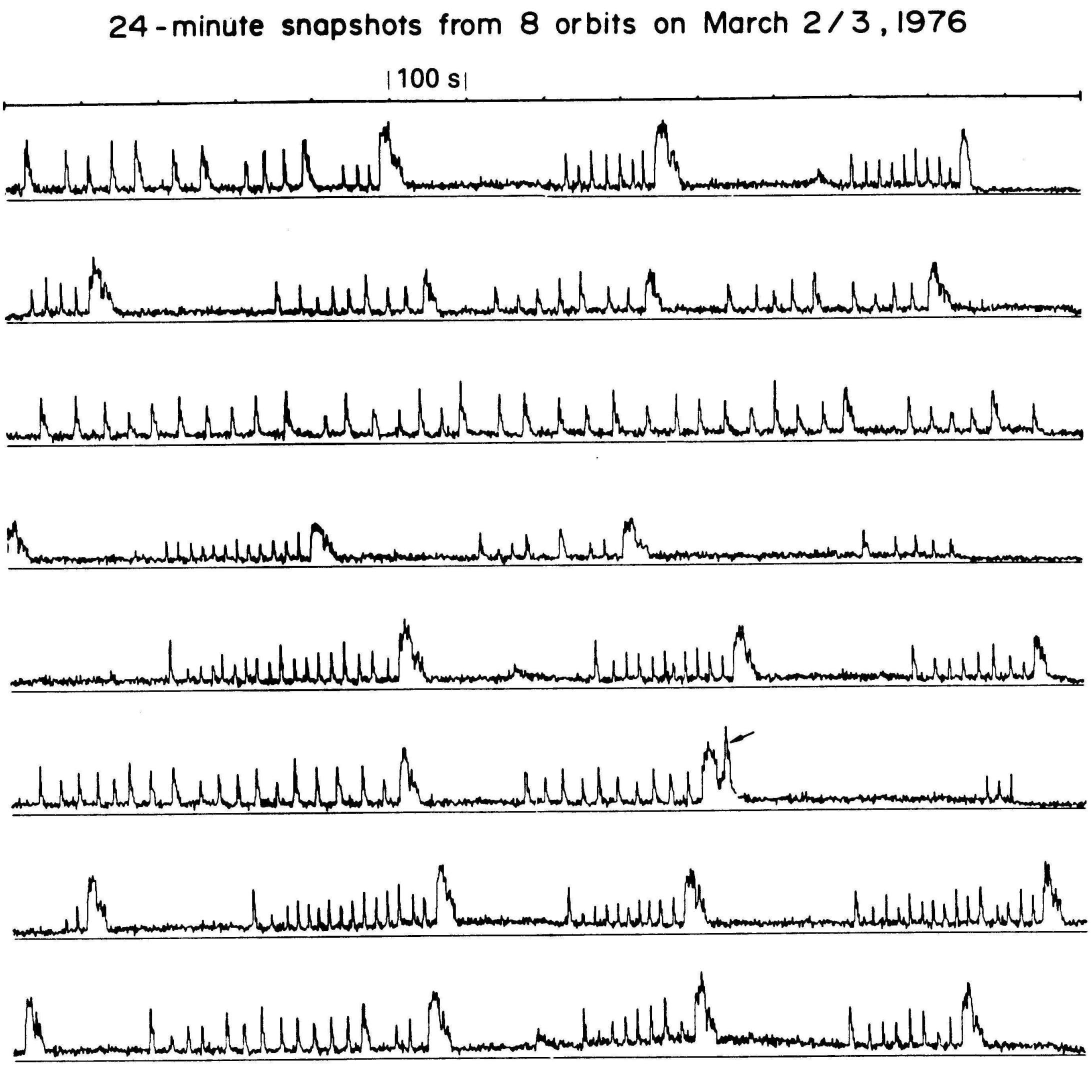

(Lewin et al., 1995, Fig. 4.19)

Bursting of the “Rapid Burster” 1730—-335: Type I and Type II bursts.

Type II bursts: magnetospheric gate model: B-fi eld blocks accretion until gas pressure $>$ magnetic pressure $\Longrightarrow$ BOOM.

Bursting Pulsar

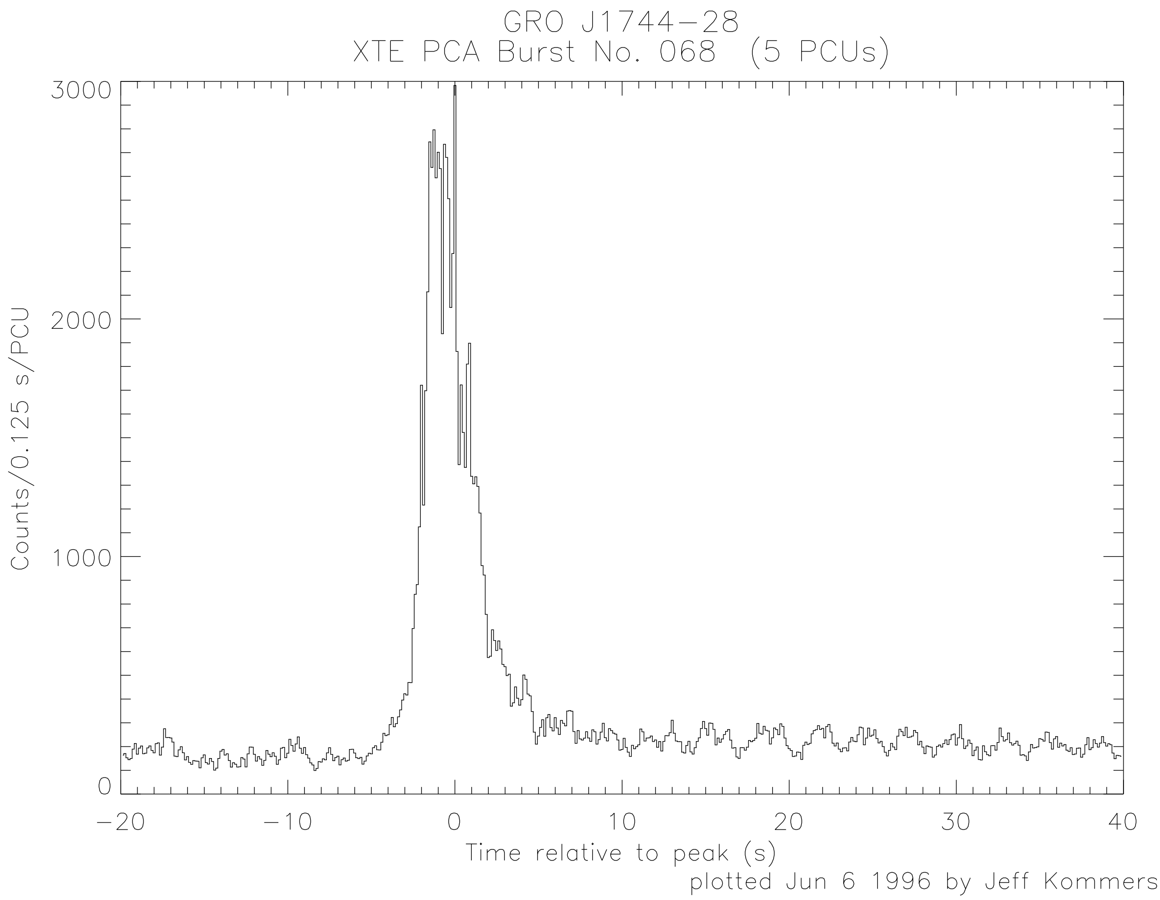

(Kommers, 1996, priv. comm.)

Before 1995 December 2: X-ray bursts and pulsations cannot occur in the same object. Then: GRO J1744-28 the bursting pulsar (see `http://space.mit.edu/home/rutledge/TRANS/trans.html`). Pulsations with 2 Hz *and* type II bursts. *Burst rate:* ∼ 20/hour, then decreasing to 1/hour. Source temporarily brightest X-ray source in the sky (several Crab), last outburst in June 1996. Orbit ∼ 2 d.

Physics not understood yet.

QPOs

Define the discrete Fourier transform as

$$X_j = \sum_{k=0}^{N-1} x_k e^{2\pi ijk/N} \quad \text{where } j \in [-(N/2) \dots (N/2) - 1] \tag{3.14}$$

for the frequencies

$$\omega_j = 2\pi\nu_j = 2\pi j/(N\Delta t) \tag{3.15}$$

($\nu_{N/2} = 1/(2\Delta t)$ = Nyquist frequency).
The power spectral density is

$$P_j = A|X_j|^2 \quad \text{where } j \in [0 \dots N/2] \tag{3.16}$$

A: Normalization constant. Often used:

- $A_{\text{Leahy}} = 2\Delta t^2/N_{\text{ph}} = 2\Delta t/X_0$ Leahy normalization
- $A_{\text{Miyamoto}} = 2\Delta t^2/(N_{\text{ph}}\langle x\rangle) = A_{\text{Leahy}}/\langle x\rangle$ Miyamoto normalization
- $A_{\text{math}} = 1/N$ (standard mathematical normalization).

where N_{ph}: number of photons observed.

QPOs

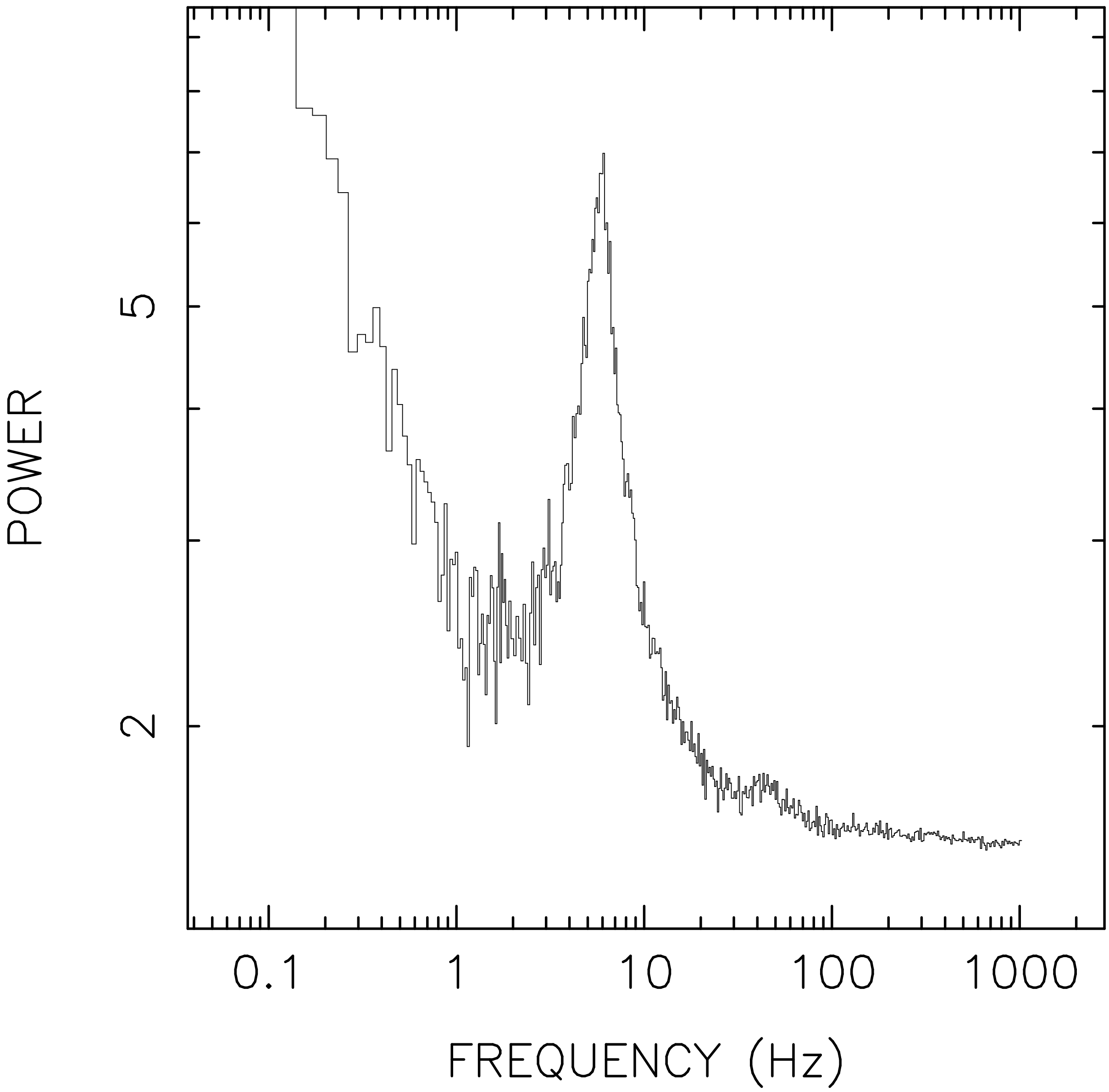

EXOSAT LMXBs have peaks in the PSD at low frequency; “quasi periodic oscillations”.

Explanation: Beat Frequency Model

IAAT

QPOs

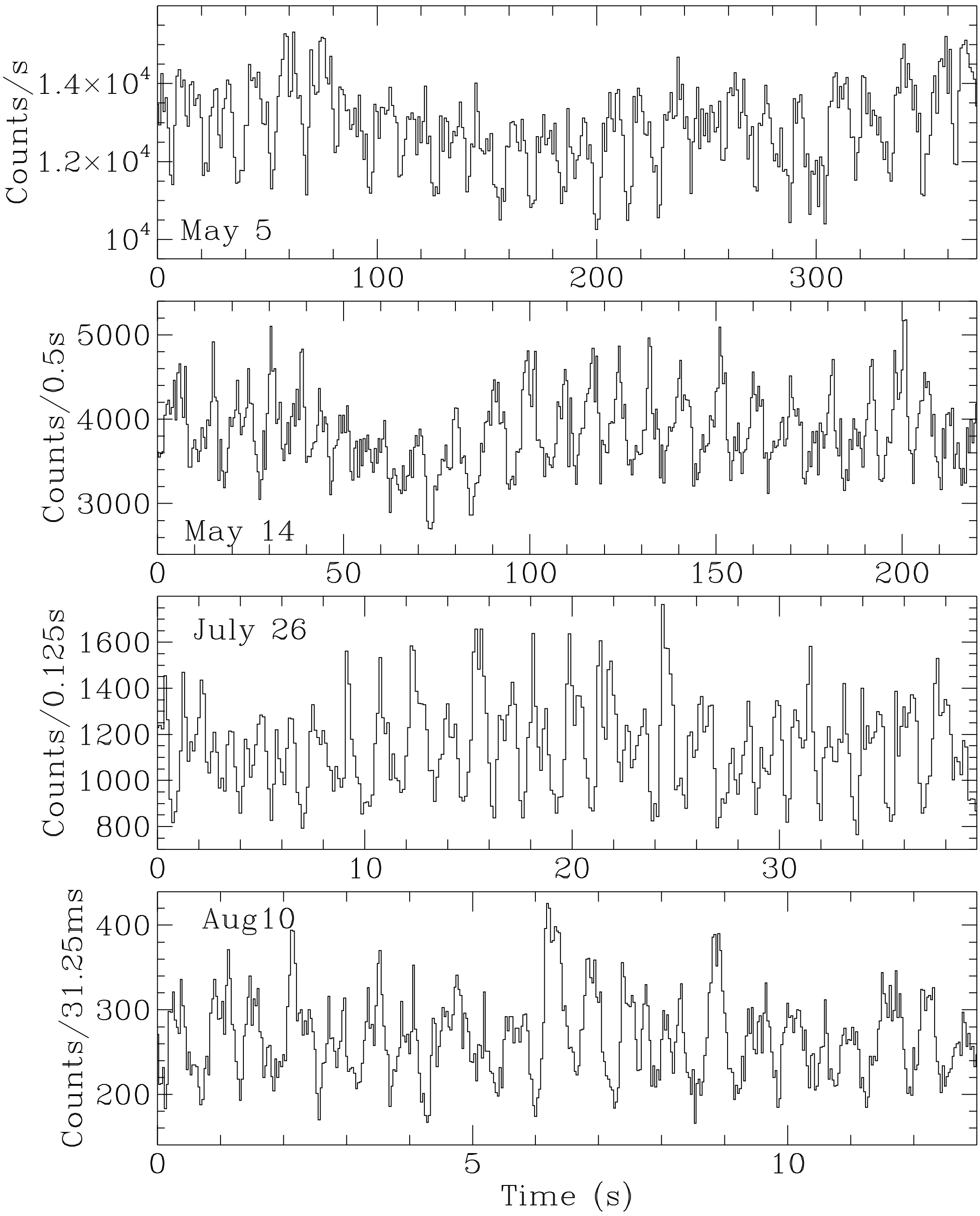

The Microquasar and BHC GRS 1915+105:

Morgan, Remillard, Greiner, 1997, *ApJ*, 482, 993

RXTE/PCA, 2–20 keV, 0.067, 0.114, 0.65, and 1.8 Hz

QPOs

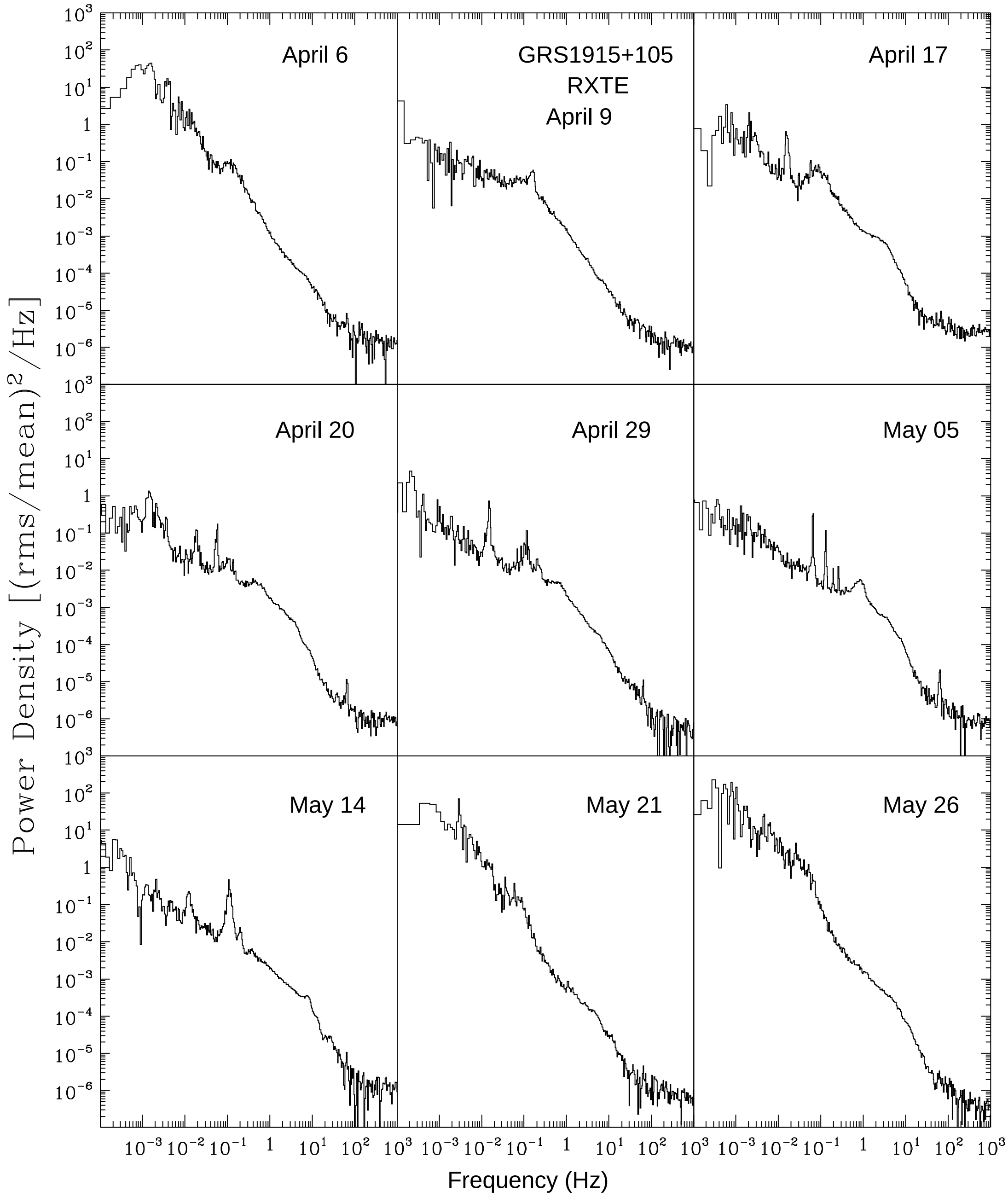

"center frequency": e.g., resonant frequency of Lorentzian

"relative rms amplitude": $\sqrt{\int \text{QPO}\,\mathrm{d}\nu}$,

above: $\text{rms}_{67} = 0.5 - 1.6\,\%$

"Q-value": $\nu_{\text{center}}/\Delta\nu_{\text{FWHM}}$,

above: $Q_{67} \approx 20$

QPOs

"The kHz QPO are the most important scientific result to date of RXTE".
(http://heasarc.gsfc.nasa.gov/docs/xte/Greatest_Hits/khz.qpo.html)

RXTE PCA: $\Delta E = $ 2-25 keV, $A_{\text{eff}} = $ 5000 cm^2, $\Delta t = 1\,\mu$s

Sco X-1

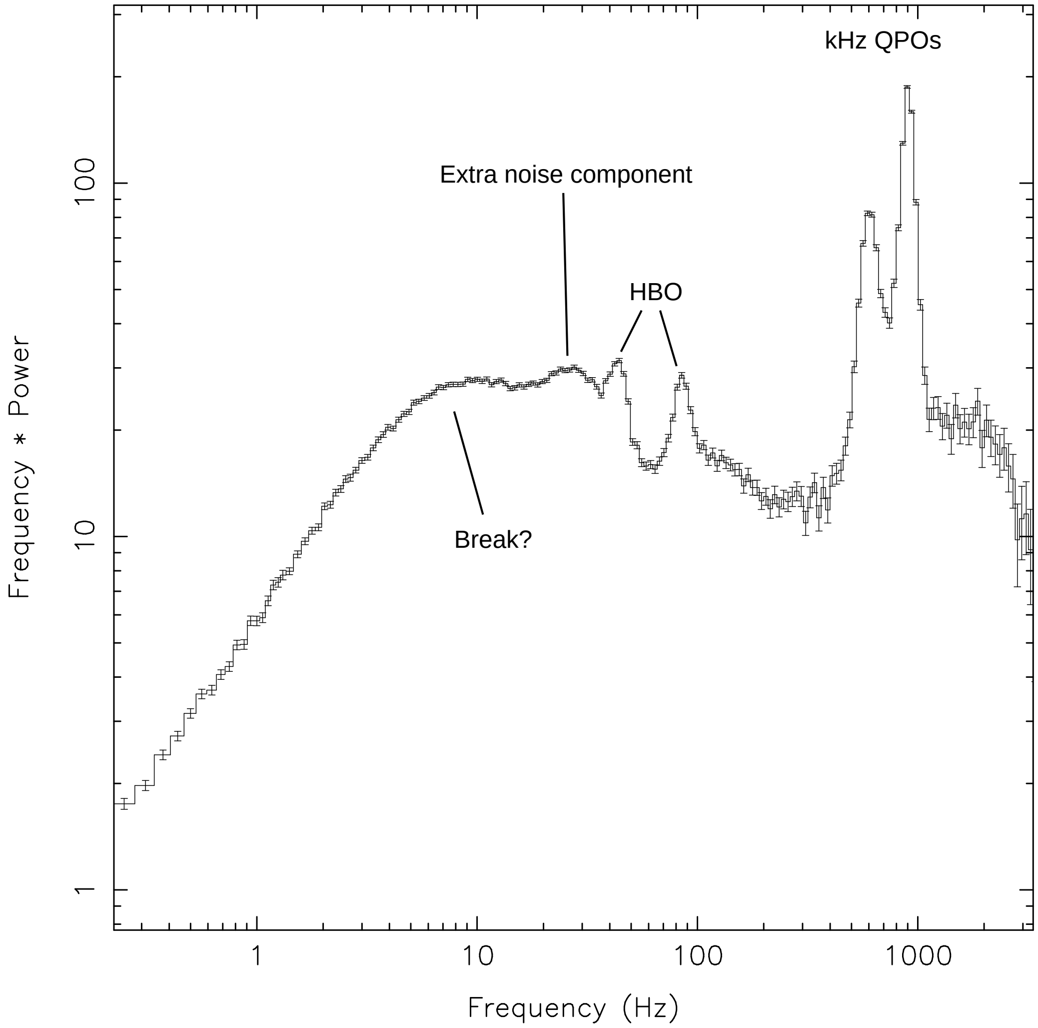

van der Klis et al., 1996, IAUC 6319 Wijnands & van der Klis, 1999, *ApJ*, 514, 939

QPOs

- >3 characteristic frequencies:
  "LF QPOs" (ν_{LF}): $0.1 - 100$ Hz, many types
  "kHz Twin Peaks" (ν_1, ν_2): $200 - 1400$ Hz
- "real" kHz QPOs only for neutron star binaries, mostly persistent LMXBs (but: Microquasars!), $\sim$ 20 kHz QPO sources are known, mostly showing double peaks
- Keplerian orbit frequency:

$$\nu_{\text{orb}} = \left(\frac{GM}{4\pi^2 R_{\text{orb}}^3}\right)^{1/2} \approx 1200\,\text{Hz} \left(\frac{R_{\text{orb}}}{15\,\text{km}}\right)^{-3/2} m_{1.4}^{1/2}$$

- innermost stable circular orbit (ISCO), Schwarzschild geometry:
  $R_{\text{ISCO}} = 6GM/c^2 \approx 12.5 m_{1.4}$ km
  $\Longrightarrow$ maximum stable frequency:
  $\nu_{\text{ISCO}} \approx (1580/m_{1.4})$ Hz
- spin corrections can be several 10%

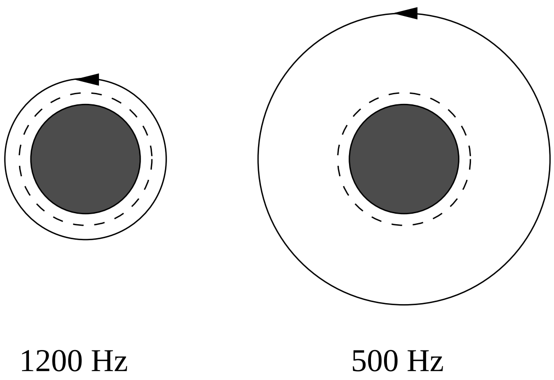

IAAT

QPOs

beat: preferred Keplerian orbit & spin frequency

Magnetospheric BFM:

- preferred radius = Alfvén radius
- orbiting clump ($\nu_{\text{Alfvén}}$)
  modulated by B-field (ν_{spin})

$\Longrightarrow$ can explain LF QPOs, $5 - 50\,\text{Hz}$

Sonic Point BFM:

- preferred radius = where radial inflow velocity becomes supersonic, near ISCO
- orbiting clump ($\nu_{\text{sonic}} > \nu_{\text{spin}}$)
  is causing bright footpoint near surface,
  footpoint: upper kHz QPO, $\nu_2 = \nu_{\text{sonic}}$
- clumps are irradiated with $\nu_{\text{spin}} \longrightarrow$
  footpoint emission is modulated with beat between ν_{sonic} and ν_{spin},
  footpoint modulation: lower kHz QPO,
  $\nu_1 = \nu_{\text{beat}}$

$\Longrightarrow$ can explain twin kHz QPOs but ...

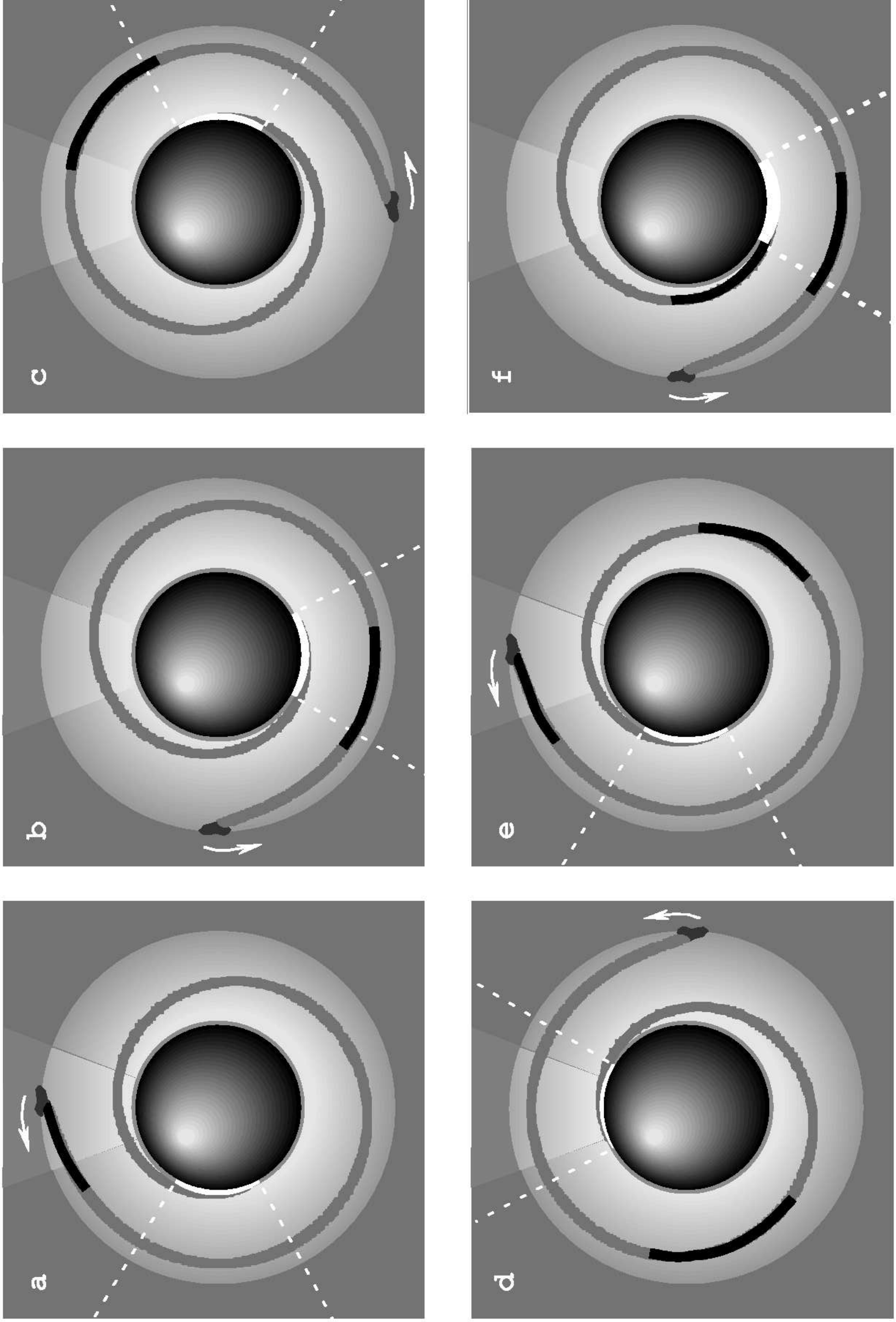

Miller et al., 1998, *ApJ*, 508, 791

QPOs

Varying frequency separation between the kHz QPOs of different sources:

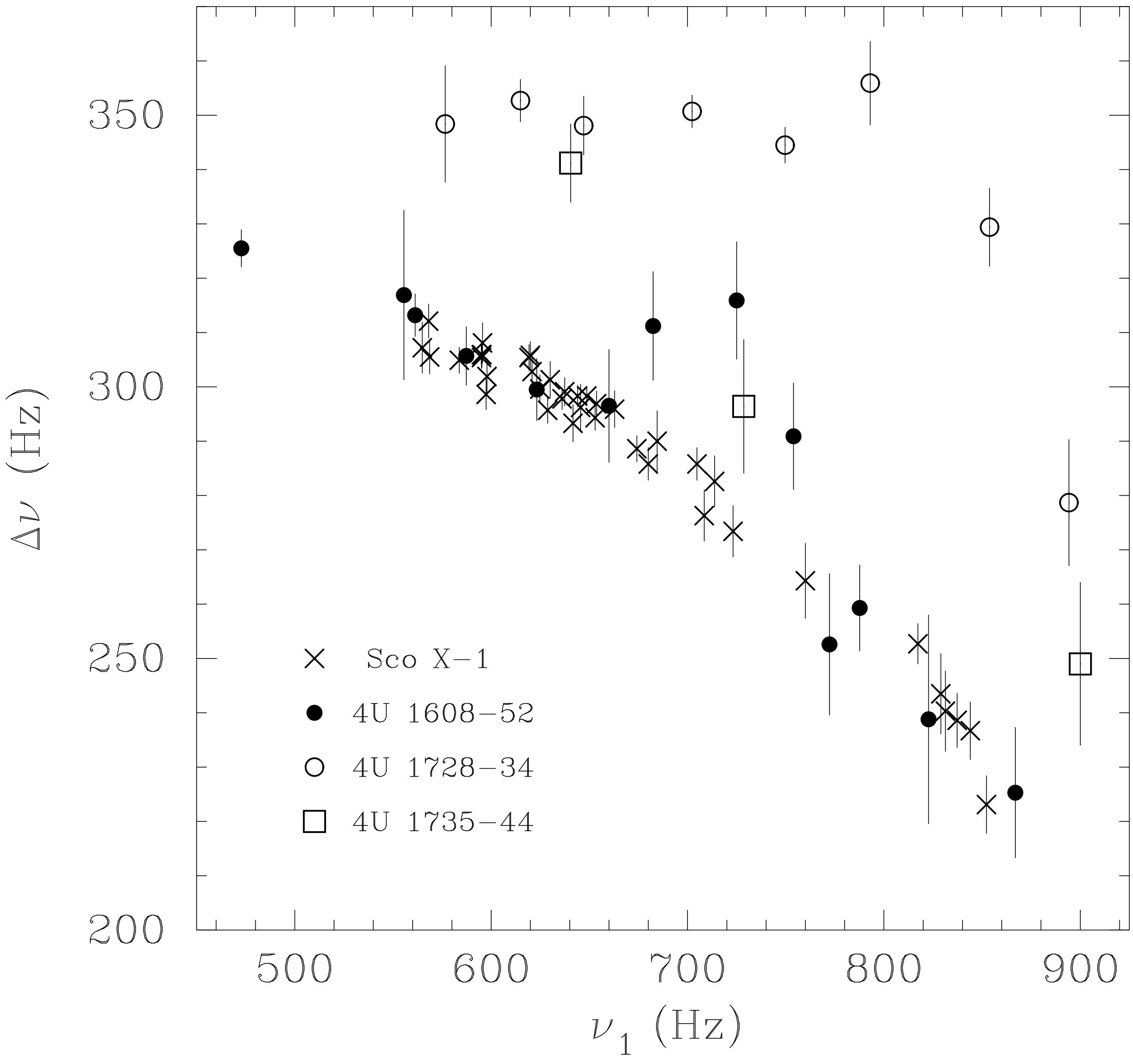

van der Klis, 2000, *ARA&A*, 38, 717

QPOs

Properties & problems of the SPBFM:

- needs surface
  $\Longrightarrow$ not valid for BHC sources
- Keplerian motion inside $r_{\text{Alfvén}}$
- r_{sonic} is depending on $\dot{M}$
  $\Longrightarrow$ varying ν_2 can be explained
- $\Delta\nu = \nu_2 - \nu_1$, constant, can be $< \nu_{\text{spin}}$
  $\Longrightarrow$ varying $\Delta\nu$ cannot easily be explained
- predicts additional frequencies (differing from precession model)

QPOs

Relativistic Precession Model

GR: free-particle orbits show characteristic frequencies

- disk is disrupted near ISCO, forming blobs
- blob orbits are inclined and eccentric

- orbit frequency: upper kHz QPO, ν_2
- periastron precession: lower kHz QPO, ν_1
- relativistic frame dragging $\longrightarrow$ "wobble of the orbital plane": nodal precession (Lense-Thirring)

  $\nu_{\text{LF}} = 2 \times \nu_{\text{nod}}$

  $\nu_{\text{nod}} = 8\pi^2 I \, \nu_2^2 \nu_{\text{spin}} / c^2 M,$

  (I: moment of inertia)

Stella & Vietri, 1998, *ApJ*, 492, L59

Vietri & Stella, 1998, *ApJ*, 503, 350

QPOs

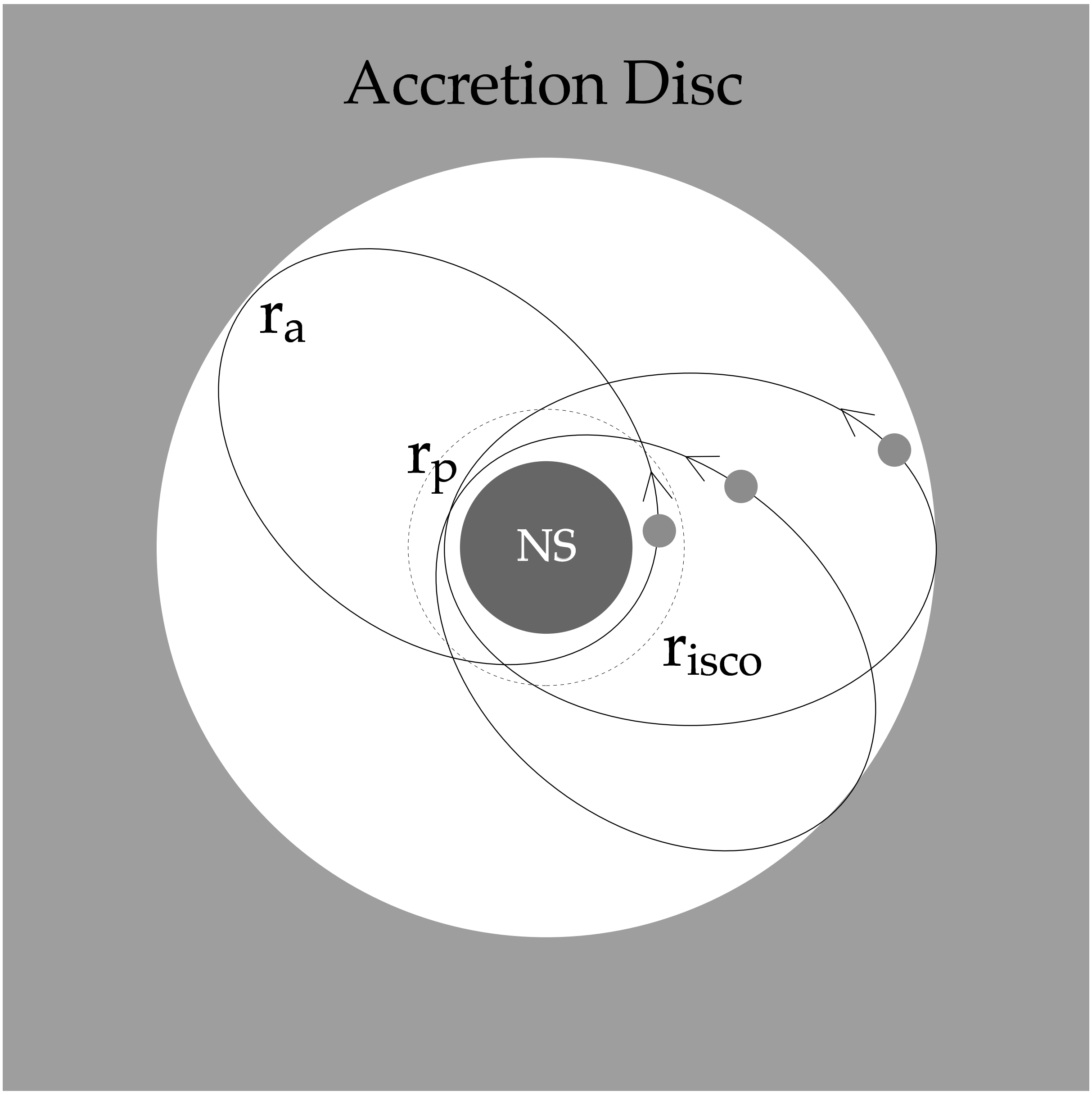

Marković & Lamb, 2000, astro-ph/0009169

QPOs

Varying frequency separation between the kHz QPOs of different sources:

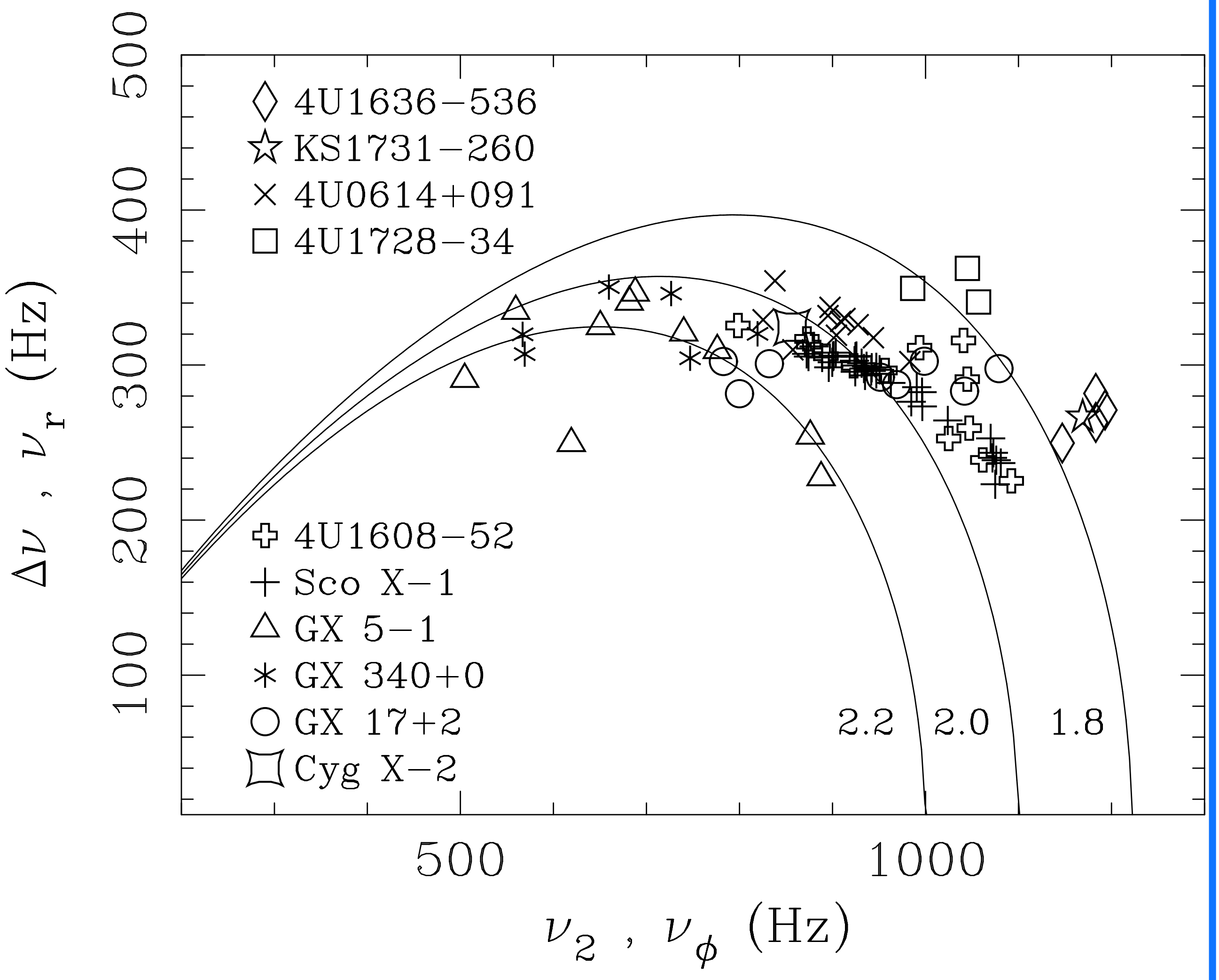

Stella & Vietri, 1999, *Phys. Rev. Lett.*, 82, 17

QPOs

Properties & problems of the RPM:

- does not need surface
  $\Longrightarrow$ also valid for BHC sources
- can explain $\Delta\nu$ (more or less)
- how to disrupt the disk?
  how to create compact clumps?
  how to maintain tilted orbits?
- how to create the flux modulations?
- other frequencies could be more important

QPOs

Promises:

- constrain M and R (via kHz QPOs)
  $\Rightarrow$ constrain EOS for neutron stars
- constrain spin
  ("holy grail", LMXB/ms radio pulsar evolution?!)
- constrain B-field (via LF QPOs)
- observe GR effects

Difficulties:

- observations (varying $\Delta\nu_{\text{kHz}}$, ν-correlations) triggered evolution of many different models ($>$ 12)
- no individual model does address all issues (i.e, generation of flux modulation, . . .)
- models predict different ν_{spin} and M, e.g.,
  BFM: $\nu_{\text{spin}} = 250 - 350$ Hz
  RPM: $\nu_{\text{spin}} = 300 - 900$ Hz
- what about "surface models"? $\Longleftrightarrow$
  big question:
  do BHCs show the same behavior as neutron star XRBs?

High-Mass XRB

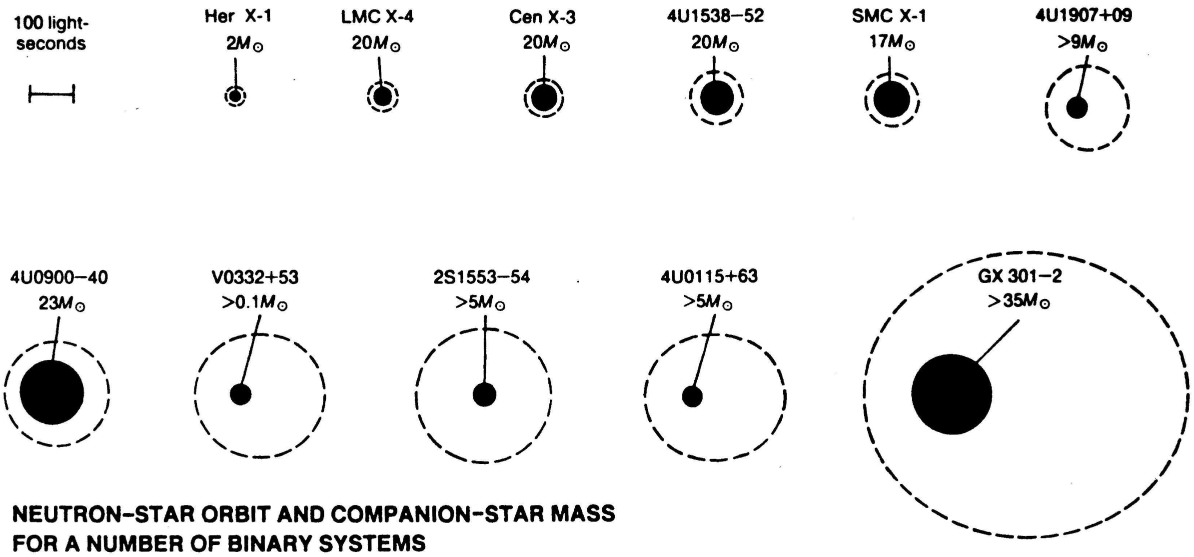

Charles and Seward, Fig. 7.7a

High-Mass X-ray Binaries: Donor star has early spectral type (O, B), and mass $M \gtrsim 10\,M_\odot$.

Dominant accretion mechanisms: Wind Accretion or Accretion Disk. Optical emission dominated by O or B star.

HMXB: System Parameters, I

Table 1.3. *The orbital periods of HMXBs*

Source	Alternative name	Orbital period (d)	Properties[a]	Reference
X2030+407	Cyg X−3	0.2	WR	1,2,3
X0532−664	LMC X−4	1.4	SG, P	4,5,6
X0538−641	LMC X−3	1.7	Be, BHC	7
X1119−603	Cen X−3	2.1	SG, P	8
X1700−377	HD153919	3.41	SG	9
X1538−522	QV Nor	3.73	SG, P	10,11
X0115−737	SMC X−1	3.89	SG, P	12
X0540−697	LMC X−1	4.22	SG, BHC	13
X1956+350	Cyg X−1	5.6	SG, BHC	14
X1907+097		8.38	B, P	15
X0900−403	Vela X−1	8.96	SG, P	16
X1657−415		10.4	SG?, P	17
X0114+650	V662 Cas	11.6	SG	18
X1909+048	SS433	13.1	SG, J	19
X0535−668	A0538−66	16.7	Be, T, P	20
X0115+634	V635 Cas	24.3	Be, T, P	21
X0236+610	LS I +61 303	26.45	Be	22
X1553−542		30.6	Be?, T, P	23
X0331+530	BQ Cam	34.25	Be, T, P	24
X1223−624	GX301−2	41.5	SG, P	25,26,27
X2030+375		45–47	Be, T, P	28
X0535+262	HD245770	111	Be, T, P	29
X1258−613	GX304−1	133?	Be, P	30
X1145−619	Hen 715	187.5	Be, P	31

[a]The source properties are indicated by 'SG' - supergiant, 'Be' - Be star, 'P' - pulsar, 'BHC' - black-hole candidate, 'T' - transient, 'WR' - Wolf–Rayet, 'J' - Jets.

References: [1]Parsignault *et al.* 1972; [2]Sanford & Hawkins 1972; [3]van Kerkwijk *et al.* 1992; [4]Li *et al.* 1978; [5]White 1978; [6]Chevalier & Ilovaisky 1977; [7]Cowley *et al.* 1983; [8]Schreier *et al.* 1972b; [9]Jones, Forman and Liller 1973; [10]Becker *et al.* 1977; [11]Davison, Watson and Pye 1977; [12]Schreier *et al.* 1972b; [13]Hutchings *et al.* 1983; [14]Webster & Murdin 1972; [15]Marshall & Ricketts 1980; [16]Ulmer *et al.* 1972; [17]Chakrabarty *et al.* 1993; [18]Crampton *et al.* 1985; [19]Crampton *et al.* 1980; [20]Johnston, *et al.* 1980; [21]Rappaport *et al.* 1978; [22]Taylor & Gregory 1982; [23]Kelley *et al.* 1983b; [24]Stella *et al.* 1985; [25]Watson *et al.* 1982; [26]Kelley *et al.* 1980; [27]White *et al.* 1978; [28]Parmar *et al.* 1989c,d; [29]Priedhorsky & Terrell 1983a; [30]Priedhorsky & Terrell 1983b; [31]Watson *et al.* 1981.

White et al., 1995, Tab. 1.3

HMXB: System Parameters, II

Table 1.4. *Pulse periods from X-ray binaries*

Source	Alternative name	Pulse period (s)	Orbital period (d)	Type	Reference
X0535−668	A0538−66	0.069	16.7	HMXB	1
X0115−737	SMC X−1	0.71	3.89	HMXB	2
X1656+354	Her X−1	1.24	1.7	LMXB	3
X0115+634	V635 Cas	3.6	24.3	HMXB	4
X0332+530	BQ Cam	4.4	34.25	HMXB	5
X1119−603	Cen X−3	4.8	2.1	HMXB	6
X1048−594		6.4		?	7
X2259+587		7.0		LMXB	8
X1627−673		7.7	0.029	LMXB	9
X1553−542		9.3	30.6	HMXB	10
X0834−430	GR0834−430	12.2	-	?	11
X0532−664	LMC X−4	13.5	1.4	HMXB	12
X1417−624		17.6		HMXB	13
X1843+009		29.5		?	14
X1657−415		38	10.4	HMXB	15
X2030+375		42	45.6	HMXB	16
X2138+568	Cep X−4	66		?	17
X1836−045		81		?	14
X1843−024		95		?	14,34
X0535+262		104	111	HMXB	18
X1833−076	Sct X−1	111		?	19
X1728−247	GX1+4	114	304?	LMXB	20,21,22
X0900−403	Vela X−1	283	8.96	HMXB	23
X1258−613	GX 304−1	272	133?	HMXB	24,25
X1145−614		298		HMXB	26,27
X1145−619		292	187.5	HMXB	26,27
X1118−615	A1118−61	405		HMXB	28
X1722−363		413		?	29
X1907+097		438	8.38	HMXB	30
X1538−522	QV Nor	529	3.73	HMXB	31
X1223−624	GX301−2	696	41.5	HMXB	32
X0352−309	X Per	835		HMXB	33

References: [1]Skinner *et al.* 1982; [2]Lucke *et al.* 1976; [3]Tananbaum *et al.* 1972; [4]Cominsky *et al.* 1978; [5]Stella *et al.* 1985; [6]Giacconi *et al.* 1971; [7]Corbet & Day 1990; [8]Gregory & Fahlman 1980; [9]Rappaport *et al.* 1977; [10]Kelley *et al.* 1983b; [11]Grebenev & Sunyaev 1991; [12]Kelley *et al.* 1983a; [13]Kelley *et al.* 1981; [14]Koyama *et al.* 1990a; [15]White & Pravdo 1979; [16]Parmar *et al.* 1989d; [17]Koyama *et al.* 1991a; [18]Rosenberg *et al.* 1975; [19]Koyama *et al.* 1991b; [20]Lewin *et al.* 1971; [21]White *et al.* 1976a; [22]Strickman *et al.* 1980; [23]McClintock *et al.* 1976; [24]Huckle *et al.* 1977; [25]McClintock *et al.* 1977; [26]White *et al.* 1978b; [27]Lamb *et al.* 1980; [28]Ives *et al.* 1975; [29]Tawara *et al.* 1989; [30]Makishima *et al.* 1984; [31]Davison *et al.* 1977; [32]White *et al.* 1976a; [33]White *et al.* 1976b; [34]Koyama *et al.* 1990b.

White et al., 1995, Tab. 1.4

X-rays probing stellar winds, I

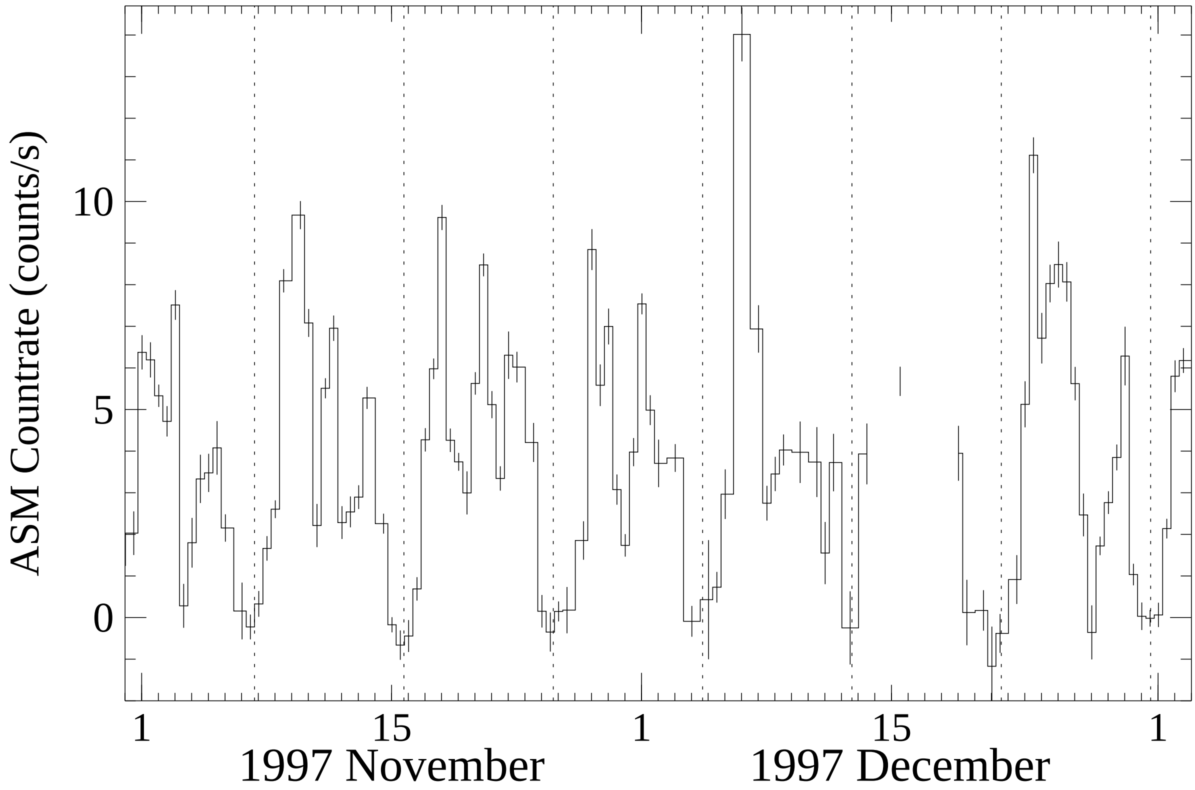

RXTE All Sky Monitor lightcurve of Vela X-1: Eclipses at dotted lines. Note rapid variability of long-term lightcurve $\Longrightarrow$ Can be traced to variations of absorbing column along line of sight.

IAAT

X-rays probing stellar winds, II

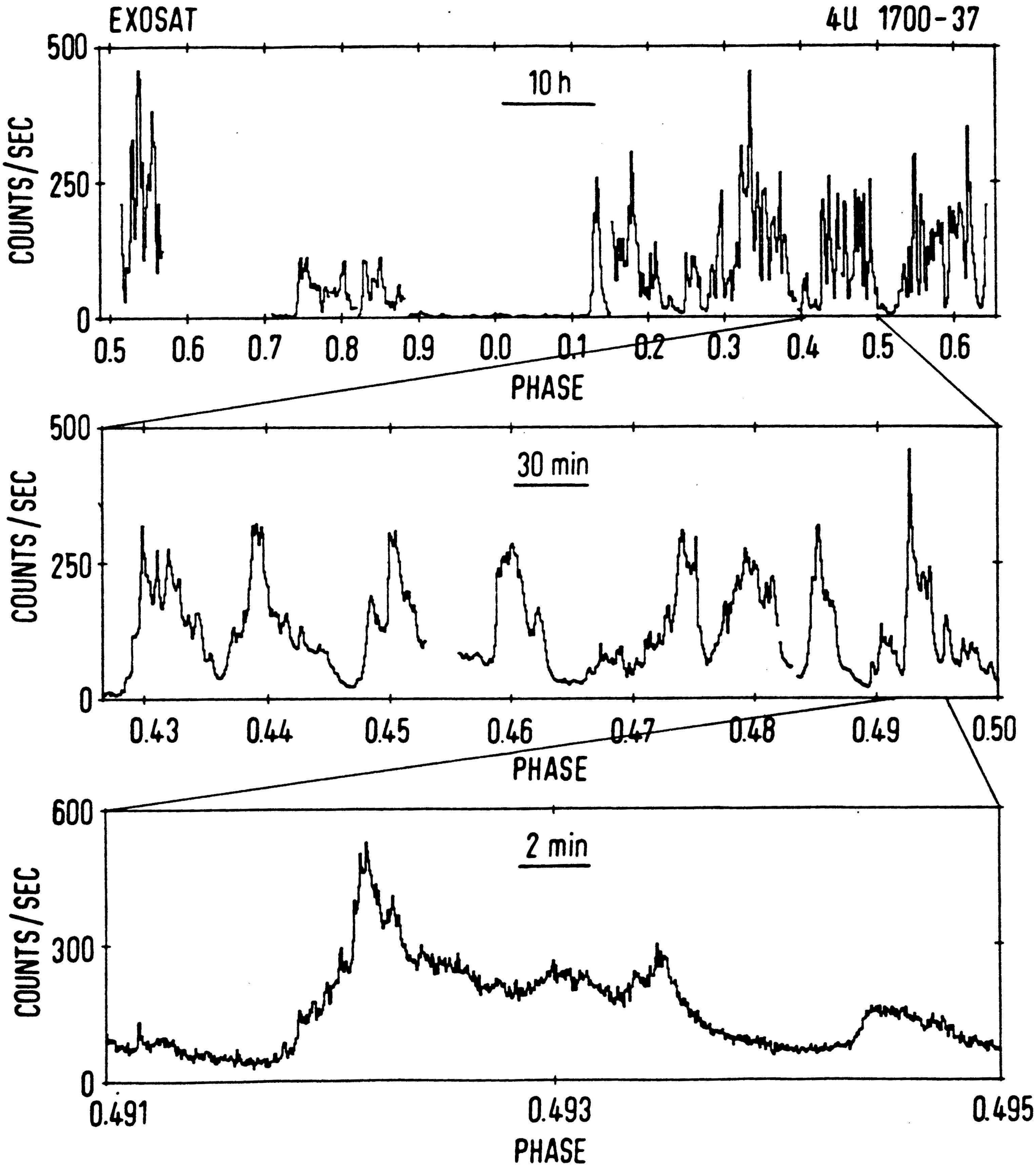

Violent X-ray absorption on all timescales in the wind accreting system 4U 1700−377.

Charles & Seward, Fig. 7.12

Magnetospheric Accretion, I

So far: ignored fact that central neutron star has (strong) magnetic field ($\sim 10^{12}$ G). Far-field:

$$B(r) = \left(\frac{R_\star}{r}\right)^3 B_\mathrm{p} \quad \text{hence} \quad P_\mathrm{mag} = \frac{B^2}{8\pi} = \left(\frac{R}{r}\right)^6 B_\mathrm{p}^2 \qquad (3.17)$$

On the other hand, the accreting material has a ram-pressure

$$P_\mathrm{ram} = \rho \mathrm{v}^2 \quad \text{or} \quad P_\mathrm{ram} = \frac{\dot{M}}{4\pi r^2}\left(\frac{2GM}{r}\right)^{1/2} \qquad (3.18)$$

assuming free fall ($\mathrm{v} = (2GM/r)^{1/2}$) and spherical symmetry ($\dot{M} = 4\pi r^2 \rho \mathrm{v}$).

For $P_\mathrm{mag} > P_\mathrm{ram}$, magnetic field dominates $\Longrightarrow$ plasma couples to magnetic field lines at the Alfvén radius

$$r_\mathrm{mag} = \left(\frac{8\pi^2}{G}\right)^{1/7} \left(\frac{R_\star^{12} B_\mathrm{p}^4}{M\dot{M}^2}\right)^{1/7} \qquad (3.19)$$

For $R_\star = 10$ km, $B = 10^{12}$ G, $M = 1.4\,M_\odot$, and $\dot{M} = 10^{-8}\,M_\odot/\mathrm{a}$, $r_\mathrm{mag} \sim 3500$ km.

For typical NS parameters, the accretion close to the NS is completely dominated by the magnetic field.

Magnetospheric Accretion, II

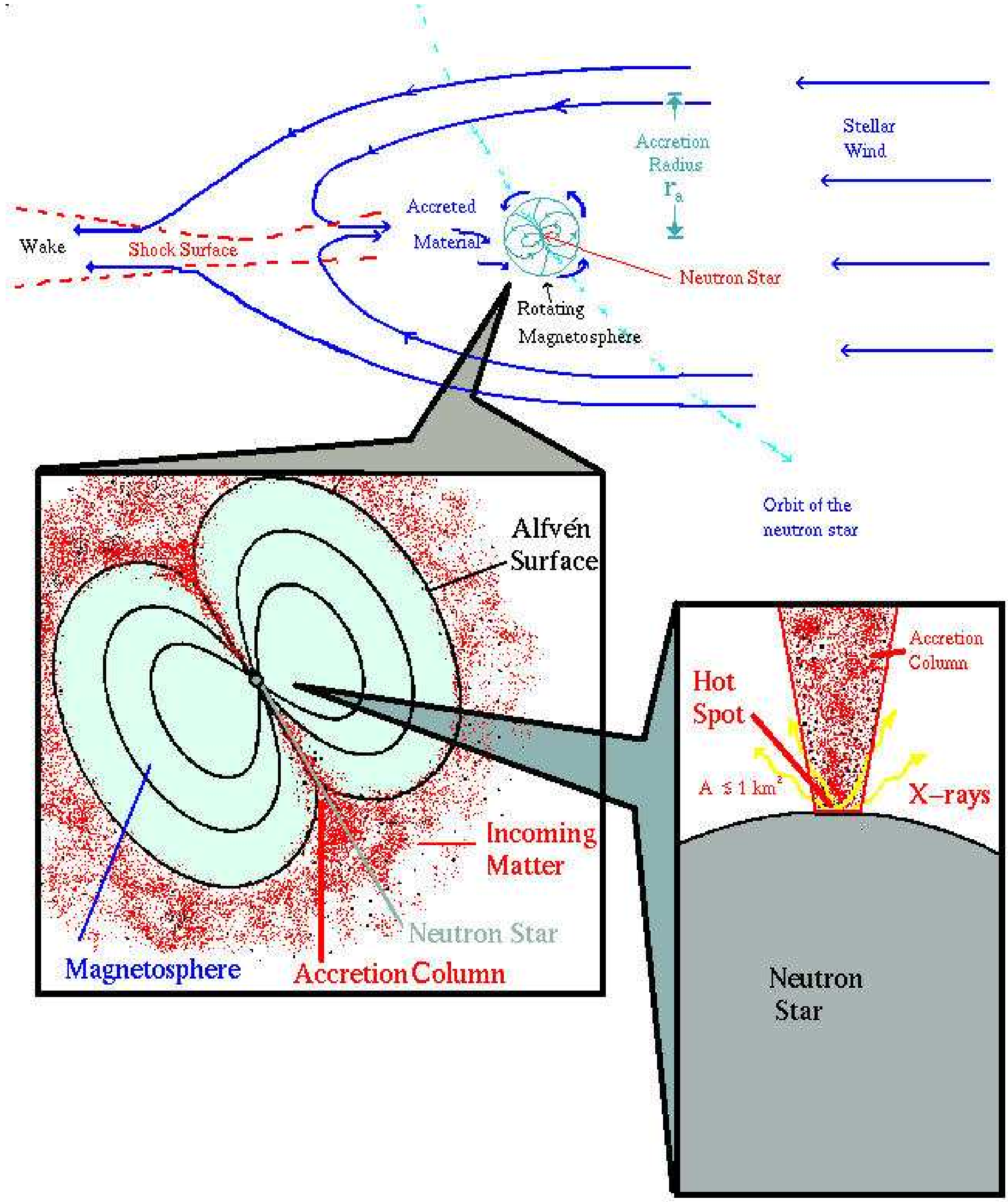

courtesy I. Negueruela

Magnetospheric Accretion, III

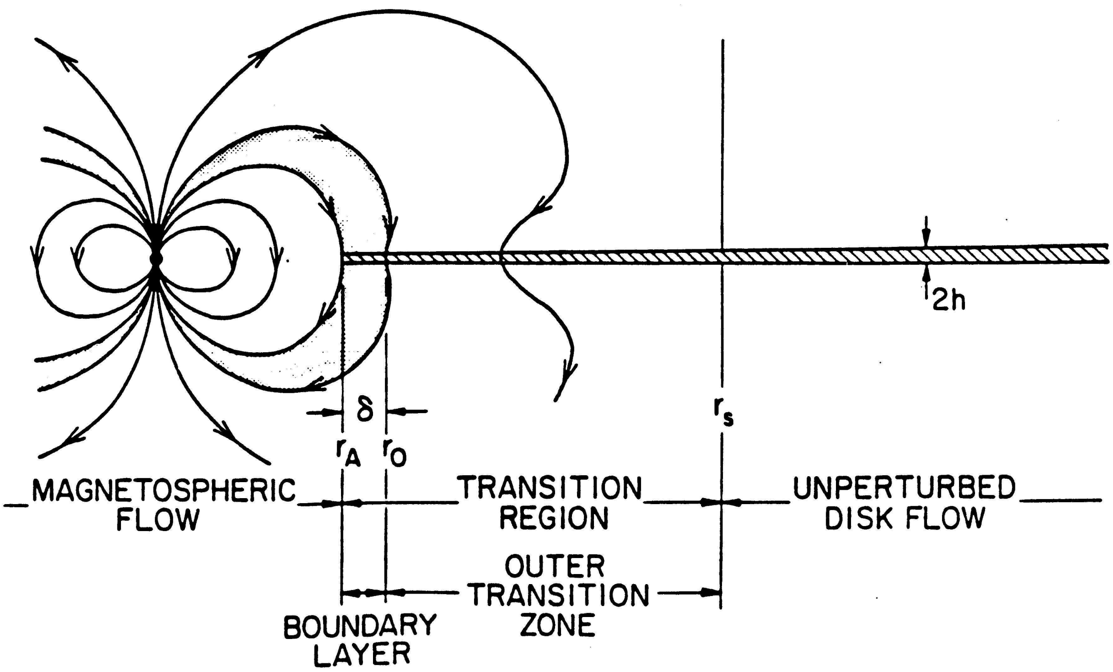

Coupling between magnetic field and accretion disk: accretion disk excerts torque onto NS:

$$I\dot{\omega} = \dot{M} r_{\mathrm{mag}}^2 \Omega_{\mathrm{K}}(r_{\mathrm{mag}}) \tag{3.20}$$

where $I = 2/5 \cdot MR_\star^2$ moment of inertia of NS, and $\Omega_{\mathrm{K}}(r_{\mathrm{mag}} = (GM/r_{\mathrm{mag}}^3)^{1/2}$ the Kepler frequency at r_{mag}.
The luminosity of the source is

$$L = \frac{GM\dot{M}}{r_{\mathrm{mag}}} \tag{3.21}$$

After some tedious algebra (Gosh & Lamb, 1979), one obtains

$$\frac{\dot{P}}{P} \propto -\left(L^{6/7}P\right) \tag{3.22}$$

Magnetospheric Accretion, IV

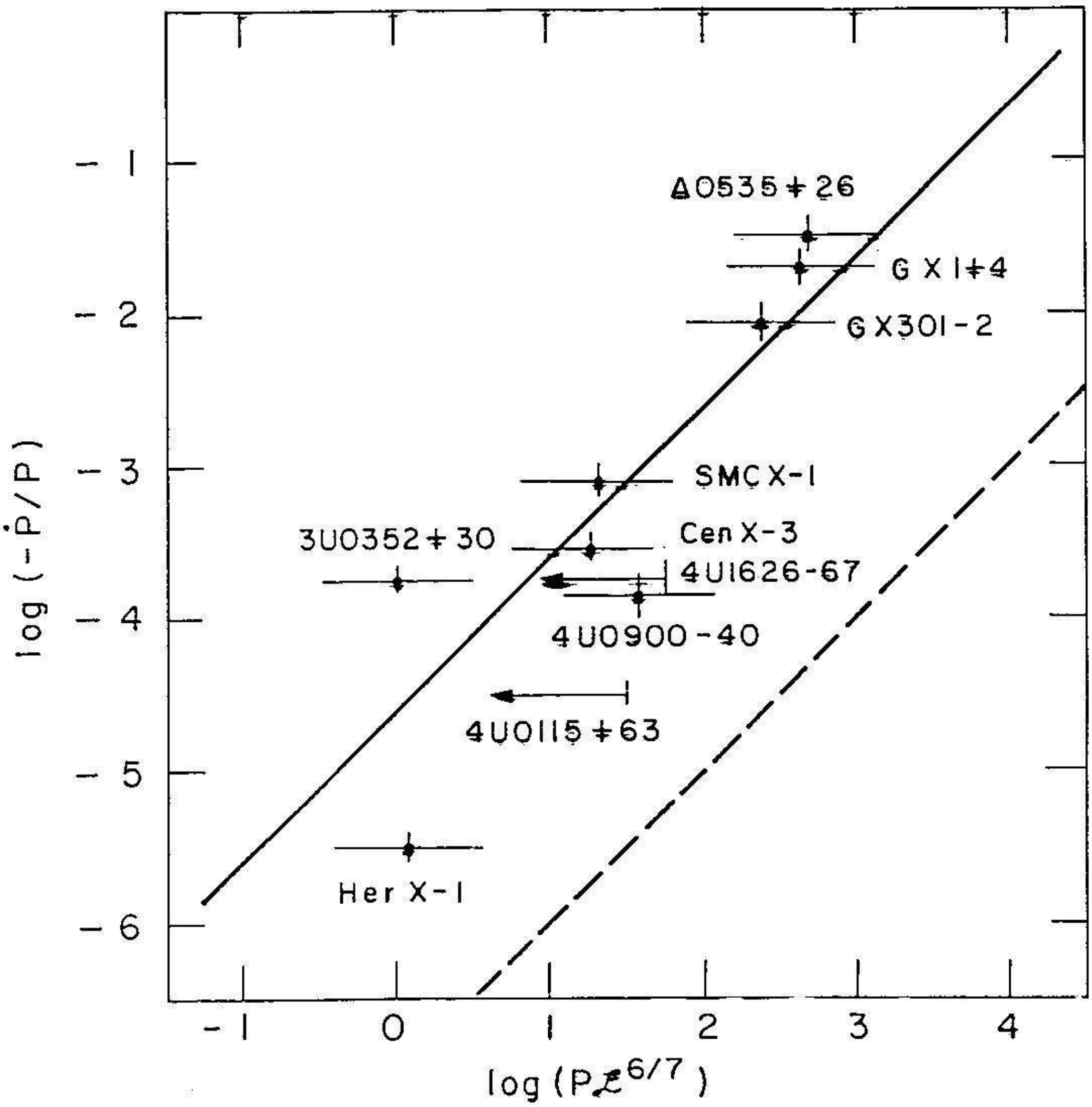

(Rappaport & Joss, 1977)

Observations and prediction of Gosh & Lamb magnetospheric accretion model agree.

Pulse Histories

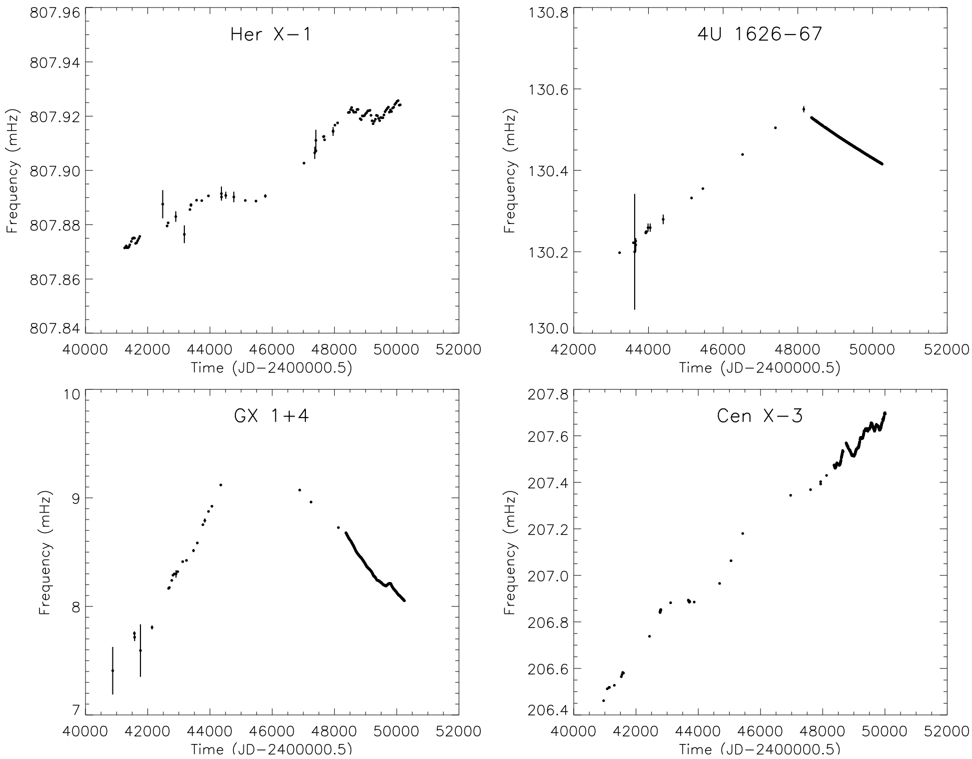

(Bildsten et al., 1998)

Real place of matter coupling to B-field is *not* $r_{\rm mag}$. Result are changes of the neutron star spin: Predominantly, a spin up (spin period *shortens* with time) is observed, but sometimes the period change is erratic or dominated by a spin down (spin period *increases* with time).

Whether a spin up or spin down occurs depends on whether matter couples to the magnetic field inside or outside of $r_{\rm mag}$.

Fan Beam vs. Pencil Beam

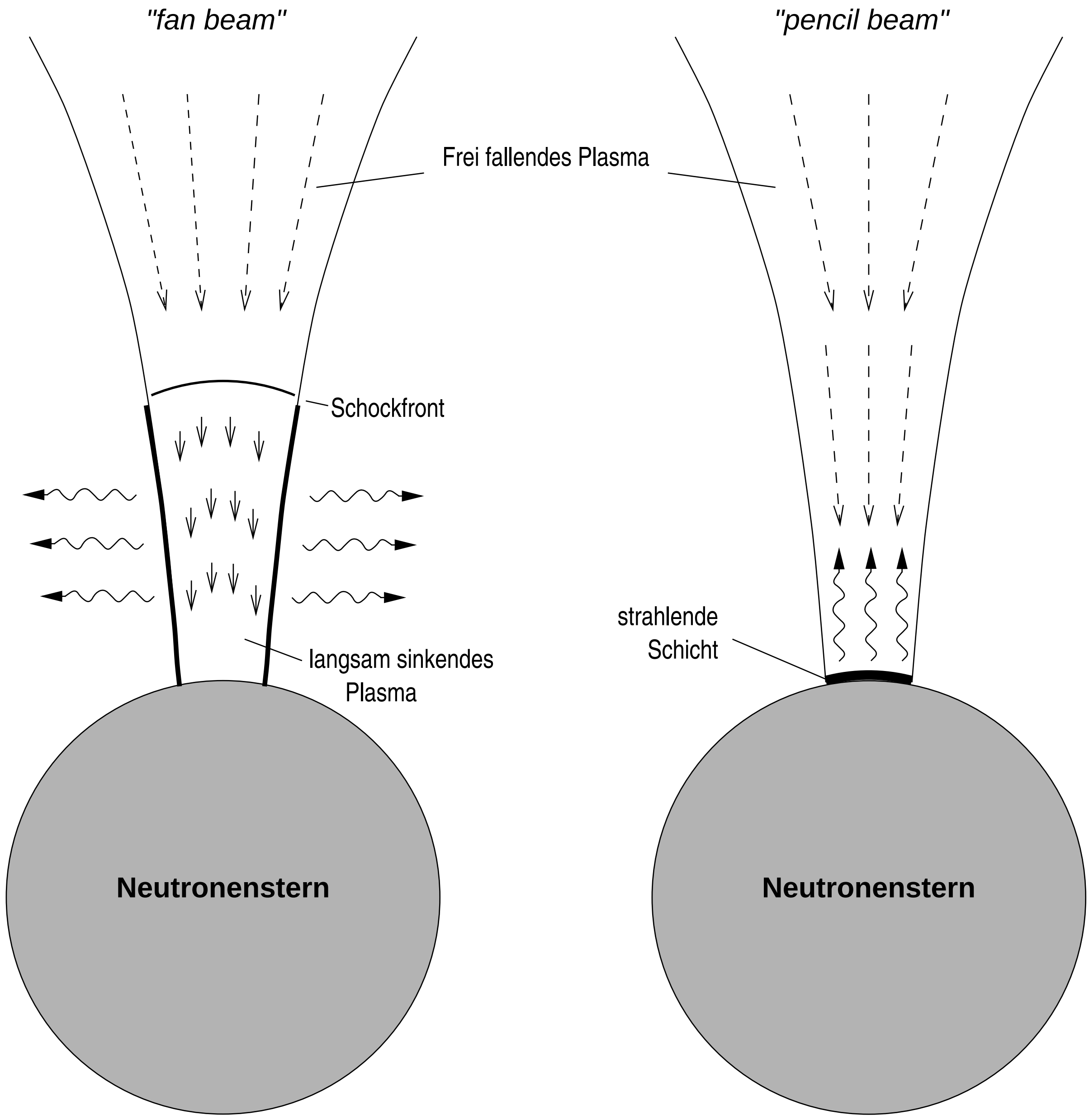

(Kretschmar 1996, Dissertation AIT, Abb. 2.9 [after Harding 1994])

Typical mass accretion rates XXXXXX

Pulse Variability

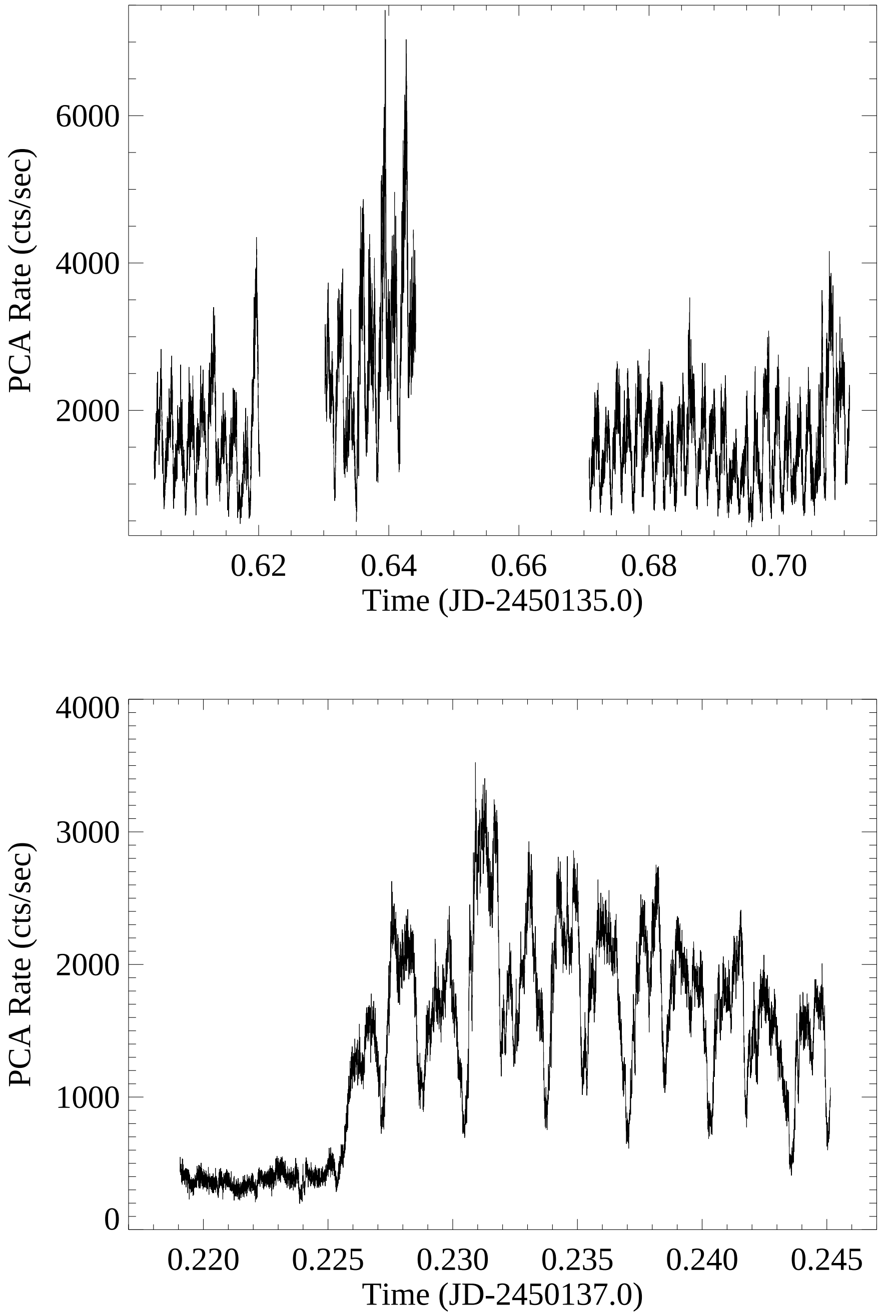

(Kreykenbohm et al., 1999)

Pulse Profi les

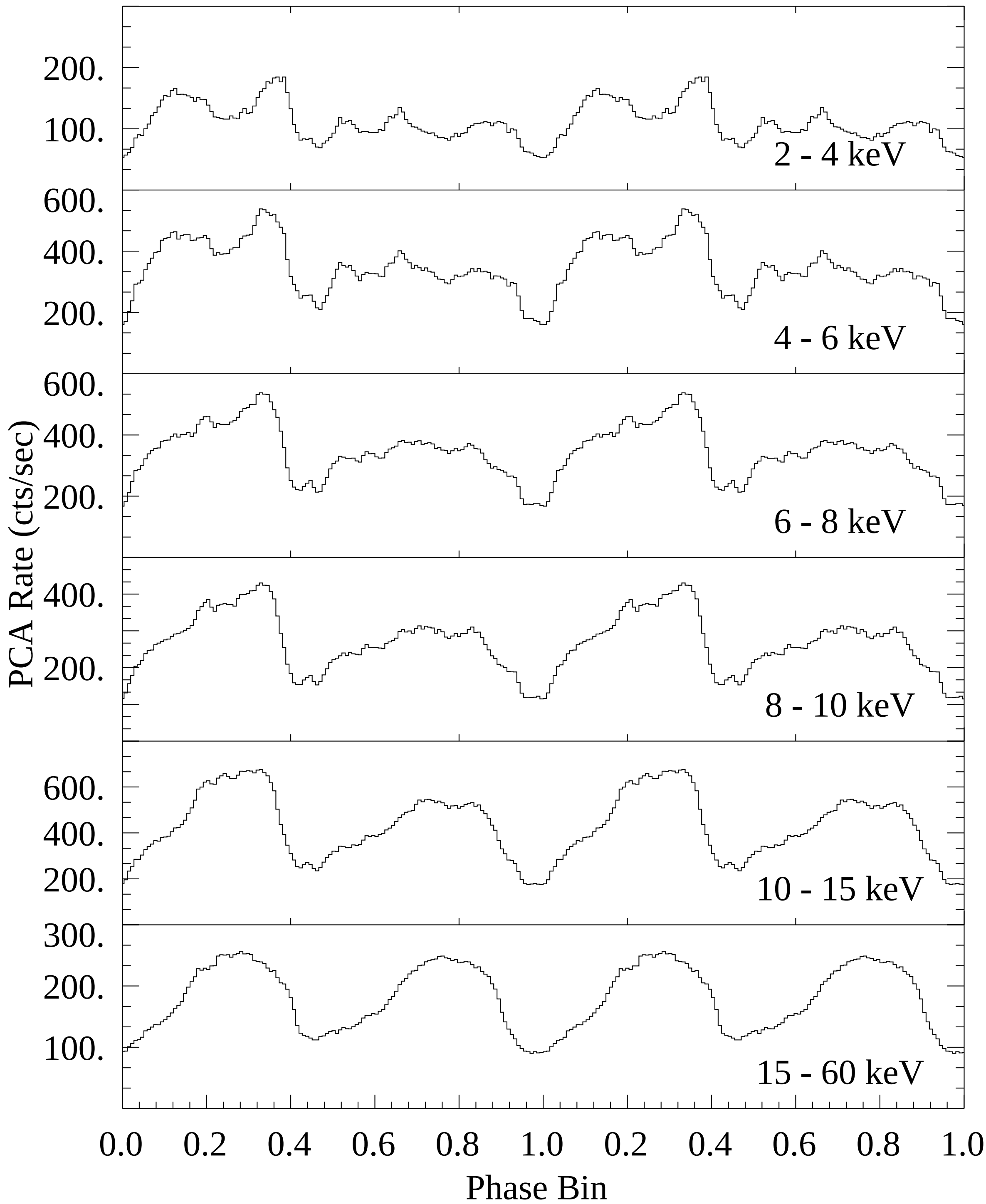

(Kreykenbohm et al. (1999))

Vela X-1: Energy dependent pulse profile.

Landau Levels

Important physical process due to strong field at NS poles: Quantization of electron energies perpendicular to the magnetic field lines (Landau levels):

$$E_n = m_e c^2 \sqrt{1 + \left(\frac{p_\parallel}{m_e c}\right)^2 + 2n\frac{B}{B_{crit}}} \quad (3.24)$$

where $p_\parallel$: momentum of electron parallel to B-field, n the major quantum number, and

$$B_{crit} = \frac{m_e^2 c^3}{e\hbar} \approx 4.4 \times 10^{13}\,\mathrm{G} \quad (3.25)$$

(*critical magnetic field*, $E_{cyc} = m_e c^2$).
For $B \ll B_{crit}$ distance between Landau levels:

$$E_{cyc} = E_{n+1} - E_n = \frac{\hbar e}{m_e c} B = 11.6\,\mathrm{keV}\left(\frac{B}{10^{12}\,\mathrm{G}}\right) \quad (3.27)$$

(12 − B_{12}-rule).

IAAT

Cyclotron Resonance Features

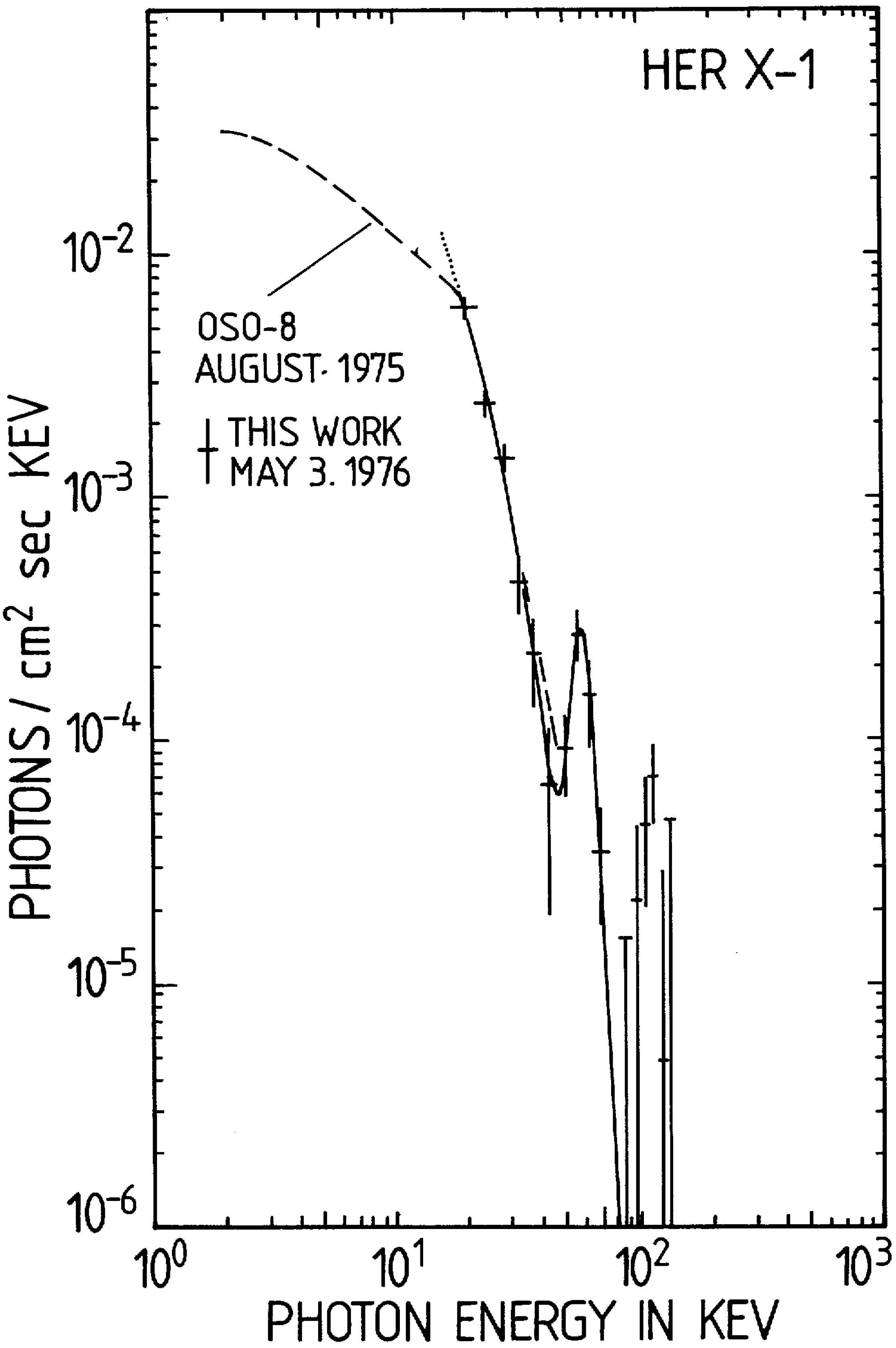

IAAT

Trümper et al. (1978)

CRFs: Summary

Object	P_{puls} (sec)	P_{orb} (days)	E_{cyc} (keV)	Companion
Her X-1	1.24	1.7	38	A9-B
4U0115+63	3.6	24.31	12,23,36?	Be
X0331+53	4.37	34.25	28.5,56?	Be (BQ Cam)
Cen X-3	4.8	2.09	27.1	O6.5II (V779 Cen)
X2259+586	6.98	?	5?,10?	single?
4U1626-67	7.66	1.7	38	KZ TrA
LMC X-4	13.5	1.408	19-23?	O7IV
GS1843+00	29.5	?	18-22	?
GS2137+57	66.2	?	29	Be?
A0535+26	105	110.58	55?,110	Be
Vela X-1	283	8.96	25?,58	B0.5Ib
4U1907+09	438	8.38	19	B2 III-IV
4U1538-52	530	3.73	20, 40	B0I
GX 301-2	690	41.5	40	B1.2Ia (Wray 977)

(Heindl, 1999, priv. comm.)

Black Holes

Stars end their life as one of three different kinds of compact objects:

white dwarf: $\rho \sim 10^{5\ldots6}\,\mathrm{g\,cm^{-3}}$, $R \sim R_{\mathrm{earth}}$,
Equilibrium between gravitation and pressure of ([relativistically] degenerate) electrons
$M < 1.44\,M_\odot$ (Chandrasekhar-Limit).

neutron star: $\rho \sim 10^{13}\ldots10^{16}\,\mathrm{g\,cm^{-3}}$,
$R \sim 10\,\mathrm{km}$, at this density β-decay
($\mathrm{p} + \mathrm{e}^- \longrightarrow \mathrm{n}$), i.e., star consists mainly of neutrons $1.44\,M_\odot < M \lesssim 3\ldots4\,M_\odot$
(Oppenheimer-Volkoff Limit).

black hole: above OV-Limit: no stable configuration known $\Longrightarrow$ star collapses at infinitum $\Longrightarrow$ black hole. horizon at
$R_\mathrm{S} = 2GM/c^2 = 3(M/M_\odot)\,\mathrm{km}$
(Schwarzschild radius), $M \gtrsim 4\,M_\odot$.

Black Holes

Observation: determine mass.

Since inclination i usually not known, can only determine mass function

$$\text{MF} = \frac{M_2^3 \sin^3 i}{(M_1 + M_2)^2} = \frac{a_1^3 \sin^3 i}{U^2} \tag{3.28}$$

(lower limit for M_2)

Most black holes have MF $\gtrsim 2\,M_\odot$, there are a few with MF $> 5\,M_\odot$.

since also MF sometimes not determined: classification as black hole *candidate* (BHC).

First BHC discovered in 1965, identified in 1972 (Cygnus X-1). End of 1970s: LMC X-3 and LMC X-1.

Today $>$30 BHC known, 3 are “safe” BH.

Black Holes

BHC can be both, HMXB and LMXB:

Soft X-ray Transients: Low mass X-ray Binaries with a BH. Transient behavior, outbursts due to triggered mass transfer/accretion. Most BHC.

Persistent Black Hole Candidates: High Mass X-ray Binaries, always seen, about five sources known (Cyg X-1, LMC X-1, LMC X-3,. . .)

Microquasars: Most probably LMXBs, strong radio emitters with jets

Black Holes

Orosz, 2001, priv. comm.

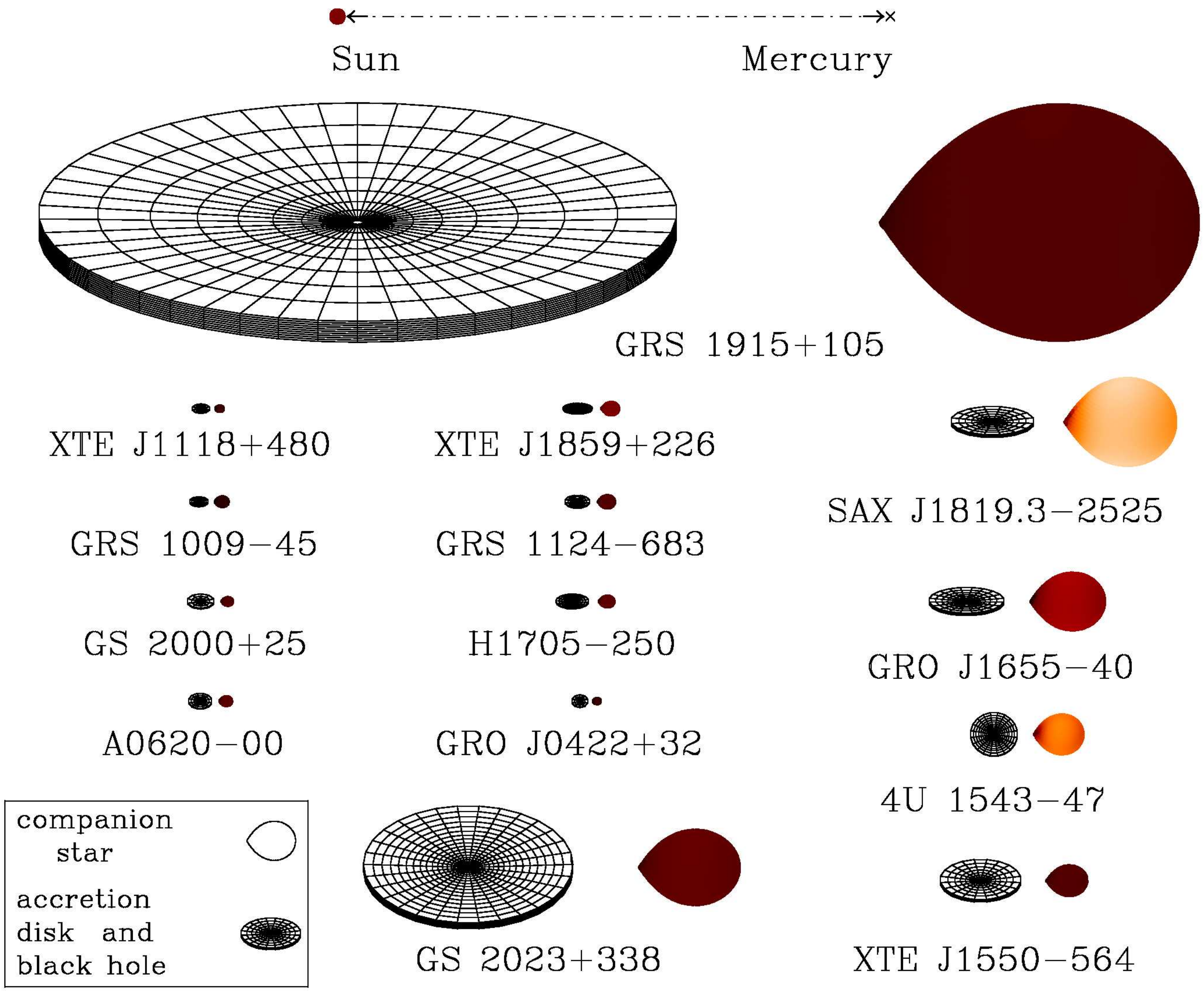

Black Holes

astrophysics of BHC: study of accretion processes

Simpler than NS/WD: no surface, no magnetic fields.

more difficult than NS/WD: large accretion rates, modification of X-ray spectrum by hot gas,. . .

$\Longrightarrow$ we have good observational material, a rough physical understanding, many (basic) questions are open.

Relativistic effects not too important, they are more crucial in active galactic nuclei

Transient Black Hole Candidates

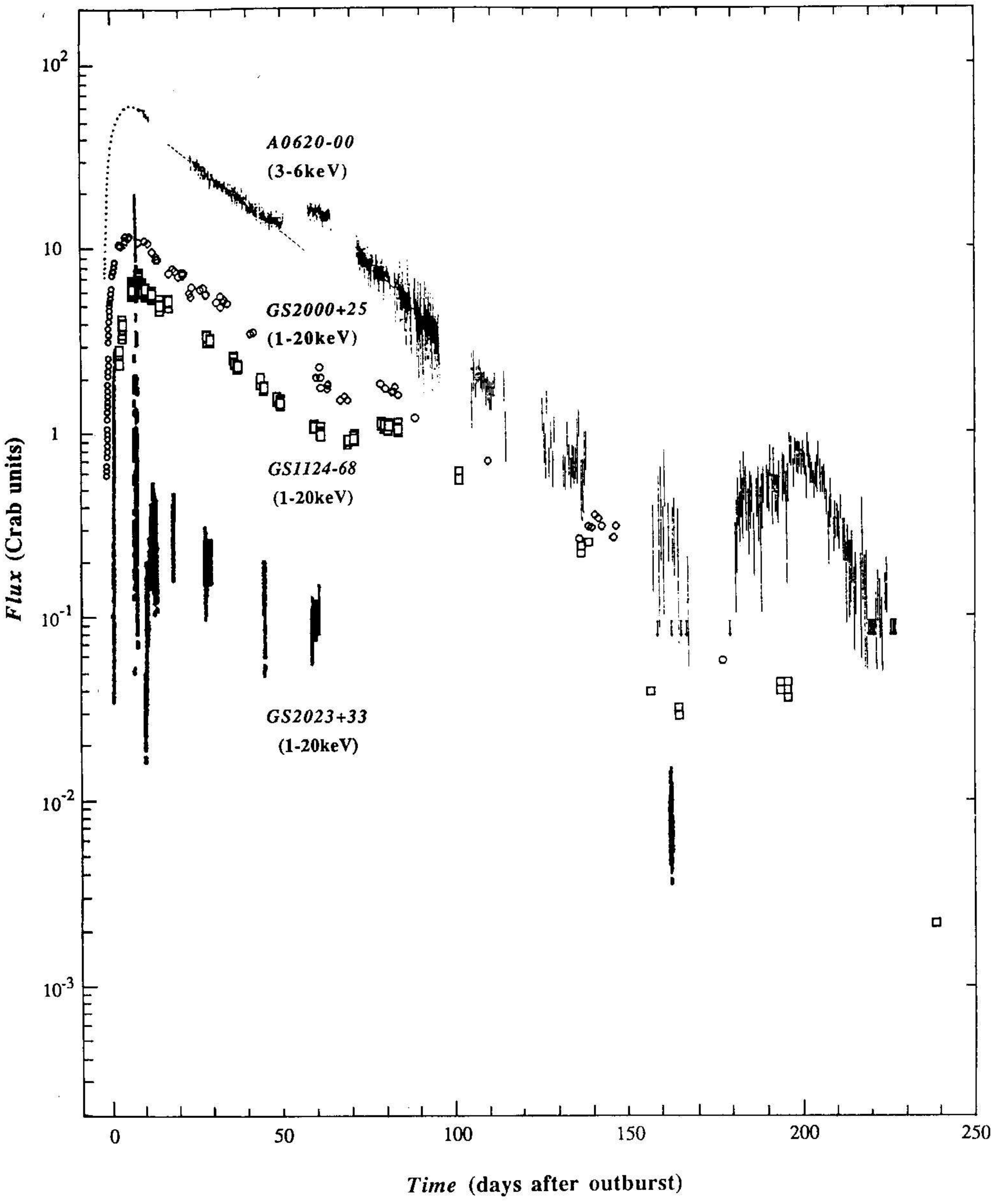

Tanaka, 1995

Transient Black Hole Candidates

light curve during outburst:

- fast raise, exponential decay (FRED)
- secondary reflare, about 50–80 d after primary maximum
- third hump after a few hundred days

Observations

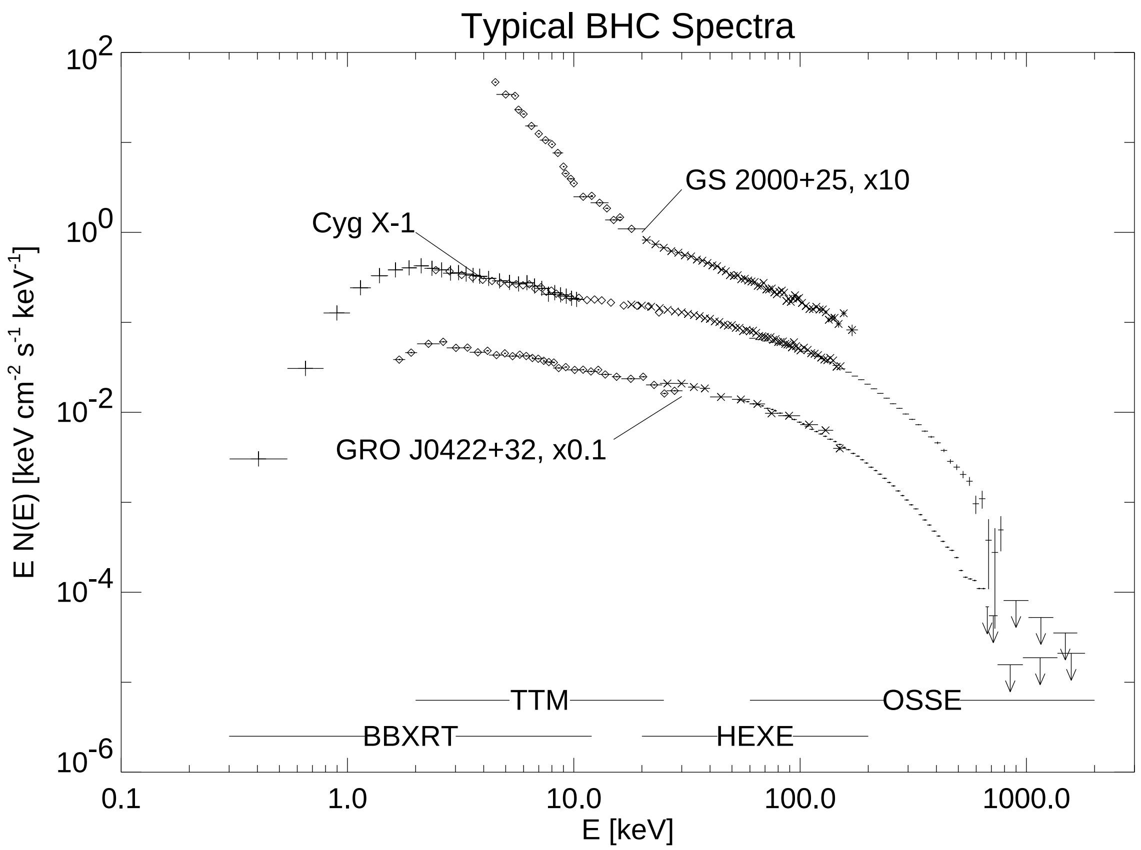

1970–1995: Single pointed observations:

- Some sources exhibit thermal X-ray spectrum ⟹ accretion disk!
- Many sources exhibit power law spectrum
- presence of Fe Kα line emission at 6.4 keV ⟹ "cold material" (disk?)

Because of this: "states of black holes":
high/soft state: accretion disk dominates.
low/hard state: power law dominates.

Hard State, I

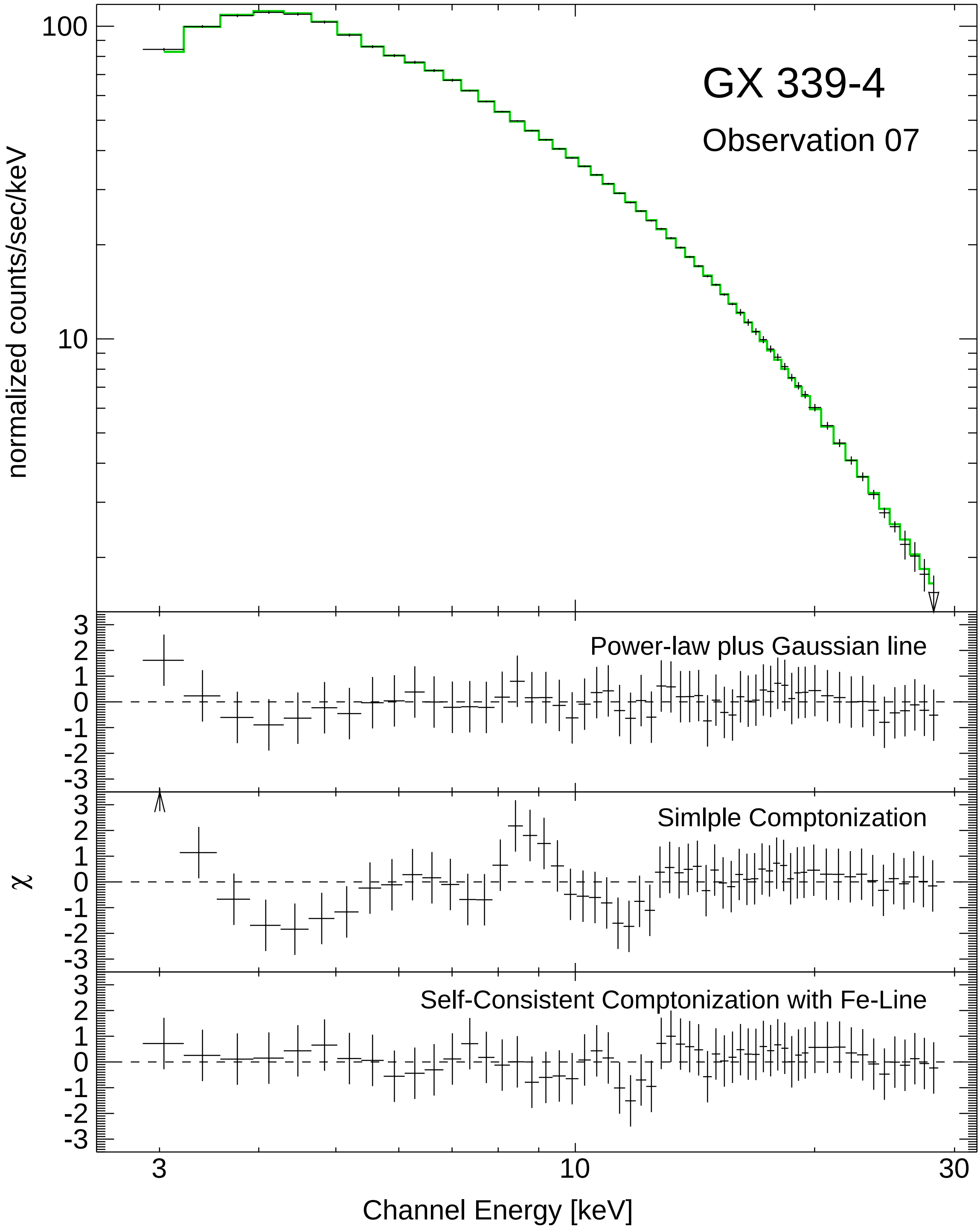

Application of Comptonization Models on GX 339−4 (Wilms et al., 2000)

⟹ good agreement between theory and observations

Hard State, II

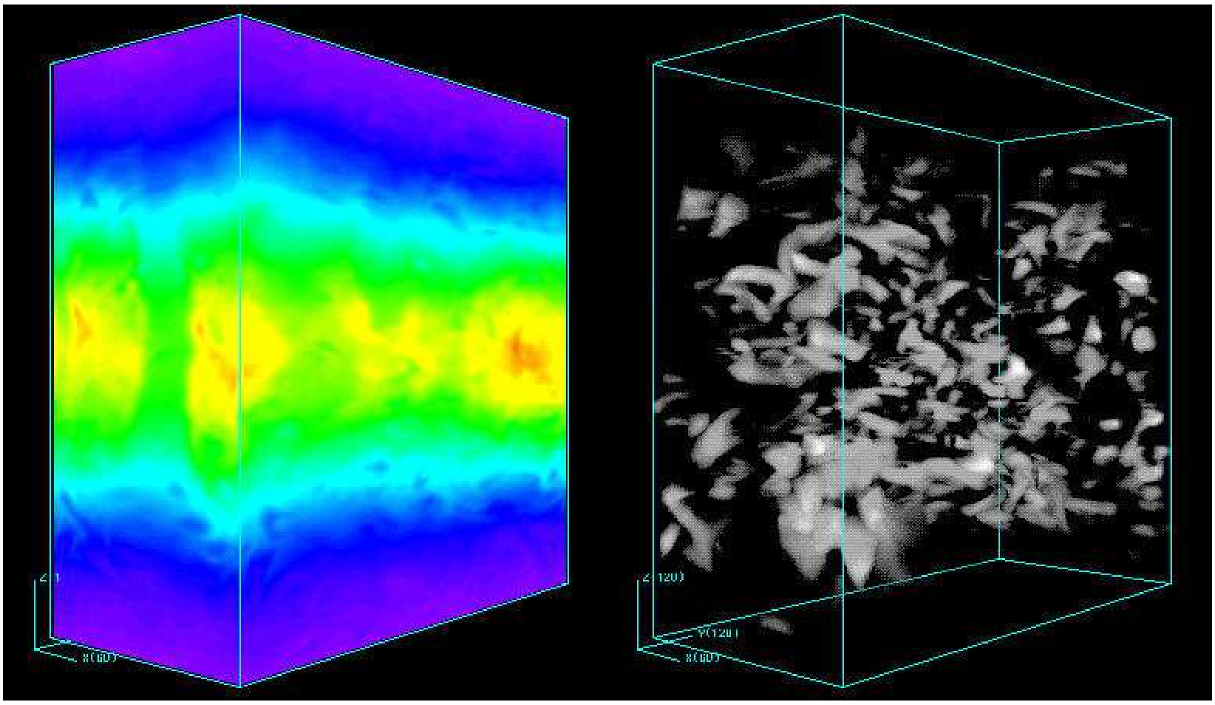

cross section through “sandwich corona”.
left: particle density,
right: B-Field (Stone, priv. comm.)

Comptonizing medium is probably of magnetohydrodynamical origin

Possible mechanism: Magnetorotational Instability (MRI, aka Balbus-Hawley Instability; possibly MRI is also source of disk viscosity [α parameter. . .]).

Hard State, III

The location of the Comptonizing medium (accretion disk corona) is unclear:

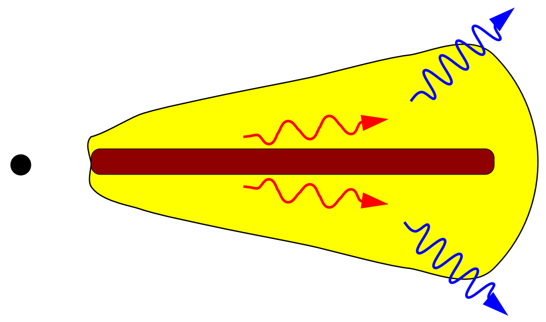

Sandwich geometry
(Haardt & Maraschi, 1993)

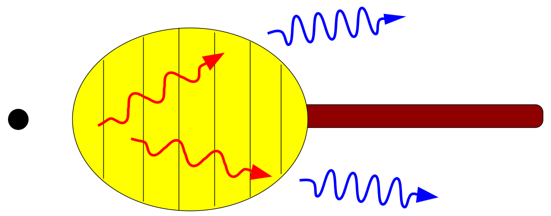

Advection dominated accretion flow (ADAF)
Narayan (1996),
Esin et al. (1997, 2000)

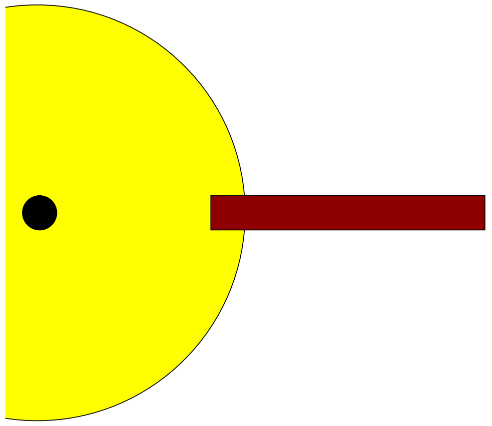

"Sphere+Disk geometry"
Dove et al. (1997),
Zdziarski et al. (1998)

Hard State, IV

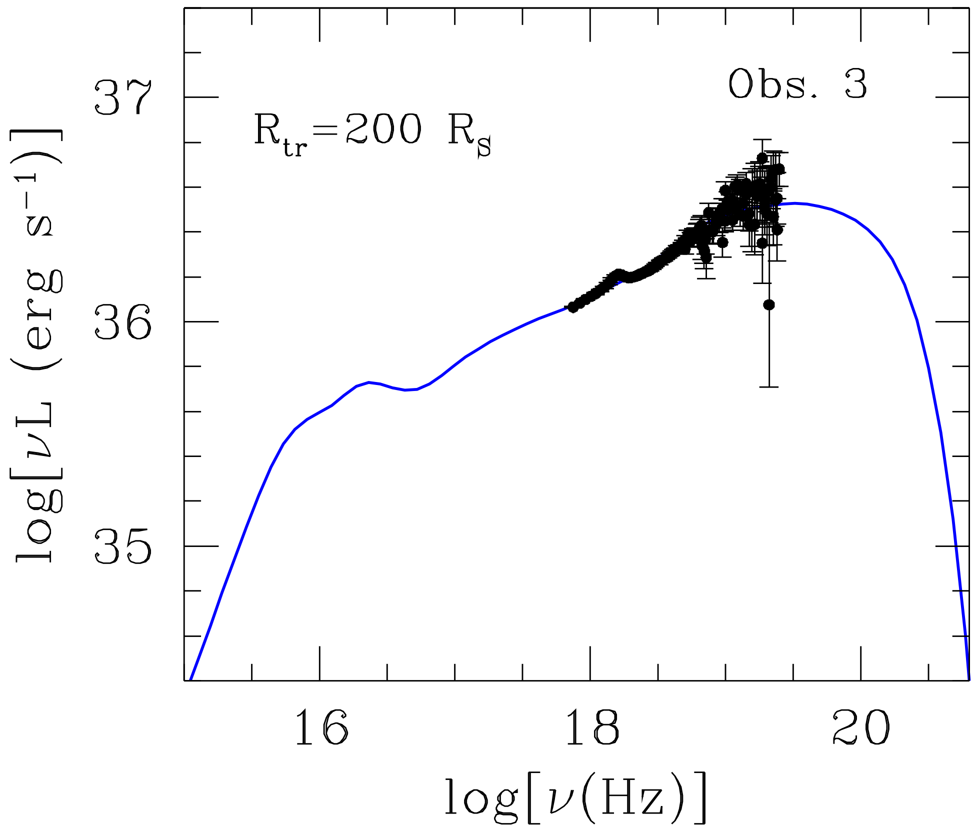

ADAF fit for GX 339−4, observed radio flux is 7 mJy at 843 MHz (Wilms et al., 2000)

- Sandwich-Geometry not self consistent, as corona is cooled too effi ciently (Dove et al., 1997).
- ADAF in many sources not possible since synchrotron peak too strong (e.g., Wilms et al., 2000).
- Sphere+Disk explains spectrum but not short term variability (z.B. Nowak et al., 1999)...

⟹ accretion geometry is not understood!

Long Term Variability

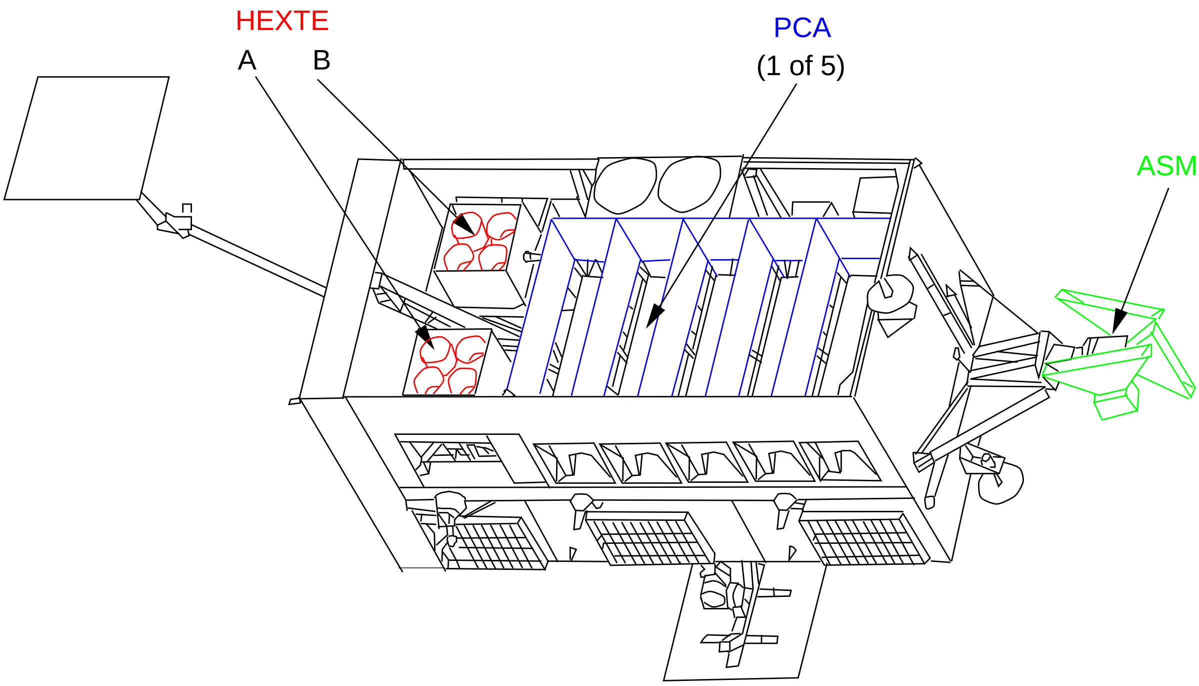

more insight through systematical, year long observing campaigns instead of "Snapshots", possibly with the Rossi X-ray Timing Explorer (RXTE, NASA, since 1996).

Tübingen campaigns

Cyg X-1: 1997–today (RXTE, radio, optical; Pottschmidt et al., 2000, 2001)

LMC X-1: 1997/1998 (RXTE; Wilms et al., 2001)

LMC X-3: 1997–1999, 2001–heute (RXTE; Wilms et al. 2001), 1990–1995 (optical [Amsterdam]; Brocksopp et al., 2001).

GX 339−4: 1998 (RXTE; Wilms et al. 2001), 2000 (XMM-Newton, BeppoSAX)

LMC X-3, I

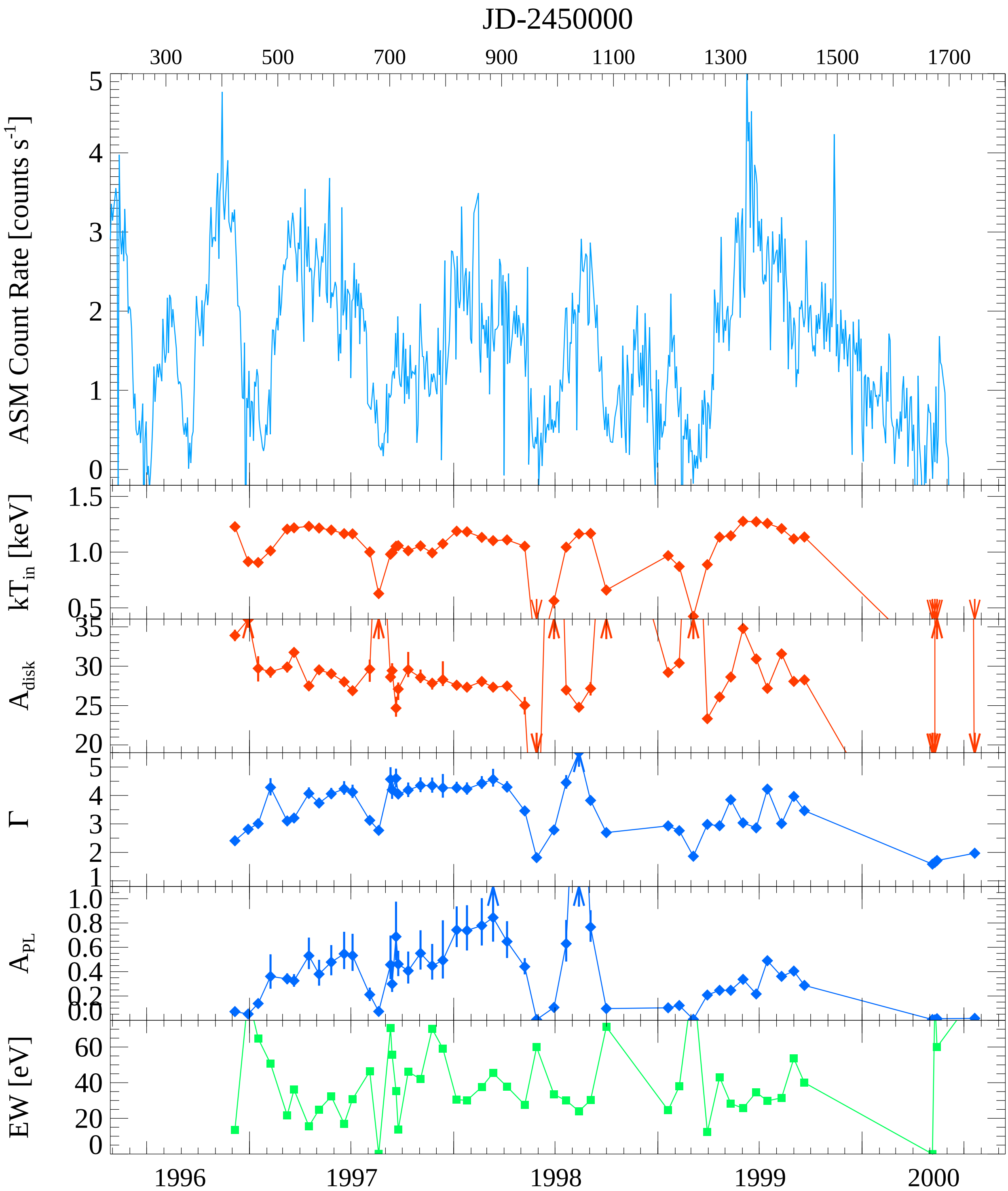

LMC X-3: variation of X-ray spectral parameters (Wilms et al., 2001)

LMC X-3, II

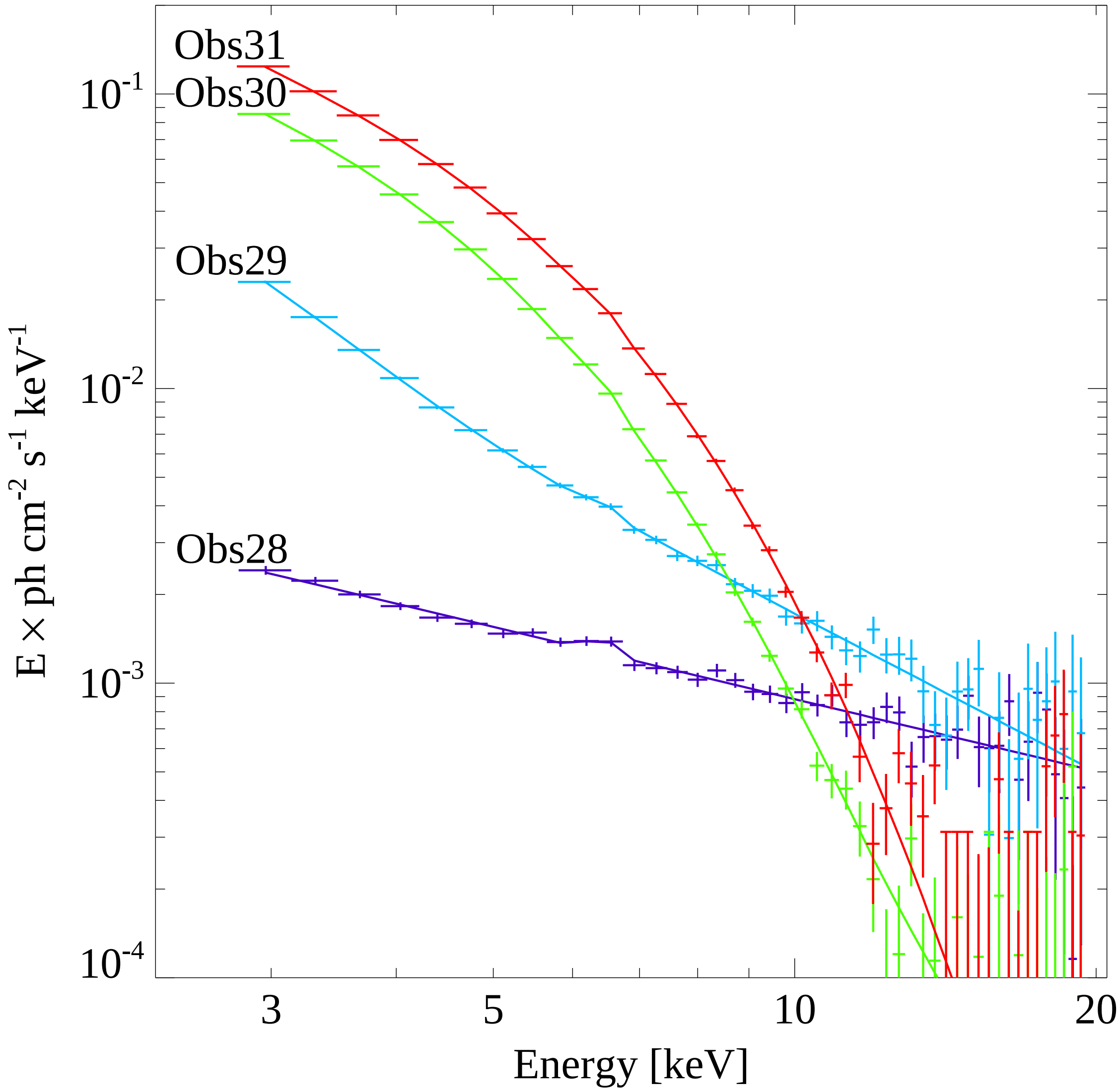

Wilms et al., 2000, 2001

LMC X-3 exhibits quasi-periodical transitions between the soft state and the hard state for $L \lesssim 5\% L_{\text{Edd}}$

$\Longrightarrow$ accretion disk corona is not always there!

similar things known from most BHC (z.B. Cyg X-1, XTE J1550,. . .)
$\Longrightarrow$ MRI does not work for large L, ($\propto \dot{M}$).

State Transitions

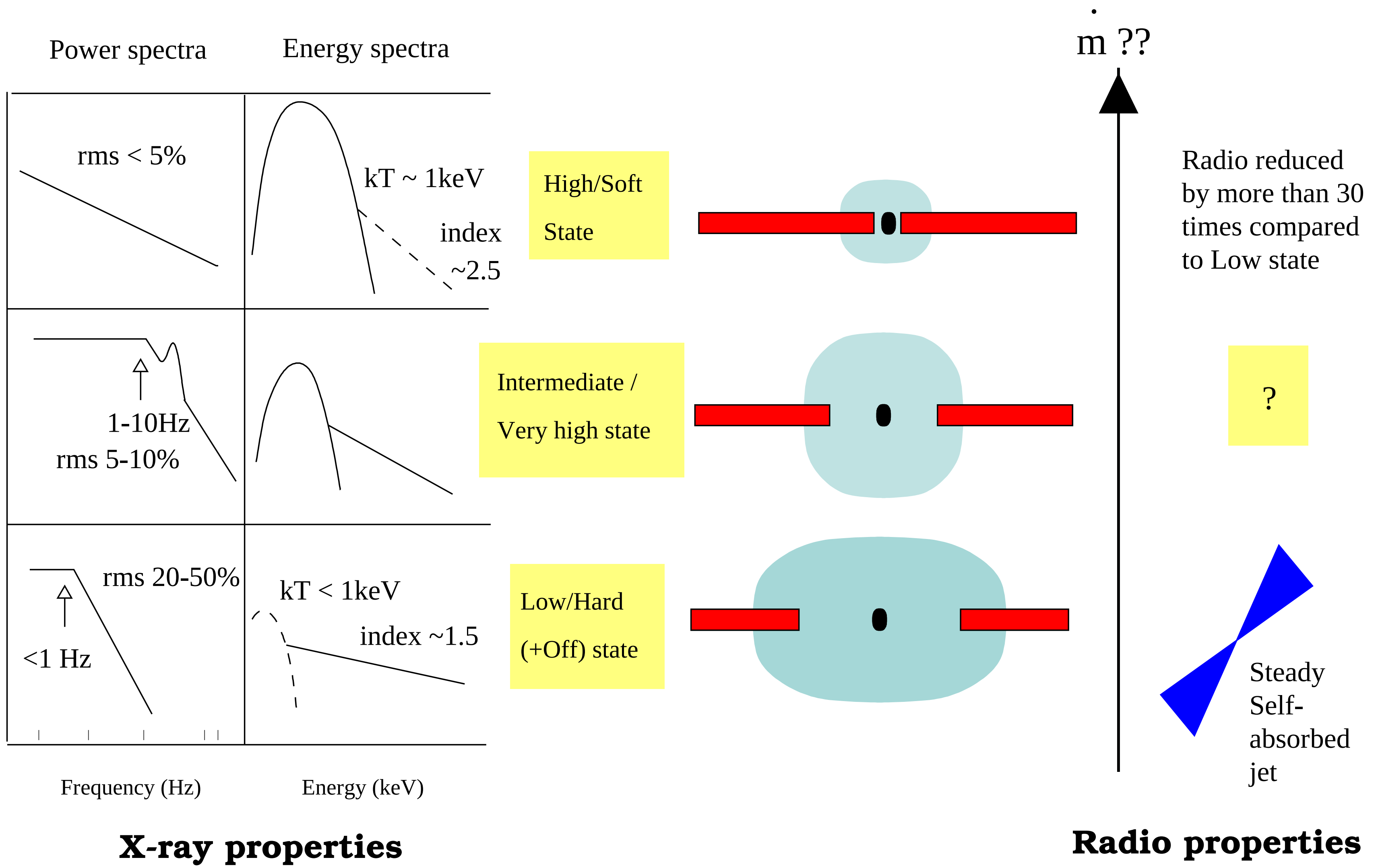

Fender 2000

Cyg X-1

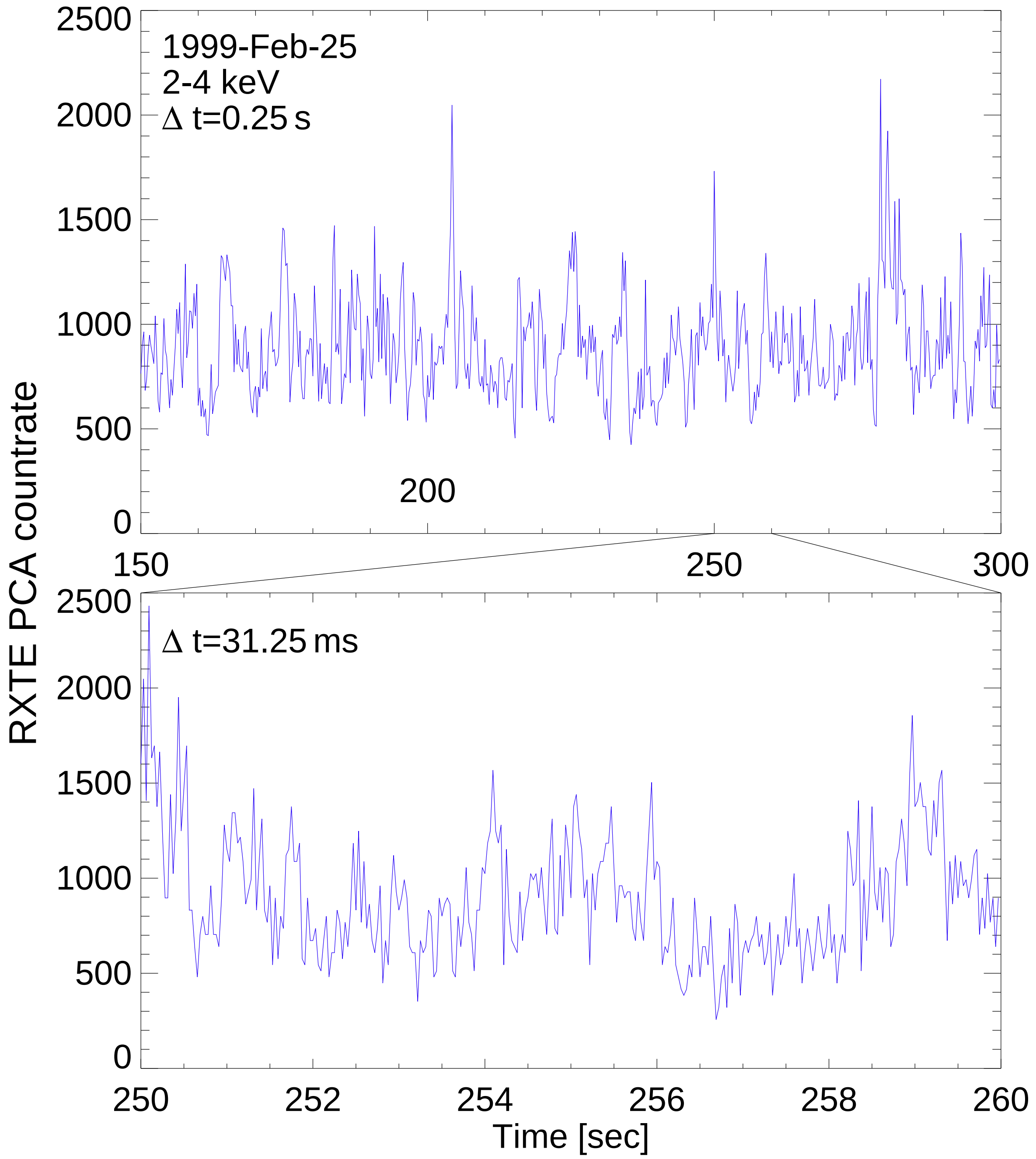

More clues from time behavior.

Cyg X-1

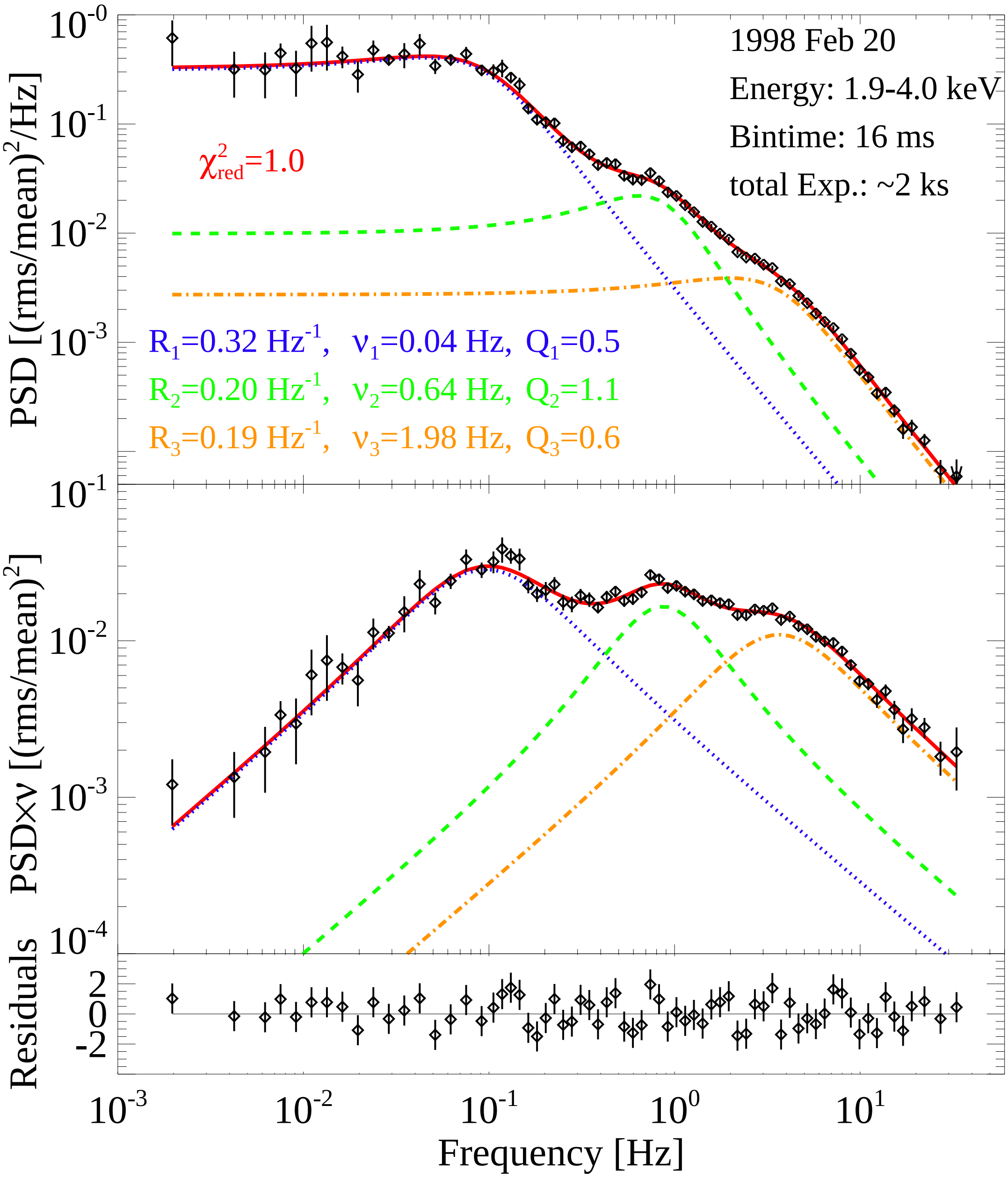

variability described as "red noise" with characteristic frequencies that are perhaps related to accretion disk oscillations (Diskoseismology).

Cyg X-1

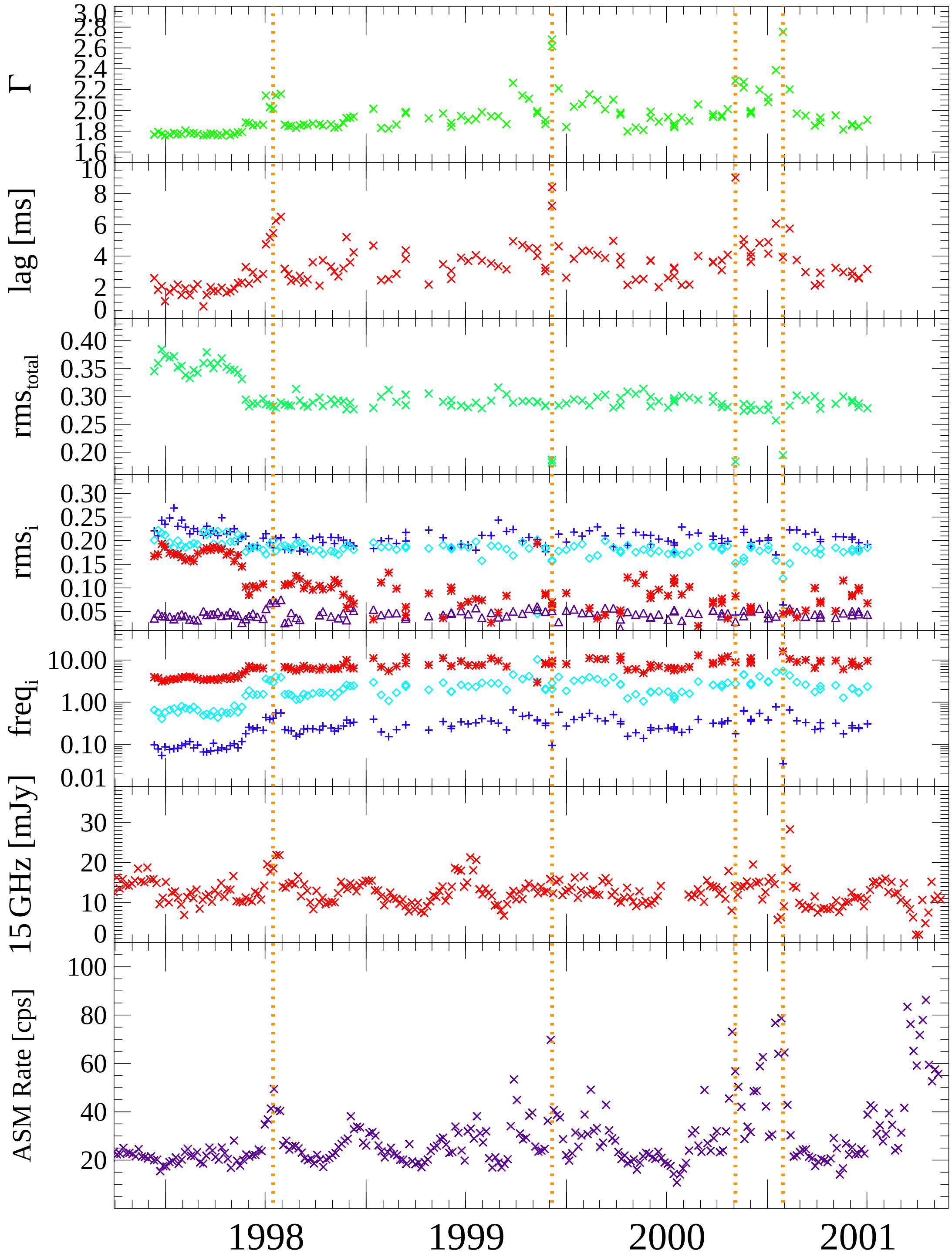

Pottschmidt et al. 2001

Evolution of PSD parameters with time ⟹ "failed state transitions"

Cyg X-1

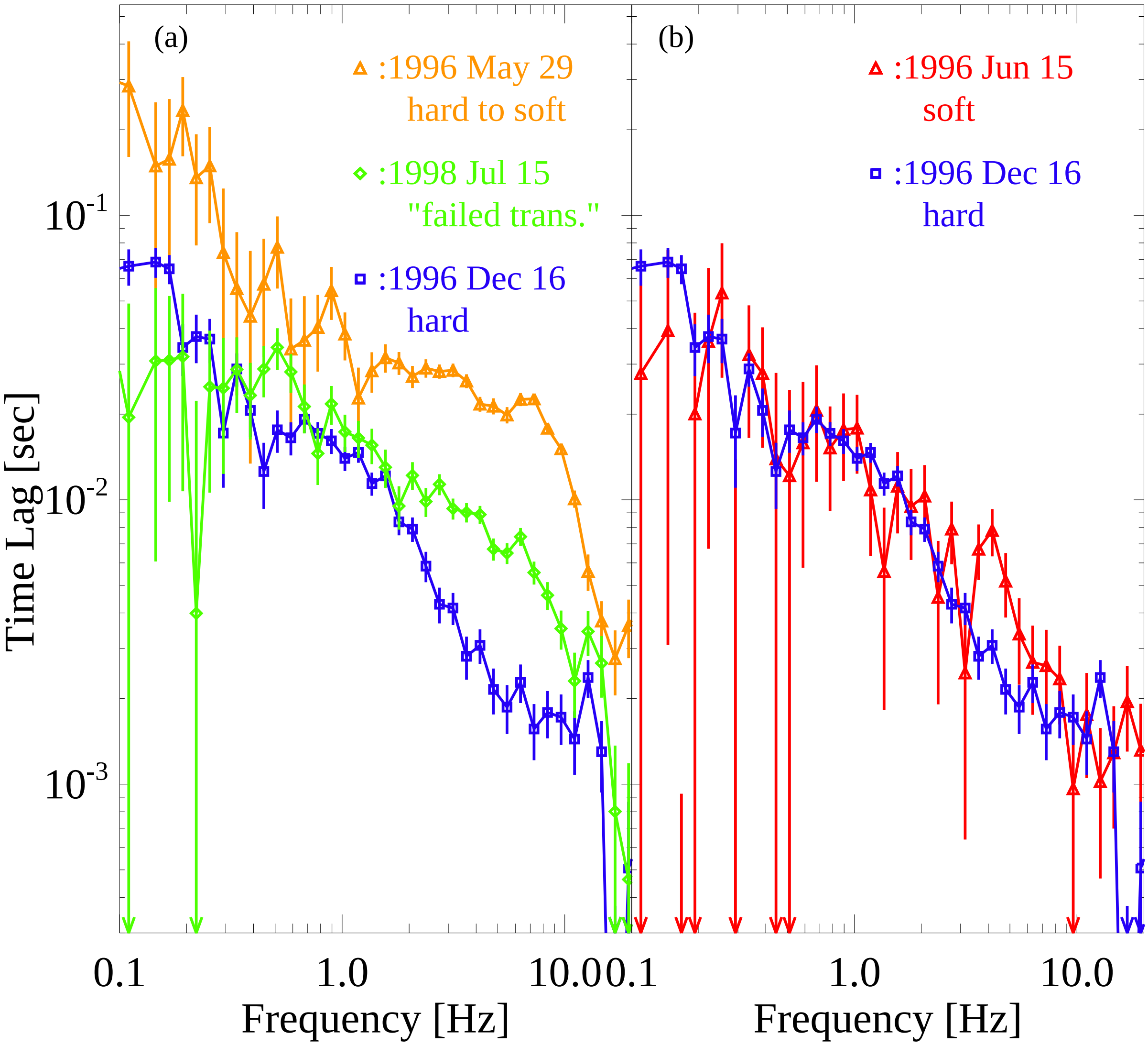

Pottschmidt et al., 2000

The fourier frequency dependent “Lag” changes only *during* state changes.

during hard and soft state, lags are identical $\Longrightarrow$ origin of lag independent of accretion disk corona.

Cyg X-1

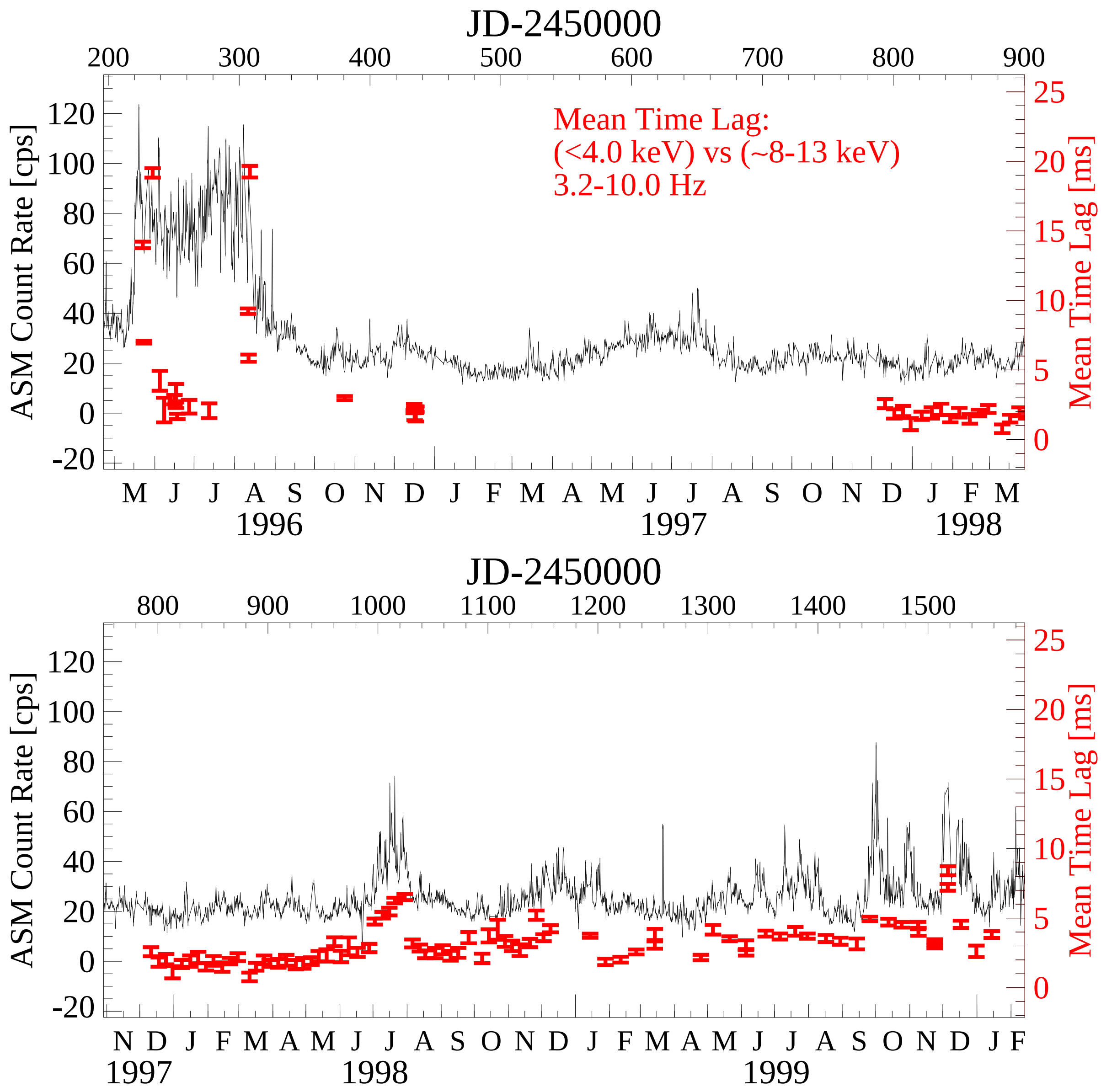

Pottschmidt, Wilms, et al., 2000

Evolution of lag between two energy bands. Lag is signifi cantly larger during state changes ⟹ change of source geometry?

IAAT

Microquasars, I

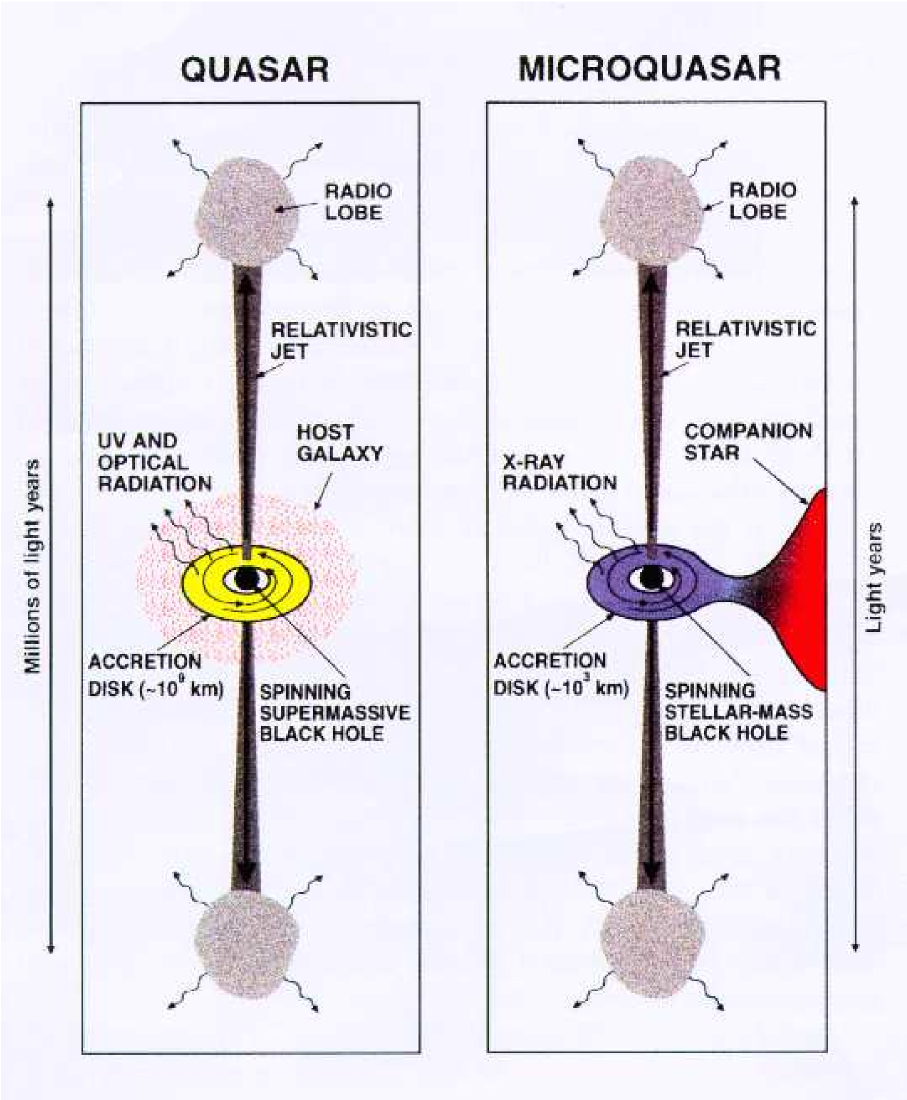

Microquasar: BHC with strong radio jets; "superluminal motion"

Three sources known:

- GRS 1915+105 (discovered 27 July 1994)
- GRO J1655-40
- XTE J1550-564

IAAT

Microquasars, II

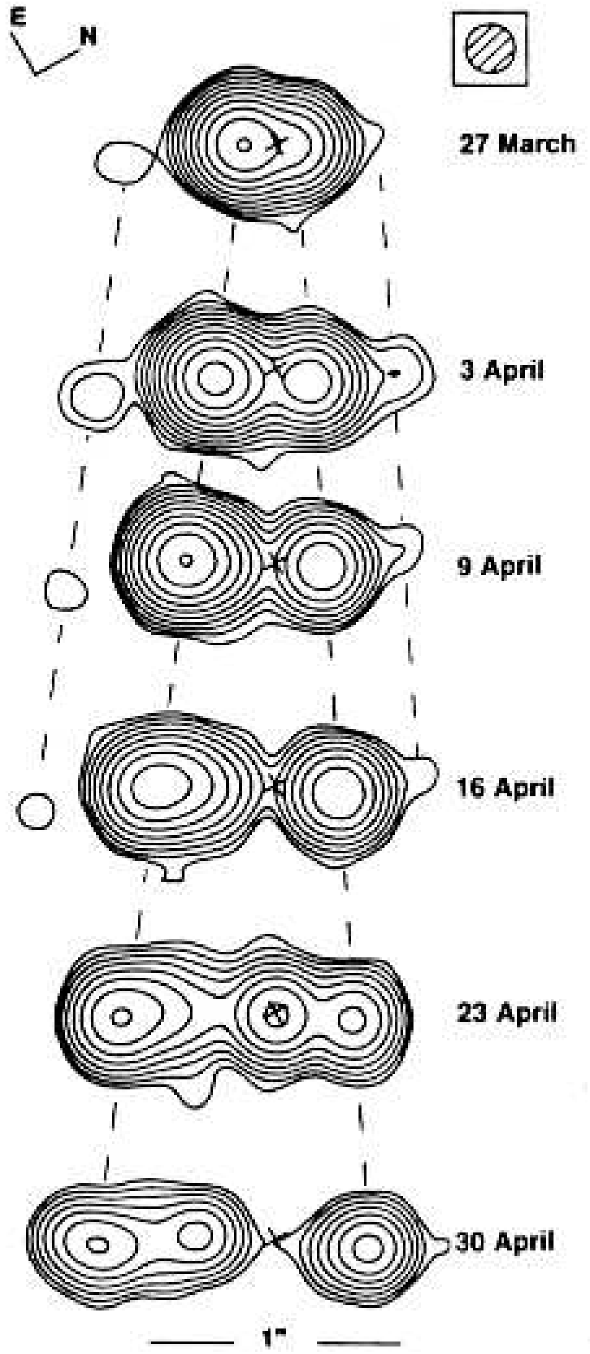

March/April 1994 (VLA, Mirabel et al., 1994)

ballistical motion of clumps: apparent velocity:

- $(0.65 \pm 0.08)c$ und $(1.25 \pm 0.15)c$, i.e. Superluminal Motion!
- before 1994: only known from AGN (z.B. 3C273)
- Theory: Projection effect

Measured fluxes consistent with relativistic Doppler boosting

Superluminal Motion

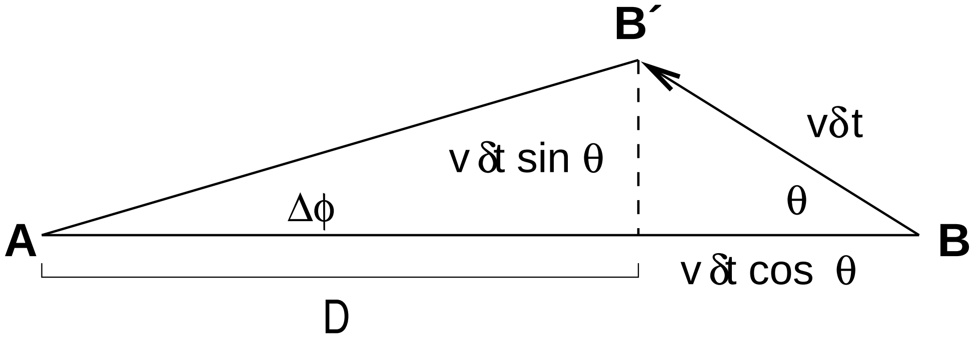

light emitted at position B and B' with time difference δt:

Observer A measures time difference:

$$\Delta t = \delta t(1 - \beta \cos\theta) \tag{3.29}$$

Observer A measures transversal velocity:

$$\beta_\mathrm{T} = \frac{v \sin\theta}{c(1 - \beta\cos\theta)} = \frac{\beta\sin\theta}{1 - \beta\cos\theta} \tag{3.30}$$

$\gamma = (1 - \beta^2)^{-1/2}$, $\beta = v/c$ with $\beta_\mathrm{T}^- = 0.65$ and $\beta_\mathrm{T}^+ = 1.25$:

$$\beta = (0.92 \pm 0.08)c$$
$$\theta = (70 \pm 2)^\circ$$

maximum transversal velocity: $\beta_\mathrm{T}^\mathrm{max} = \beta\gamma \approx \gamma$

GRS 1915+105

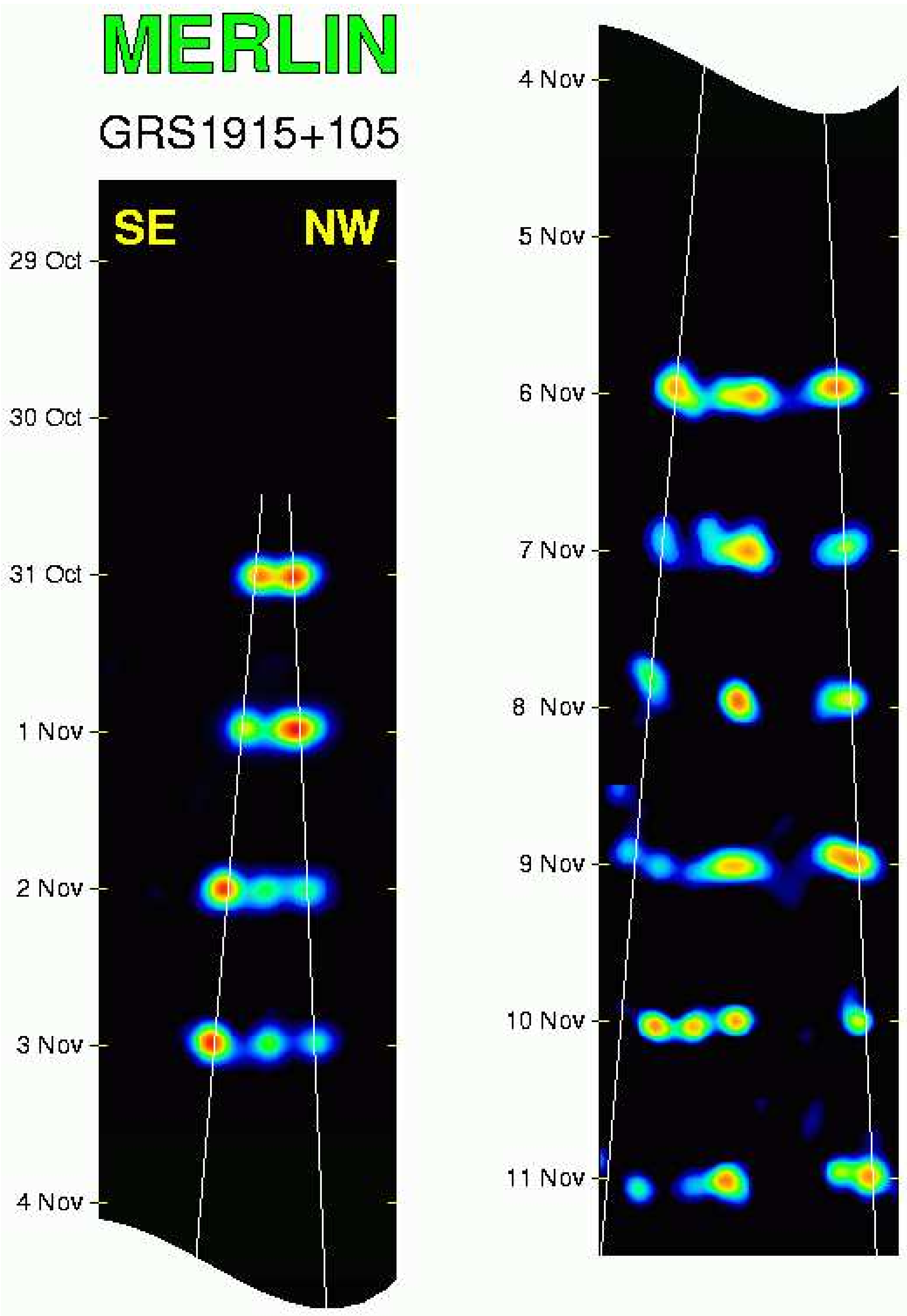

Superluminal Motion in GRS 1915

GRS 1915+105

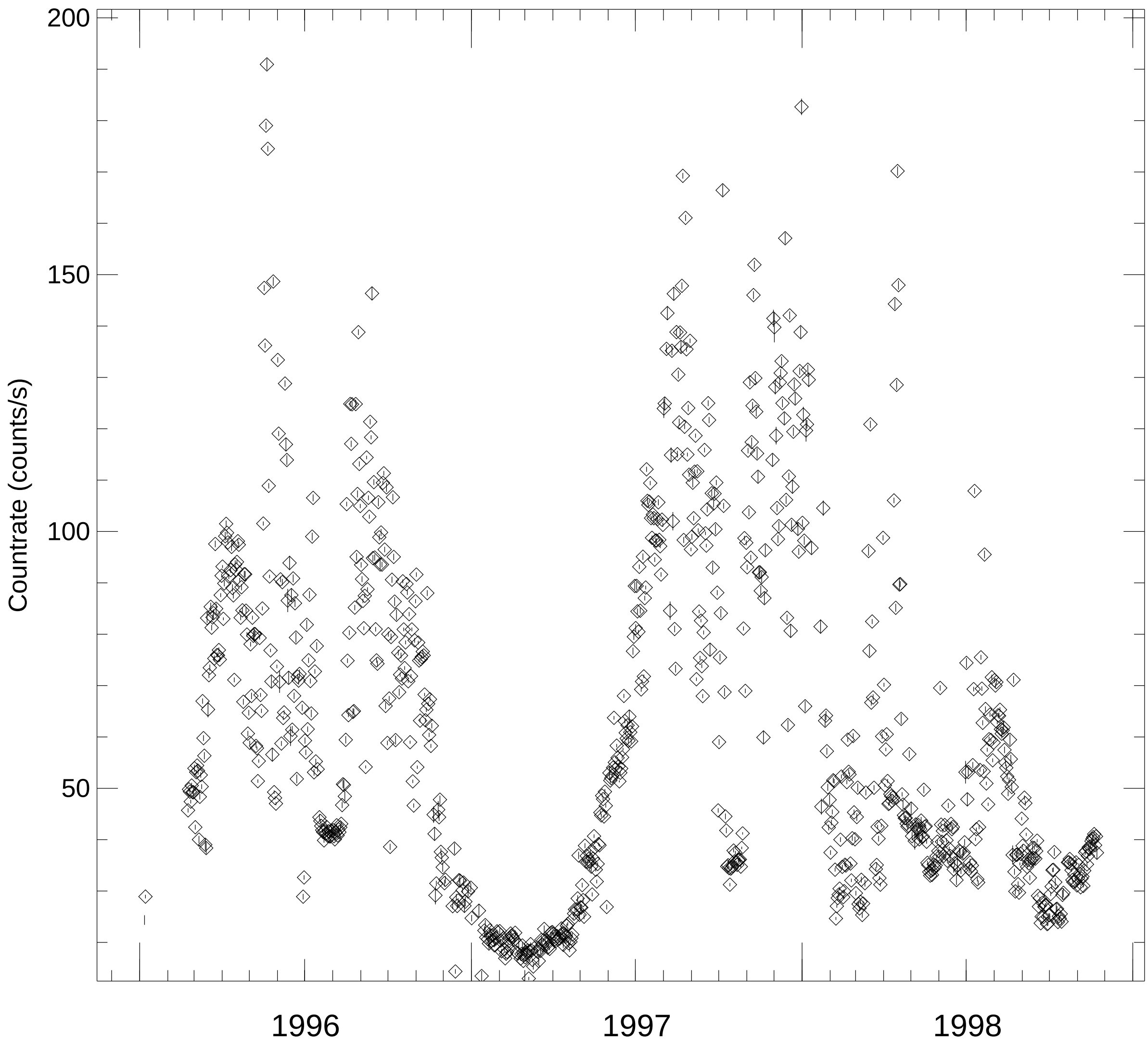

RXTE ASM lightcurve

Although transient, outburst behavior very different from soft X-ray transients.

GRS 1915+105

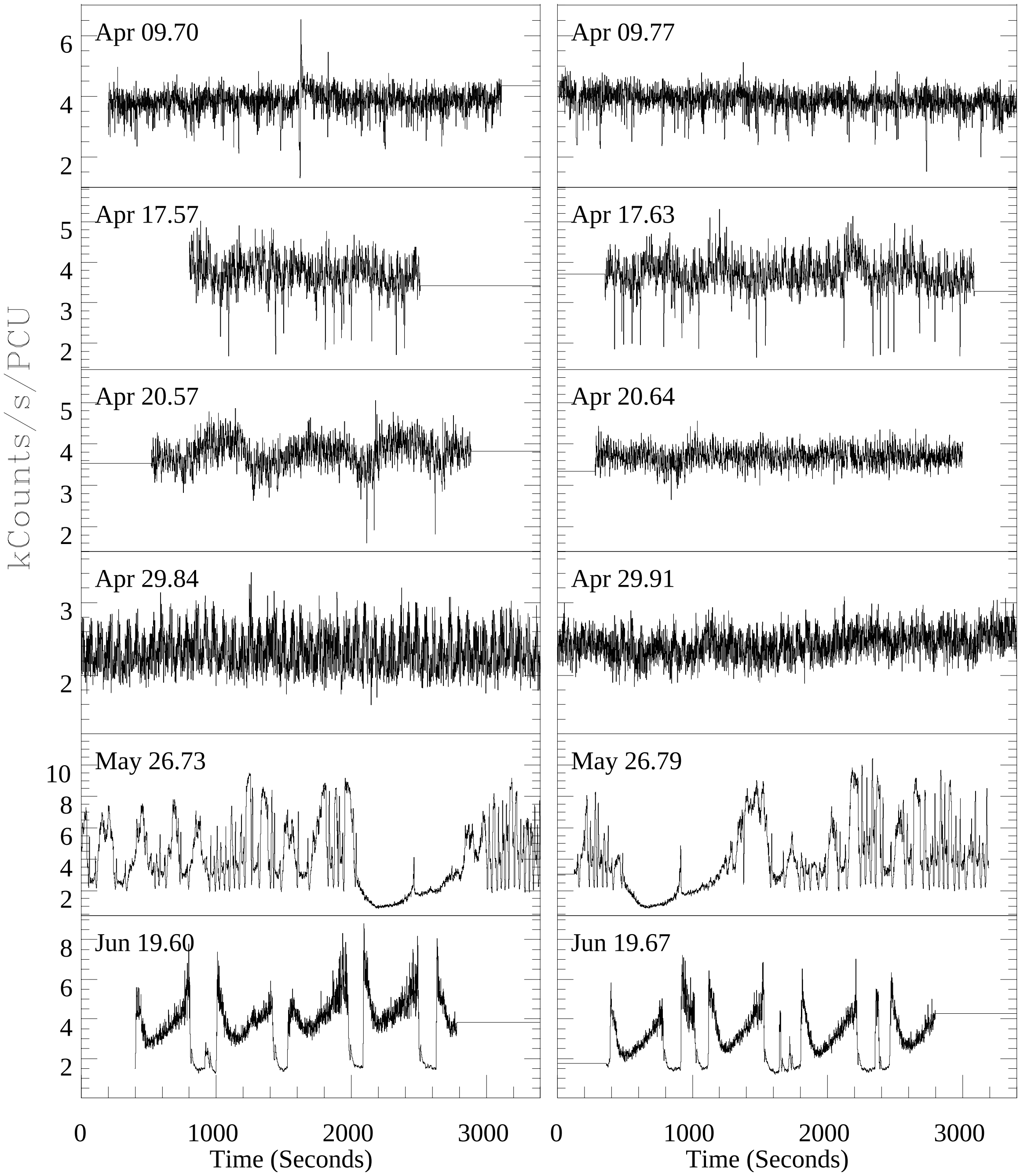

Short term variability is also weird: Brightness Sputters, Large-Amplitude Oscillations (Greiner et al., 1996)

GRS 1915+105

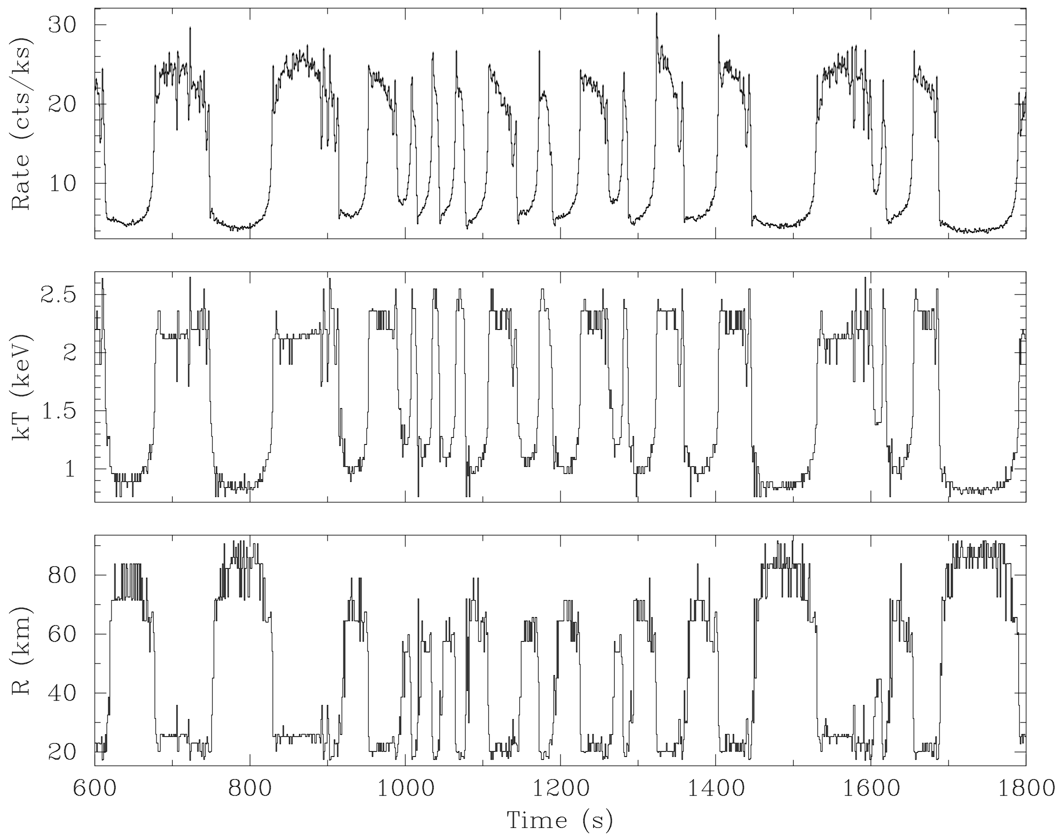

Belloni et al., 1997

Possible explanation via fast emptying out of accretion disk (accretion disk instability on viscous timescale?), slow refill via $\dot{M}$.

GRS 1915+105

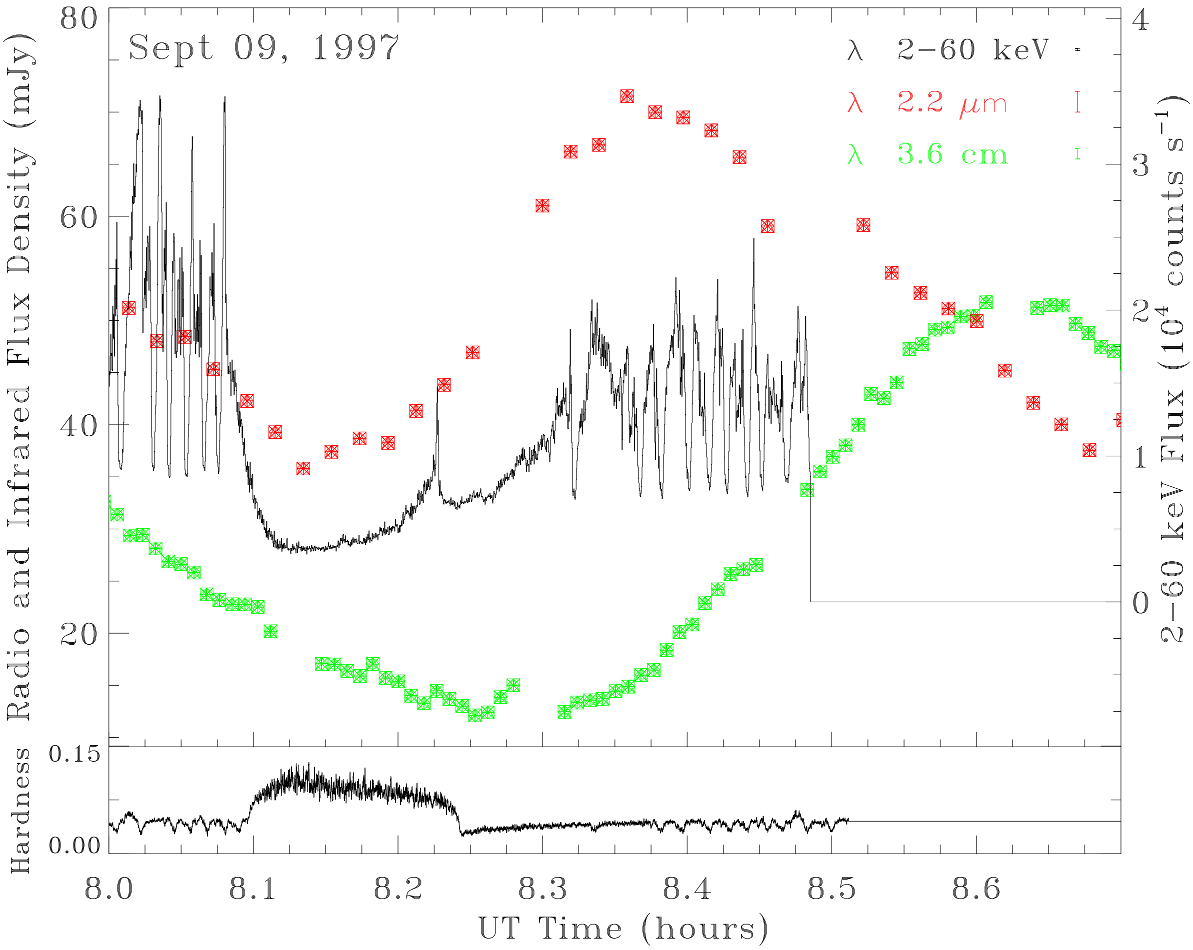

- X-Rays (PCA): 50 s QPO, Dip with short flare
- IR (UKIRT): Flare starts after short X-ray flare
- Radio (VLA): Flare starts 16 min after IR Flare (adiabatic expansion; effect of λ dependency of optical thickness for synchrotron radiation)

$\Longrightarrow$ Hypothesis (Mirabel et al., 1998): Inner disk empties out, material released as adiabatically expanding plasma cloud that emits synchrotron radiation (“Minijet”)

Bibliography

Blondin, J. M., 1994, ApJ, 435, 756

Giacconi, R., Gursky, H., Kellogg, E., Levinson, R., Schreier, E., & Tananbaum, H., 1973, ApJ, 184, 227

Kreykenbohm, I., Kretschmar, P., Wilms, J., Staubert, R., Kendziorra, E., Gruber, D., & Rothschild, R., 1999, A&A, 341, 141

Maloney, P. R., Begelman, M. C., & Pringle, J. E., 1996, ApJ, 472, 582

Schandl, S., 1996, A&A, 307, 95

Stelzer, B., Wilms, J., Staubert, R., Gruber, D., & Rothschild, R., 1999, A&A, 342, 736